Definition of injury mechanism and related physical parameters based on datasets from PMHS tests and advanced HBM simulation

EUROPEAN COMMISSION
DG RTD

SEVENTH FRAMEWORK PROGRAMME
THEME 7
TRANSPORT - SST
SST.2007.4.1.2: Human physical and behavioral components
GA No. 218516

THORAX
Thoracic injury assessment for improved vehicle safety

Deliverable No.	THORAX D2.4
Deliverable Title	Definition of injury mechanism and related physical parameters based on datasets from PMHS tests and advanced HBM simulation
Dissemination level	Public
Written By	Eric Song; Erwan Lecuyer; Xavier Trosseille (Gie Re Pr) M. Mendoza-Vazquez; Johan Davidsson (Chalmers)
Checked by	Johan Davidsson (Chalmers)
Approved by	Paul Lemmen (Humanetics)
Issue date	May 11, 2012

Executive summary

The THORAX project was initiated to study thoracic injuries for a wide variety of car occupants and transfer research results into test and design tools. Task 2.3 - Injury mechanism – was designed to achieve the following objectives:

- Characterization of injury mechanisms of the most relevant thoracic injury types as defined in WP1;
- Definition of assessment criteria for use in an improved THOR frontal crash test dummy as well as in Human Body Models. An injury criterion is considered as relevant if it is restraint-independent, capable to discriminate between different loading conditions.

To achieve these objectives, two approaches were planned: 1) Traditional approach: it consists of analyzing existing PMHS tests and injuries and suggesting injury mechanisms. 2) HBM-based approach: it consists of using Human Body Models to identify the most relevant global injury criteria. This document, assigned as Deliverable D2.4-M24, reports results obtained. All results are dealing with the human body model simulations since the traditional approach was not performed due to limited data available.

Activities using the HBM-based approach were split into two parts:

- Studies into the definition of injury assessment criteria, conducted by Gie Re PR (LAB PSA Peugeot Citroën Renault) using an updated version of the HUMOS2 model called HUMOS2LAB.
- Studies into the thoracic stiffness and the contributions of the various elements in the thorax to this stiffness, conducted by Chalmers, using an modified version of the THUMS model, and by Gie Re PR, using the HUMOS2LAB model.

Each of these activities included a first step into validation of the models for their purpose followed by application studies.

Main results of the studies into assessment criteria include:

- A human body model, the HUMOS2LAB, was validated with respect to four types of biomechanical data: 1) global force and deflection-based corridors, 2) rib strain profile, 3) spacial repartition of rib fractures and 4) ribcage damage evolution versus loading severity, under different loading types and regarding different impact directions.
- A series of simulations using the HUMOS2LAB model were performed, forming a “virtual” PMHS tests database. Five loading types were covered by this database: 3 points shoulder-lap belt restraint, 3 points shoulder-lap belt + airbag restraint, and airbag only restraint in sled test environment, airbag and cylinder impactor loading in static environment. For each simulation, rib fracture outcome was established and different metric of ribcage deflection were recorded.
- Based on these “virtual” PMHS tests, excessive strain, provoked mainly by bending, was identified as mechanism of rib fractures.
- It was demonstrated that maximum peak strain of ribs does not predict number of fractured ribs correctly. It was suggested to directly use the NFR (Numbers of Fractured Ribs) as a global injury criterion. A scheme to use the NFR on a mechanical dummy, where ribs always remain in elastic state, is proposed. The NFR

offers potential to be a universal injury criterion - restraint independent, impact direction independent and suitable for evaluating different levels of injuries.
- A more usual metric, named as Combined Deflection and noted as Dc, is also proposed. This metric is a global deflection-based predictor for serious injury (more than six fractured ribs). Injury curve and risk curve constructed with this criterion do not vary significantly from one loading type to another. It has potential to candidate as a restrain-independent injury predictor.
- Both the above mentioned criteria have been reported to the THORAX team and have been considered in the demonstrator THOR dummy. For the Combined Delfection criterion multiple point chest deflection measurement device (3D-ITRRAC) was developped. For the evaluation of the NFR criterion the chest cage of the demonstrator was instrumented with a suitable numbers of strain gages.

Main results of the studies into the thoracic stiffness included:

- The Total HUman Model for Safety version 3.0 was modified by including a finely meshed ribcage, and thoracic flesh and material properties and contact conditions were updated.
- The modified THUMS force-deflection response of the torso was then validated against three different PHMS data sets:
    - the pendulum impact test as in Neathery (1974) using the corridors as defined in GESAC (2005).
    - the four different Table Top tests configurations, hub, belt, double diagonal and distributed, as in Kent et al (2003).
    - the three different states, including intact, denuded and eviscerated, of the PMHS torsos in table top tests as in Kent et al (2005).
- The modified THUMS kinematic response was validated in the Gold Standard configuration, the UVa sled test as in Shaw et al (2009).
- A parametric study was carried out using the developed Table Top and Gold Standard sled conditions to clarify the contribution of the thoracic organs and tissue properties on the overall thoracic response, and to support the ATD design.
- The parameter changes include changes of material stiffness, here denoted weak states, and design changes that made its torso resemble that of an anthropometric test device. Examples of these weak states are weaker costal cartilage, ribs and intercostal muscles whereas examples of ATD-like designs are remove the internal organs, horizontal clavicle and divided sternum.
- The parameters measured were total stiffness change, coupling between the upper and lower chest regions and coupling between the right and left chest regions and particularly the calculated combined deflection criterion (DC).
- In summary, the modified Total HUman Model for Safety (THUMS) version 3.0 showed a response very close to that of PMHS.
- Related to the studies into combined deflection criterion it can be concluded that:
    - THUMS showed an inverse relationship between coupling and chest stiffness. This implies that for THUMS, an increase in chest stiffness is followed by a decrease in both the C and dD.
    - The whole kinematic response of THUMS was not substantially affected by the weak states. Weak intercostal muscles and weak ribs were the states with largest differential deflection (dD). The smallest dD values were found when the cartilage was made shorter and ribcage was made stiffer in combination with removal of the internal organs.
    - For THUMS in the sled tests condition, the C and dD peak values varied in amplitude and timings. Since the DC value is reported as one single value,

corresponding to its maximum, and the DC is calculated as the sum of C and dD, it is important to consider their timing.

- Related to the thoracic stiffness studies and introduction of ATD design changes using the THUMS model it can be concluded that:
  - The kinematic response of THUMS was changed the most when ATD-like changes were introduced. The results suggest that small changes on THOR ribcage stiffness will not affect its kinematic response, but changes on its clavicle and thoracic mass distribution will probably do.
  - Different tests on THOR indicate that it has a stiffer response than PMHS (Shaw et al. (2005)). The parametric study has shown that the weak ribs state decreased the effective stiffness. Hence, a reduction in the THOR chest stiffness could be achieved by a substantial decrease in the thickness or height of the ribs in the THOR.
  - The jacket in the THOR is intended to represent the intercostal muscles and fat tissue. From the simulations with the THUMS we found that there is a risk that the THOR jacket will influence the chest response differently for different load cases. For hub loads, the jacket would be engaging a small surface and therefore underestimating its contribution on the chest response as compared to distributed load for which the jacket would be engaging a large rib cage surface.
  - The state with the anteriorly displaced clavicle shielded the belted upper chest.
  - Different states experienced a change on the displacement pattern in the coronal plane. This pattern change could modify the deflection results. For example, a larger caudal rib rotation may be interpreted as a larger rib compression. It is therefore suggested that the biofidelity requirements include 3D displacements of the anterior end of the rib relative the spine and not only the compression relative to the spine.

- Related to the thoracic stiffness studies using the HUMOS2LAB model it can be concluded that:
  - Organ simplification (i.e. without representing organs, such as lungs and heart, and using rigid connections between the ribs and the spine) does not fundamentally change the thoracic behavior. The main features of rib strain profile remain the same, and the global stiffness decrease of the thorax may be compensated in a mechanical dummy by using stiffer rib materials. These conclusions suggest that it may not be necessary to represent organs and rib-spine joints in a mechanical dummy.

Contents

1 General introduction

Around 41,600 people were killed and more than 1.7 million injured in European road accidents in 2005 (European Commission, 2006b). Accident studies showed that thoracic injuries are one of the dominant causes for fatalities and injuries in car crashes. Motivated by this the THORAX project was started in February 2009 to study thoracic injuries for a wide variety of car occupants and transfer results into test and design tools. In order to maximise the safety benefits gained from new vehicle and restraint technology for various genders, ages, and sizes of occupants, these tools will have to be much more sensitive to the in-vehicle occupant environment than is the case with existing test tools.

WP2 of THORAX aimed at delivering a set of biomechanical requirements for enhanced shoulder thorax complex of crash-test dummies of different sizes & ages for the test conditions identified. A key activity of WP2 was to study injury mechanisms and governing parameters using human body models done under task 2.3. This report presents the results of this task which fed into the concept dummy design of task 2.4 and the dummy design in WP 3.

The goals of task 2.3 were to characterization injury mechanisms of the most relevant thoracic injury types as defined in the accident studies done under COVER / THORAX WP1 and define related assessment criteria for use in an improved THOR frontal crash test dummy as well as in Human Body Models.

1.1 Results of accident studies

Accident surveys for the THORAX project were done in COVER WP1 and in THORAX WP1. In COVER the statistical analysis were done using databases from the UK, France and Germany. In THORAX WP1 in-depth studies were done, comparing the real world performance with crash test performance.

Main conclusions of this work in relation to task 2.3 are:

- Fractures to the ribs and then the sternum are the most frequently occurring types of fractures. They therefore represent a priority injury type when considering AIS _ 2 torso injuries.
- Injuries to the lungs are the most frequently occurring visceral injuries to the torso. In both the CCIS and GIDAS sample, the heart is the next most frequently injured torso organ.
- Younger occupants can sustain AIS _ 3 lung injuries without an AIS _ 3 series of rib fractures. This may have implications regarding the mechanism of injury and the ability of an advanced dummy thorax to detect the loading which is responsible.

Hence most important injuries to be considered in THORAX are the rib fractures and the lung injuries. Previous projects like APROSYS have shown that Human Body models can be dealing with rib fracture injuries. Lung injuries on the other hand are too complex and the soft tissue modelling in HBM's is not that advanced to deal with this type of injuries. Therefore these have to be considered using the traditional apporach of analyzing PMHS tests.

1.2 Approach

To achieve these objectives of task 2.3, two approaches were planned: 1) Traditional approach: it consists of analyzing existing PMHS tests and injuries and suggesting injury mechanisms. 2) HBM-based approach: it consists of using Human Body Models to identify

the most relevant global injury criteria. Finally, only the HBM-based approach was used. The traditional approach was not performed due to limited data available. Activities using the HBM-based approach were split into two parts:

- Studies into the definition of injury assessment criteria, conducted by Gie Re PR (LAB PSA Peugeot Citroën Renault) using an updated version of the HUMOS2 model called HUMOS2LAB.
- Studies into the thoracic stiffness and the contributions of the various elements in the thorax to this stiffness, conducted by Chalmers approach using an modified version of the THUMS model, and by LAB, using the HUMOS2LAB model.

1.3 Report layout

This report follows the above mentioned activities, covering the studies into the assessment criteria in chapter 2, and the studies into the thoracic stiffness and the contributions of the various elements in the thorax to this stiffness in chapter 3 and 4. Each chapter starts with a short introduction followed by a section on the validation and the applications. Each chapter ends with conclusions. Chapter 5 provides with general conclusions.

2 Traditional approach

In the traditional approach existing and new PMHS data were to be analyzed to suggest improved chest injury criteria. One of the challenges using this approach was to design operations that made data from existing PMHS experiments available for the analysis. One example of such an operation would be to recalculate chest band data from PMHS experiments carried out in the past so that it could be expressed in the same system as used in more recent PMHS experiments. In these more recent experiments multiple chest deformations were determined using advanced film analysis. Unfortunately, the suggested operations were found to be less robust than desired and could only be applied to a limited data set. Due to this the traditional approach would, using the available data, lack statistical power. As a result the traditional approach was not completed.

2.1 Introduction

Sternal deflection is an injury criterion used by current regulation and consumer tests (such like US-NCAP, EURO-NCAP …) worldwide to assess thoracic injury risk. However, this criterion has some serious limits regarding its applications.

Kent et al. (2003) showed that the risk curve in terms of sternal deflection is restraint dependent when measured with H-III dummy. As shown in Figure 1, the risk curve relative to impactor loading is completely different from that of airbag loading and that of belt loading. This dependency to restraint type raises a serious interrogation on the relevance of the criterion for its use on the H-III dummy. It means that it is incorrect to compare injury risk between these loading types. It means also that the risk curve established using different loading types is no relevant.

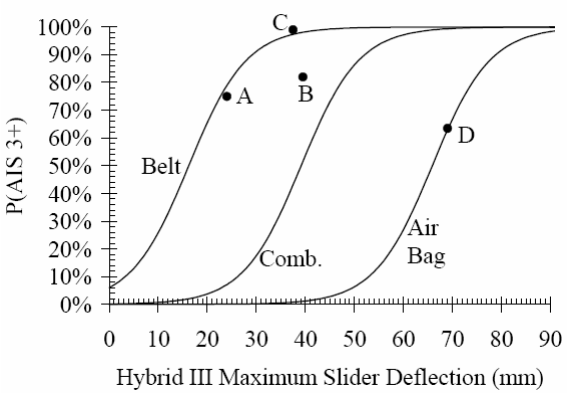

Figure 1. Risk curves for AIS3+, constructed for the Hybrid III dummy in terms of maximum slider deflection (Kent et al. 2003)

A more elaborated injury criterion, Cmax (maximum chest compression), was evaluated by Kent et al. (2003) based on 93 cadaver tests. They found that the Cmax is not sensitive to loading types when measured on cadavers (Figure 2). Bose et al. (2009) studied the application of the Cmax on the THOR dummy and found that the risk curve is also restraint-dependent with the dummy (Figure 3).

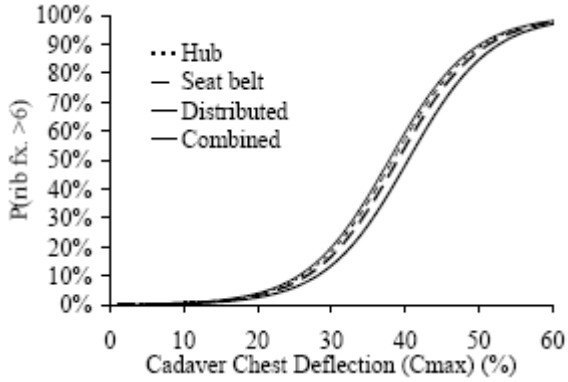

Figure 2. Restraint-type insensitivity of Cmax when measured directly on cadavers (Kent et al. 2003)

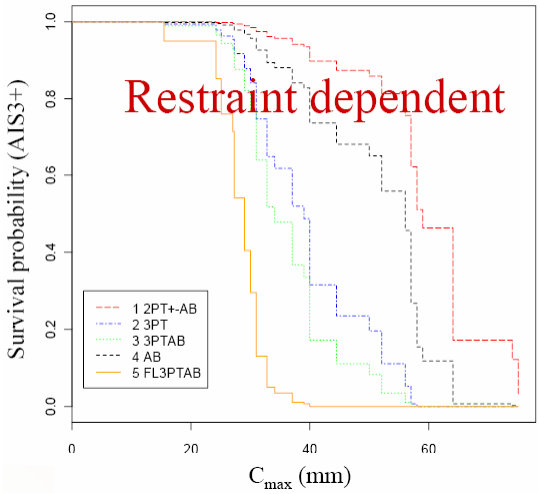

Figure 3. Risk curves for AIS3+, constructed for the THOR dummy in terms of Cmax (Bose et al. (2009).

In the FP7 THORAX Project, Task 2.3 aims at identifying injury mechanisms of the thorax and defining corresponding physical parameters (i.e. injury criteria) which are:

- Restraint-independent
- Capable of discriminating between different loading conditions
- Applicable to a mechanical dummy.

The contribution of the LAB to Task 2.3 consists of investigating mechanism of rib fractures and identifying relevant injury criteria by using a human body model.

This document reports progress achieved so far by LAB. First, it presents the validation of the HUMOS2LAB human body model which was used to conduct current study (section 2.2). Then, findings regarding mechanism of rib fractures are reported in section 2.3. In section 2.4 and 2.5, two candidates as global injury criteria are presented respectively, one based on global thoracic deflection measurement, and the other based on rib strain measurement along the ribs. This chapter ends with conclusions.

2.2 Evaluation of HUMOS2LAB human body model

2.2.1 HUMOS2LAB model

The thorax model used in this study was an improved version of the HUMOS model. The HUMOS model is a full human body finite elements model developed by a consortium of universities, research institutes and car manufacturers (Robin 2001). Its mesh was constructed based on the geometry of a single subject whose mass, stature and seated height were close to a mean European male. However, the subject presented a more massive torso and less massive lower extremities, typical for an aged person. LAB (Laboratory of Accidentology and Biomechanics) was in charge of the shoulder and the thorax modeling in the first phase of the HUMOS model development in the Radioss^{TM} FE code. The HUMOS model was scaled to other body sizes, and was further updated with respect to new biomechanical data available in the following phases of its development (Vezin et al. 2005). The HUMOS 50th percentile male model in the Radioss^{TM} code was used in this study. Regarding the thorax part of the HUMOS model, the cortical bone of the ribs and the sternum was represented by shell elements, and the trabecular bone by solid elements. The cartilage between the sternum and the ribs was also represented by solid elements. The muscles and internal organs, such as the heart, lungs, stomach and liver were represented by solid elements. An elasto-plastic material law was used to model the cortical bone, an elastic material law for the trabecular bone and cartilage, and a Boltzman material law for the organs and muscles. The vertebrae were considered as rigid bodies, the connections between them were modeled with general springs. The same was done for the connections between the ribs and the vertebrae. Figure 4 provides an overall view of the HUMOS 50th male model, and Figure 5 shows the thorax part of the model.

A number of modifications were made to the HUMOS model at the LAB. The objective was to make the model representative of the behavior of a human thorax, not only in terms of global responses, but also in terms of local responses, such as the strain profiles and rib fractures. The following sections present the main modifications performed. To facilitate the expression, the modified model will be referred as the HUMOS2LAB model in the following sections.

Cortical bone thickness of ribs. In the original HUMOS model, the cortical bone thickness is constant for all ribs. This simplification may be acceptable for a thorax model dedicated to represent global responses of the thorax, but may be inappropriate when the target is to simulate rib fractures. The strain level of a rib depends on its cortical bone thickness, so does the rib fracture outcome. Based on the data collected by means of rib scanning (Charpail et al. 2005), a regional thickness variation was defined across the ribs, each region receiving its own cortical bone thickness. Figure 6 illustrates the variation.

Figure 4. Overall view of the RadiossTM HUMOS 50th male model.

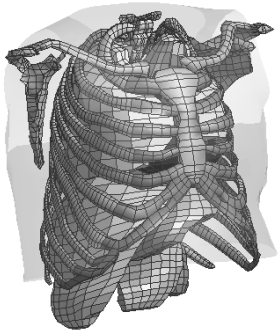

Figure 5. Thorax part of the HUMOS model.

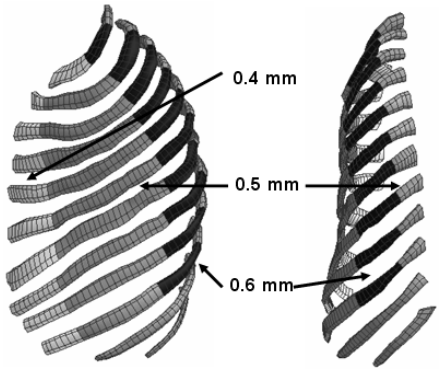

Figure 6. Regional variation of the cortical bone thickness across the ribs.

Mechanical properties of ribs. An elasto-plastic material law (Law 02 in the Radioss™ FE code) was used to model the cortical bone of ribs in the original HUMOS model:

$$\sigma = a + b\varepsilon_p^n \qquad (1)$$

Where, σ is the effective plastic stress; n is the hardening exponent; a is the yield stress; b is the hardening parameter.

In the HUMOS2LAB model, the same law was used, but with a new set of parameters (Table 1). The Young's modulus and the yield stress were those determined by Kemper et al. (2005) carrying out rib tests. b was derived based on the same rib tests:

$$b = \frac{\sigma_{UT} - a}{\varepsilon_p} = \frac{\sigma_{UT} - a}{\varepsilon_{UT} - a/\sigma} = \frac{124.2 - 93.9}{0.0271 - 93.9/13900} = 1489 \qquad (2)$$

Rib fractures were modeled by a shell element deletion scheme. A shell element is deleted when the failure plastic strain is reached. The failure plastic strain was determined for the HUMOS2LAB model to represent, as closely as possible, the main features of a validation database relative to rib fractures (presented later in the Validation database Section). It is to be noted that the failure plastic strain according to Kemper's experiments was established around 20 millistrain.

Table 1. Material law for the cortical bone of the ribs.

Density	1800kg/m^3
Young's modulus	13900 MPa
Poisson's ratio	0.3
Yield stress (a)	93.9 MPa
Hardening parameter (b)	1489 MPa
Hardening exponent (n)	1
Failure plastic strain	13 millistrain

Connection between ribcage and surrouding soft tissues. In the original model, the connection between the ribcage and the surrounding soft tissues is realized by two tied interfaces. One is between the ribcage and the interior surface of the superficial muscle (Surface A); the other is between the ribcage and the exterior surface of organs (Surface B). Such a method is frequently used to connect two parts with different mesh sizes. This is the case in the HUMOS model where the elements of muscles and organs have bigger sizes than those of the ribs. By simulating the PMHS tests of our validation database, it was found that such an approach significantly stiffens the ribcage. It resulted in the formation of small stiff regions across the ribs, and consequently, the discontinuity of strain along the ribs (more details can be found in the Discussion Section). To solve this problem, these two tied interfaces were replaced by two general interfaces (Type 7 interface in Radioss^{TM}). These interfaces allow force transmission between the ribcage and the surrounding soft tissues, and relative sliding between them. However, the surfaces in interaction can separate freely with this type of interface. To ban the separation between the ribcage and the surrounding tissues, a tied interface was defined between Surface A and Surface B. In this way, the ribcage was sandwiched between the surrounding soft tissues. It is to be noted that Surfaces A and B have similar mesh size, so there is no risk of small stiff region formation.

Connection between the spine and surrounding soft tissues. In the original model, this connection is realized by including the nodes of the surrounding soft tissues into the rigid bodies representing the vertebrae. In the HUMOS2LAB model, this approach was replaced by defining contact interfaces (Type 7 interfaces) between the spine and the surrounding tissues, this in order to render the spine more flexible. It is to be noted that, with this new approach, local separation between the spine and surrounding soft tissues may be observed, but it remains very limited. This limitation can be partially explained by the proximity of the interfaces between the ribcage, Surface A and Surface B.

2.2.2 Validation database

To validate the HUMOS2LAB model, an original validation database was established. The main characteristics of the database are briefly presented below. To facilitate the expression, a pure frontal impact will be noted as an impact at 0°, a pure lateral impact as an impact at 90°. An oblique impact will be noted according to the angle formed with respect to the direction of frontal impact.

Bouquet impactor tests at 0° and 90°. A series of PMHS tests were carried out by Bouquet et al. (1994, 1998) using a flat rigid disc, the diameter being 150mm, with a pendulum of mass equal to 23.4kg. Two velocity levels were applied for each direction, namely 3.3 m/s and 5.9 m/s. The response corridors derived include the thoracic deflection versus time, the impact

force versus time and the impact force versus the thoracic deflection. The fractured ribs were reported, but without the precise locations of the fractures.

Kroell impactor tests at 0°. A series of PMHS tests were carried out by Kroell et al. (1971, 1974) using a flat rigid disc, the diameter being 150mm, and an impactor of mass equal to 23.4kg. Three velocity levels were applied, at 4.9 m/s, 6.9 m/s and 9.8m/s. The response corridors derived include the thoracic deflection versus time, the impact force versus time and the impact force versus the thoracic deflection. The fractured ribs were reported, but without the precise locations of the fractures.

Viano impactor tests at 60°. A series of PMHS tests were carried out by Viano (1989) using a cylindrical pendulum, the diameter being 150mm, and a pendulum of mass equal to 23.4kg. Three velocity levels were applied, at 4.3 m/s, 6.5 m/s and 9.8m/s. The response corridors derived include the thoracic deflection versus time, the impact force versus time and the impact force versus the thoracic deflection. The fractured ribs were reported, but without precise locations of the fractures.

LAB impactor tests. Three PMHS tests were carried out at the LAB (Trosseille et al. 2008) using a flat rigid disc, the diameter being 150mm, and a pendulum mass of 23.4kg. A single speed (4.3 m/s) was applied at 0°, 60° and 90°. These tests present two major advantages with respect to the above impactor tests:

- Strain gauges were mounted on the ribs and strain profiles of ribs were derived,
- The in-depth autopsy allowed exactly determining the sites of fractures and the nature of each fracture: complete with displacement (D), complete without displacement (ND), partial with rupture of the external cortical bone (PE) and partial with rupture of the internal cortical bone (PI). To facilitate expression, a complete fracture with displacement will be called as a separated fracture in the following presentations.

LAB airbag tests at 0°. Five PMHS tests were carried out at the LAB with airbags - three under membrane-only loading, and two under punch-out-only loading (Lebarbé et al. 2005). The sites of fractures and their natures were reported. The strain profile was derived for the membrane-only airbag loading.

LAB airbag impacts at 90°. A series of PMHS tests were carried out at the LAB (Trosseille et al. 2008). Different loading levels were achieved by varying the distance between the subject and the airbag support plate (98mm, 115mm, 125mm, 137mm, 157mm, 189mm and 205mm, respectively). The rib strain profiles, the sites of fractures and their nature were provided.

LAB airbag impacts at 60°. More PMHS tests were carried out as above but with an impact angle of 60° (Trosseille et al. 2008). The following distances were used: 114mm, 123mm, 178mm and 205mm. The rib strain profiles, the sites of fractures and their nature were provided.

LAB frontal sled tests: Four PMHS tests were carried out (Petitjean et al. 2002). The subjects were seated on a rigid seat; the velocity change was 56km/h. Two subjects were restrained by a combined restraint system (3-point belt with a 4kN load-limiting shoulder belt plus an airbag) while the two others by a belt-only restraint (3-point belt with a 6kN load-limiting shoulder belt). The sites of fractures were provided.

In summary, this database covers:

- Different directions of impact: 0°, 60° and 90°
- Different loading types: rigid impactor, membrane-only airbag, punch-out-only airbag, sled with belt-only restraint system and combined belt and airbag restraint system.

- Different loading levels: from sub-injury level to numerous rib fractures.

2.2.3 Model validation

Based on the validation database presented above, a new validation approach was used to validate the HUMOS2LAB model. It consisted of evaluating the model at different levels, as explained in the following sections.

Global responses. The evaluation at this level aimed at comparing the response of the model to the experimental measurements such as the global thorax deflection and the global impact force. Different finite element thorax models reported in the literature focused mainly on this type of validation. In the current study, Bouquet impactor tests at 0° and 90°, Kroell impactor tests at 0°, and Viano impactor tests at 60° were used. The validation corridors were constructed in a previous published study (Lizée et al. 1998). Furthermore, the HUMOS2LAB model was also evaluated with respect to LAB airbag tests at 0°, 60° and 90°. In these tests, the force sustained by the torso was approximated by the reaction force measured behind the plate supporting the airbag. The reaction force was compared between the simulations and the tests. The variation of the force as a function of the distance between the airbag and the test subject was also compared.

It should be noted here that no tests involving belts were considered as the PMHS testdata were not yet analysed at the moment of wrting this report. This validation will be included in the final version of D2.4

Strain profiles. In the validation database, a number of PMHS tests performed at the LAB provide rib strain profiles, as illustrated in Figure 7. In order to allow for the comparison of different tests and ribs, the strains were normalized. First, an effective strain, ε_{RMS} (Root Mean Square, Equation 3) was calculated for each costal ring. Then, each strain of the costal ring was divided by the effective strain to obtain a normalized strain $\varepsilon_N(s, t)$ (Equation 4). The calculation of the effective strain was done for the costal rings instrumented with more than eight rib strain gauges. The details about the construction of the local strain profiles can be found in a preceding published study (Trosseille et al. 2008). Six profiles were thus constructed, corresponding to the impactor tests at 0°, 60° and 90°, and airbag tests at 0°, 60° and 90°, respectively. These profiles constitute a good test battery to evaluate the relevance of a model, far beyond the classic global response validation. The HUMOS2LAB model was evaluated with respect to these strain profiles.

Fracture regions. The evaluation at this level consisted of examining whether the rib fractures occurred in the same regions between the model and the PMHS tests for different loading types. It did not aim to compare either the exact fracture sites or the number of fractures for each rib, which may vary considerably from one subject to another, but rather to check whether the fracture regions, which are relatively stable, were correctly reproduced for each loading type. The PMHS tests performed at the LAB were used for this purpose since the nature and the sites of the rib fractures were clearly identified by the autopsy report.

Ribcage damage. A good indicator of the ribcage damage level is the number of fractured ribs (NFR). For a given loading type, the NFR depends on the loading severity. A fracturable model should be able to represent this variation. The HUMOS2LAB model was evaluated in this respect using impactor tests at 0°, 60°, and 90°, and LAB airbag tests at 0°, 60°, and 90°. For the impactor tests, the loading severity varies as a function of the impact velocity; for the airbag tests, it varies as a function of the distance between the airbag supporting plate and the subject tested. Like for the global response no tests involving belts were considered here as the data were still under analysis. This validation will be included in the final version of D2.4

In summary, we believe that this validation approach represents a significant advance with respect to the classic approach, which is focused mainly on the validation in terms of global responses. The classic approach is used by most finite elements thorax models reported in the literature. Our approach allows evaluation of the relevance of a thorax model at deeper layers: the interaction between the ribcage and the surrounding tissues, the ribcage deformation, the occurrence and the variation in location of rib fractures versus loading type and severity.

$$\varepsilon_{RMS}(t) = \sqrt{\frac{1}{\left((s1-sn)_{left}+(sn-s1)_{right}\right)}\left(\left(\int_{sn}^{s1}(\varepsilon(s,t))^2\,ds\right)_{left}+\left(\int_{sn}^{s1}(\varepsilon(s,t))^2\,ds\right)_{right}\right)} \quad (3)$$

where ε(s, t) is the strain measured at the curvilinear abscissa s as a function of time, s1 the curvilinear abscissa of the first gauge and sn is the curvilinear abscissa of the nth gauge.

$$\varepsilon_N(s,t) = \frac{\varepsilon(s,t)}{\varepsilon_{RMS}(t)} \quad (4)$$

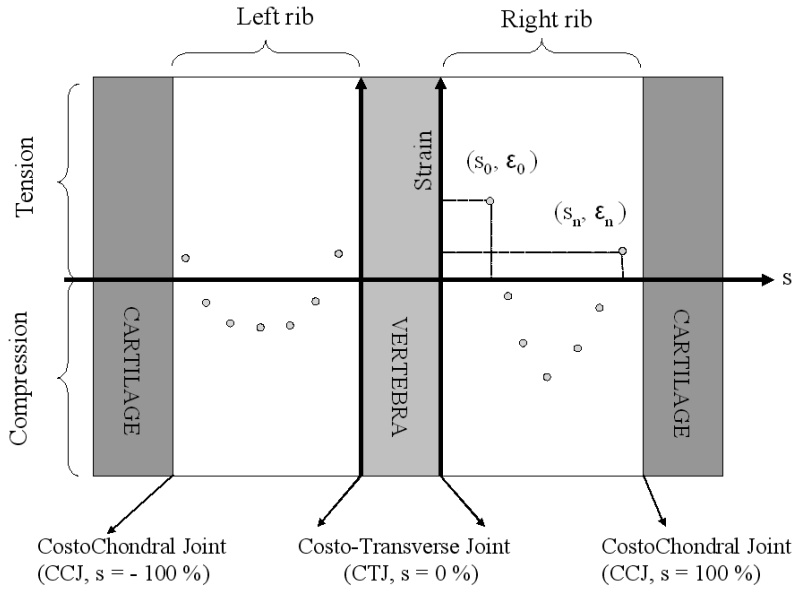

Figure 7. Schematic graph of a strain profile.

2.2.4 Results

All figures relative to the validation results of the HUMOS2LAB model were provided in the Appendix A (Figures A1-A18).

Global responses relative to impactor tests. The global responses of the HUMOS2LAB model were compared to the experimental results relative to the different impactor tests presented in the previous Section of the paper, called "Validation Database". The corridors used were developed by Lizée et al. (1998). The responses of the original model were also provided to illustrate the effects of the modifications presented above. Figures A1-A2 show the results with respect to the Bouquet and Kroell impactor tests at 0°. The thoracic deflection time history, the impact force time history, and the impact force versus deflection curve were compared. In the same way, Figure A3 shows the results with respect to the Bouquet impactor tests at 90°. For the Viano impactor tests at 60°, the impact force time history and

the impact force versus deflection curve were compared (Figures A4). The following observations were made relative to these comparisons:

- The magnitude of the impact force is similar between the model responses and the experiments. The onset of the force is close to the upper limit of the experimental corridor for frontal and oblique impacts, but to the lower limit for side impacts.
- The force-deflection curve matches the corridors in the major part, but the magnitude of the deflection generally exceeded the corridors.
- The original thorax model is way too stiff. The modifications performed allowed a considerable reduction of the peak and plateau forces, leading to a thorax model far more representative of the global responses of the thorax.

Global response relative to airbag tests. Figure A5-a compares the reaction force of the airbag support plate for the membrane-only airbag loading at 0°. The reaction force reflects the force exercised over the thorax. Similar comparison is provided in Figure A5-b for the punch-out only airbag loading at 0°, in Figure A5-c for the airbag loading at 90°, and in Figure A5-d for the airbag loading at 60°. It is to be noted that different loading severities were tested for the airbag loading at 90° and 60° by varying the distance between the airbag and the test subject. Figure A6-a compares the reaction force variation as a function of the distance between the model and the experimental results for the airbag loading at 90°. The same type of comparison for the airbag loading at 60° is provided in Figure A6-b. It is also to be noted that the reaction force was filtered at CFC180 for the model response as for the experiments. However, the model response filtered at CFC60 was also provided for the loading at 90° and 60°, where the oscillation was more important. A good match between the model and the experiments can be observed in terms of the interaction between the airbags and the test subject.

Local strain profiles. Figure A7 compares the local strain profile of the 5th rib between the thorax model and the experiments for the six loading types. A positive strain corresponds to tension and a negative strain to compression. It can be observed that the model is appropriate to represent the state of deformation for the six loading types: the regions of tension and compression, as well as the relative magnitude of strain match the experimental data well, except for the loaded side of the chest in the oblique airbag tests.

Evaluation of fracture regions. Fracture regions given by the thorax model were compared to those given by the experiments. Figures A8-A10 show the results for the impactor tests at 0°, 60° and 90°. Figures A11- A14 show the results for the airbag tests at 0°, 60° and 90°. Figures A15-A16 show the results for the frontal sled tests. The following observations can be made in light of these comparisons:

- For the impactor loading at 0°, the fracture region is the anterior part of the ribs, near the cartilage. Figure A8 shows the similarity between the model and the test.
- For the impactor loading at 60°, two fracture regions can be distinguished: the anterior part and lateral-posterior part, but these regions both appear only on the impacted side of the chest. Figure A9 shows the similarity between the model and the test.
- For the impactor loading at 90°, the fractures appear in the lateral part of the ribs, and again only on the impacted side of the chest. Figure A10 shows the similarity between the model and the test.
- For the airbag loading at 90°, Figure A11 combines all fractures that occurred for the tests at all distances between the airbag and the test subject. Two principal fracture regions can be distinguished: the lateral part and the lateral-posterior part of the ribs. Figure A11 shows the similarity between the model and the experiments.

- For the airbag loading at 60°, Figure A12 combines all fractures that occurred for the tests at all distances between the airbag and the test subject. Two principal fracture regions can be distinguished: the anterior part and the lateral-posterior part of the ribs. Figure A12 shows the similarity between the model and the reference test.
- For the membrane only airbag loading at 0°, the results of the three PMHS tests showed that the rib fractures appeared in the antero-lateral part of the ribs (Figure A13). Similar results were observed with the model.
- For the punch-out only airbag loading at 0°, the results of the PMHS test showed that the rib fractures appeared in the anterior part of the ribs (Figure A14). Similar results were observed with the model.
- The fracture regions of the frontal sled tests are shown in Figures A15-A16. The simulation with a combined restraint system (3-point belt with a 4kN load-limiting shoulder belt plus an airbag) indicates two lines of fractures in the right part of the ribcage, while the simulation with a belt-only restraint (3-points belt with a 6kN load-limiting shoulder belt) shows a single line of fractures. The four PMHS tests do not allow clearly formulating such a tendency. For the left part of the ribcage, the fractures appeared in the anterior-superior part of the ribcage, in the PMHS tests as in the model. The analysis of the strain profiles observed in the THOMO/THORAX PMHS belt tests may allow a better assessment of the model. This will be done in the second issue of this report (M24).

Ribcage damage versus loading severity. Figure A17 compares the model responses to those of the experiment in terms of NFR variation versus the impact velocity for the impactor loading type. Similar comparison was provided in Figure A18 for the airbag loading type at 60° and 90°. For the airbag loading at 0°, the effects of distance were not tested with PMHS experiments. Figure A18 provides the comparison for the membrane-only loading and the punch-out loading. It is to be noted that two types of fractures were distinguished for each comparison: the number of fractured ribs (taking into account all types of fractures), and the number of ribs sustaining separated fractures (or complete fractures with displacement). Regarding the LAB experimental data, the nature of each fracture was clearly reported, distinguishing separated fractures from other types of fracture. Regarding the impactor tests carried out by Bouquet et al., Kroell et al. and Viano, the nature of fractures was not reported, so the same fracture outcome was used for comparison with the model. In the model, a fracture was established when a shell element of the ribs was deleted, and a separated fracture was established when the adjacent deleted elements form a ring. In general, a reasonable agreement between the model responses and the experiments can be observed.

2.3 Injury mechanism of rib fractures

It is generally agreed that an excessive strain leads to failure. It is reasonable to extend this general principle to ribs. However, it is not clear how an excessive rib strain is generated in a crash event. In others words, we do not know what type of loading is responsible for excessive strain of ribs. Is it traction, compression, bending, torsion, or a combination of two or more loading modes?

In the HUMOS2LAB model, plastic strain was used as a failure criterion of shell elements representing cortical bones of ribs. A rib fracture occurs when equivalent strain reaches the specified threshold of plastic strain. Consistence of rib fracture regions between the HUMOS2LAB model and PMHS tests observed in the model validation phase supports that excessive strain explains rib fracture well.

Using the HUMOS2LAB model, longitudinal rib strain (along the rib curvilinear axis) and transverse rib strain (along the rib cross section circumference) were compared. Figure 8 is an example of this type of comparison. It shows that the longitudinal strain is the main component compared to the transverse strain. Extensive examination of this type of comparison confirms the generality of this observation. It implies that measurement of strain along the rib axis is a good descriptor of strain state.

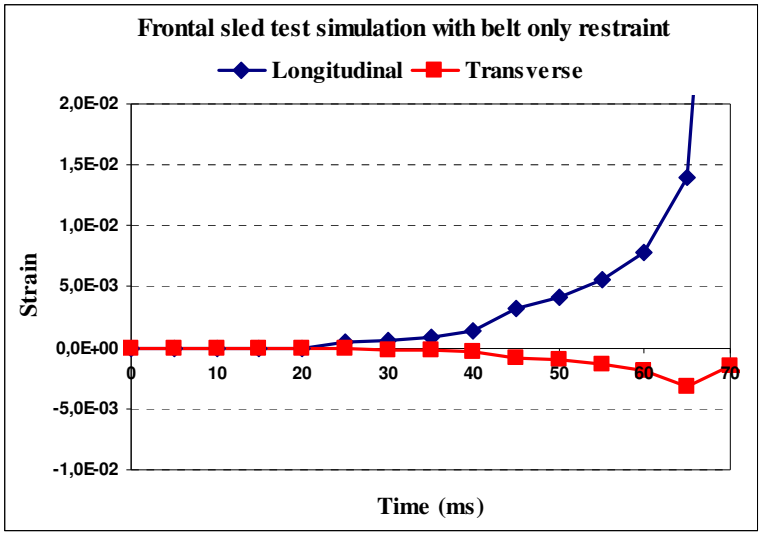

Figure 8. Comparison of the longitudinal rib strain to the transverse rib strain in the same shell element representing rib cortical bone.

In order to determine the loading modes responsible for excessive rib strain, the longitudinal strain field was examined for different HUMOS2LAB model simulations. Bending was identified as an injury mechanism in rib fractures. Figure 9 is an example for belt loading in a frontal sled test simulation, where high longitudinal strain (≥ 2%) locations are indicated in red (for traction) and in blue (for compression). One can observe that red elements and blue elements are in the opposite sides for each rib. Figure 10 plots stress in face to face shell elements at one of the rib fracture locations. It shows that the traction stress level in the external side of rib is close to the compression stress level in the internal side of rib. These characteristics were also observed for airbag only loading and for combined belt and airbag loading. Based on theses observations, it can be concluded that excessive rib strain (or rib fracture) is mainly generated by bending.

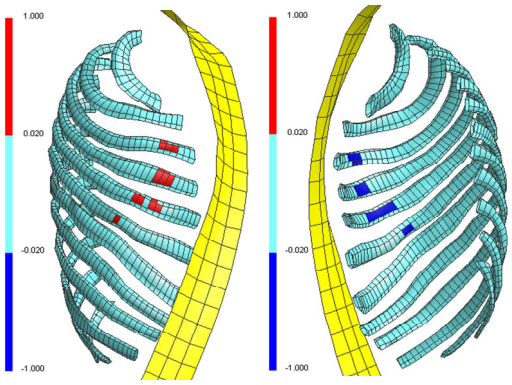

Frontal sled with belt

Figure 9. Longitudinal strain field of ribs showing that bending is the main loading mode leading to rib fracture: external side of ribs (left figure), internal side of ribs (right figure).

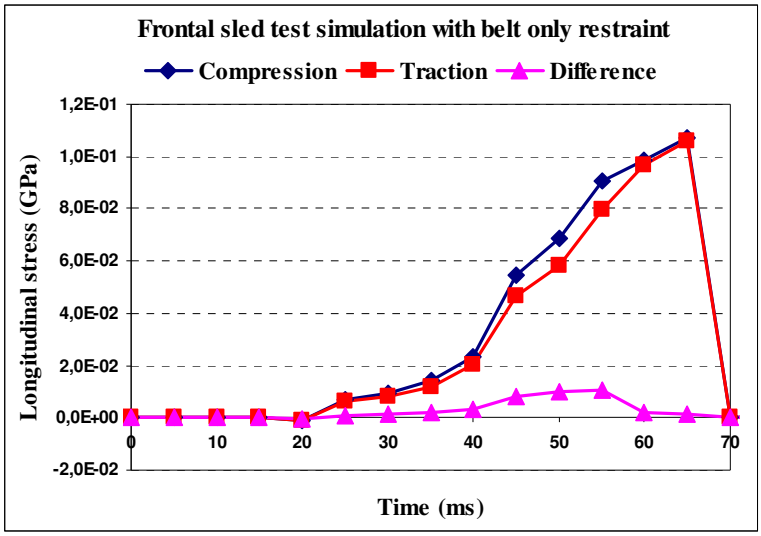

Figure 10. Stress recorded in face to face shell elements at one of the rib fracture locations for belt loading in a frontal sled test simulation.

2.4 Identification of a deflection-based injury criterion - Dc

2.4.1 Simulation matrix

The HUMOS2LAB model was used to identify a global injury criterion correlated to rib fractures but independent to loading types. That means: the relationship between the number of fractured ribs and the injury criterion candidate should be relatively stable. In other words, it should not depend on the loading types. For this purpose, the HUMOS2LAB model was submitted to different loading types:

- Static impactor
- Static airbag
- Belt only restraint in dynamic sled environment
- Airbag only restraint in dynamic sled environment
- Combined belt and airbag restraint dynamic sled environment

These loading types cover the main loading configurations used for PMHS tests in literature, but also current restraint systems used for frontal impact protection. For each loading type, different loading severities were applied in order to generate different levels of ribcage damage: from the absence to numerous fractured ribs.

Preliminary simulations showed an excessive clavicle move towards T1 at strong impact velocity in dynamic sled environment. We have modified ribs 1 cortical bone thickness from about 0.5mm to 3 mm, and render the joints between ribs 1 and T1 stiffer in order to offer a more resistant support to the clavicle.

With this enhanced clavicle-ribs 1 complex, two series of simulations were carried out. One seris corresponds to a plastic strain threshold of 1.3%, another to a plastic strain threshold of 2.4%. The reason of varying the plastic strain threshold is to examine the influence of body resistance level on injury criteria. The plastic strain threshold of 1.3% is the value used by the HUMOS2LAB model resulting from its validation. It reflects the threshold for fragile subjects

since all PMHS tests used to validate the model were carried out with aged subjects. The plastic strain threshold of 2.4% corresponds to an ultimate failure strain of 3.1% which is in line with experimental data on bones (Burstein et al (1976)) for a middle age subject (around 45 year old). Table 2 summarizes the simulations performed with plastic strain threshold of 1.3% and corresponding injury outcome. Table 3 gives similar results with plastic strain threshold of 2.4%. The injury outcome is expressed by the number of fractured ribs. A rib is considered as fractured when a separated fracture occurs on it. A separated fracture means that two face to face elements in the internal and external sides of a rib were deleted.

2.4.2 Thoracic deflection measurement

Springs with null stiffness were defined over the ribcage to measure its global deflection at different locations. Each spring records the relative displacement of the node, on which the spring is connected, with respect to the corresponding vertebra, but also with respect to its posterior extremity in order to exclude the rigid body movement of the rib relative to the vertebra. For example, the springs of the 5th rib measure the relative motion of the nodes relative to the 5th vertebra and the posterior extremity of the 5th rib. The floating ribs were not instrumented. The thoracic deflection was measured at 4 different locations for each rib, apart from the first ribs where it was measured only at two locations. To facilitate the presentation and the discussion in the following sections, the deflections measured for each rib were noted as D1, D2, D3 and D4, respectively. Figure 11 is an example for the 5th rib ring. For the first ribs, the deflections were noted as D1 and D2 in similar way.

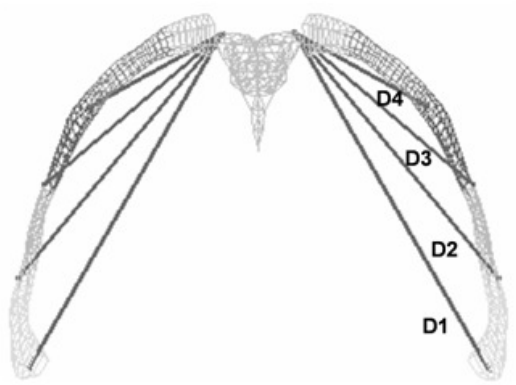

Figure 11. Position of springs measuring the global deformation of the ribcage at the 5th rib level.

More springs were defined over the ribcage to measure its global deflection in its anterior-posterior direction. They are:

- Deflection between the extremity rib 1 and the vertebrae T1
- Deflection between the extremity rib 3 and the vertebrae T4
- Deflection between the extremity rib 5 and the vertebrae T8
- Deflection between the extremity rib 7 and the vertebrae L1
- Deflection between the extremity rib 9 and the vertebrae L2

Three springs were also defined to measure thoracic deflection at levels of the upper sternum, the mid-sternum and the lower sternum.

Based on these measurements, different indicators characterizing thoracic deflection can be defined and calculated.

Table 2. Simulation matrix performed with plastic strain threshold of 1.3%

Plastic strain = 1.3%				
Model name	Test config	Severity	Loading type	NFR
20AB4R8R	Sled test	ΔV=20km/h	4kN belt+AB	3
22AB4R8R	Sled test	ΔV=22km/h	4kN belt+AB	4
23AB4R8R	Sled test	ΔV=23km/h	4kN belt+AB	8
25AB4R8R	Sled test	ΔV=25km/h	4kN belt+AB	11
30AB4R8R	Sled test	ΔV=30km/h	4kN belt+AB	12
20FD6R8R	Sled test	ΔV=20km/h	6kN belt only	2
25FD6R8R	Sled test	ΔV=25km/h	6kN belt only	5
28FD6R8R	Sled test	ΔV=28km/h	6kN belt only	5
30FD6R8R	Sled test	ΔV=30km/h	6kN belt only	7
30AB0R8R	Sled test	ΔV=30km/h	AB only, Δp*, m(t)**	1
40AB0R8R	Sled test	ΔV=40km/h	AB only, Δp, m(t)	1
40AB488R	Sled test	ΔV=40km/h	AB only, 1.07Δp, m(t)	1
40AB508R	Sled test	ΔV=40km/h	AB only, 1.11Δp, m(t)	5
40AB528R	Sled test	ΔV=40km/h	AB only, 1.15Δp, m(t)	7
40AB3R8R	Sled test	ΔV=40km/h	AB only, 1.22 Δp, m(t)	8
40AB1R8R	Sled test	ΔV=40km/h	AB only, 1.44Δp, m(t)	11
F29STR8R	Impactor	Vimpact=2.9m/s	15cm&23.4kg disc	0
F34STR8R	Impactor	Vimpact=3.4m/s	15cm&23.4kg disc	4
F43STR8R	Impactor	Vimpact=4.3m/s	15cm&23.4kg disc	6
F47STR8R	Impactor	Vimpact=4.7m/s	15cm&23.4kg disc	8
F50STR8R	Impactor	Vimpact=5.0m/s	15cm&23.4kg disc	8
OPM12R8R	Static airbag	D AB/PMHS=128mm	Unfolded AB	8
OPM15R8R	Static airbag	D AB/PMHS=158mm	Unfolded AB	6
OPM17R8R	Static airbag	D AB/PMHS=178mm	Unfolded AB	4
* Δp=differential pressure for venting; ** m(t)=mass flow law				

Table 3. Simulation matrix performed with plastic strain threshold of 2.4%

Plastic strain = 2.4%				
Model name	Test config	Severity	Loading type	NFR
30AB4R8Q	Sled test	ΔV=30km/h	4kN belt+AB	2
40AB4R8Q	Sled test	ΔV=40km/h	4kN belt+AB	3
45AB4R8Q	Sled test	ΔV=45km/h	4kN belt+AB	3
47AB4R8Q	Sled test	ΔV=47km/h	4kN belt+AB	8
50AB4R8Q	Sled test	ΔV=50km/h	4kN belt+AB	9
60AB4R8Q	Sled test	ΔV=60km/h	4kN belt+AB	10
30FD6R8Q	Sled test	ΔV=30km/h	6kN belt only	2
40FD6R8Q	Sled test	ΔV=40km/h	6kN belt only	3
45FD6R8Q	Sled test	ΔV=45km/h	6kN belt only	5
50FD6R8Q	Sled test	ΔV=50km/h	6kN belt only	8
40AB0R8Q	Sled test	ΔV=40km/h	AB only, Δp*, m(t)**	0
40AB3R8Q	Sled test	ΔV=40km/h	AB only, 1.44Δp, m(t)	0
43AB3R8Q	Sled test	ΔV=43km/h	AB only, 1.44Δp, m(t)	4
45AB3R8Q	Sled test	ΔV=45km/h	AB only, 1.44Δp, m(t)	7
50AB1R8Q	Sled test	ΔV=50km/h	AB only, 1.44Δp, 1.3m(t)	9
50AB2R8Q	Sled test	ΔV=50km/h	AB only, 1.89Δp, 1.6m(t)	12
F34STR8Q	Impactor	Vimpact=3.4m/s	15cm&23.4kg disc	0
F43STR8Q	Impactor	Vimpact=4.3m/s	15cm&23.4kg disc	4
F47STR8Q	Impactor	Vimpact=4.7m/s	15cm&23.4kg disc	4
F50STR8Q	Impactor	Vimpact=5.0m/s	15cm&23.4kg disc	6
F53STR8Q	Impactor	Vimpact=5.3m/s	15cm&23.4kg disc	7
F56STR8Q	Impactor	Vimpact=5.6m/s	15cm&23.4kg disc	8
F59STR8Q	Impactor	Vimpact=5.9m/s	15cm&23.4kg disc	8
OPM12R8Q	Static airbag	D AB/PMHS=128mm	Unfolded AB	4
OPM15R8Q	Static airbag	D AB/PMHS=158mm	Unfolded AB	2
OPM17R8Q	Static airbag	D AB/PMHS=178mm	Unfolded AB	0
* Δp=differential pressure for venting; ** m(t)=mass flow law				

2.4.3 Identification of a global injury criterion

In order to examine whether an injury criterion is loading type-dependent, we are going to use a concept named “injury curve”. An injury curve is defined as the relationship between injury outcome and injury predicator. Regarding rib fractures, it is the number of fractured ribs that is used to express injury outcome. Figure 12 is an example of injury curve for airbag only restraint in dynamic sled environment.

The traditional injury risk curve was also used to evaluate loading dependency of an injury predicator. Since a human body model represents a single subject (there is no individual dispersion), the resulting risk curve presents always a vertical slope which separates injury area from non-injury area. The injury risk is either 0% or 100%, and there is no intermediate risk level. Figure 13 is an example of risk curve.

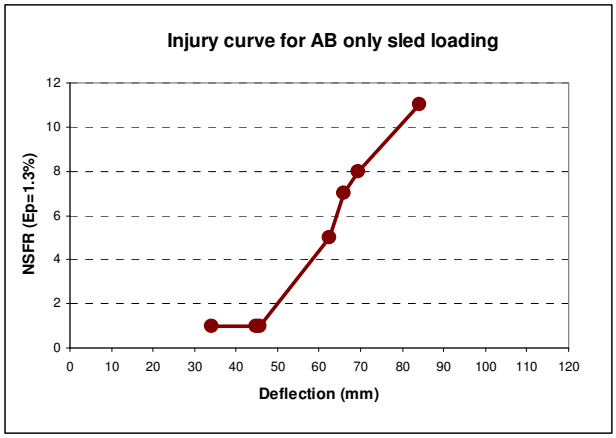

Figure 12. Example of injury curve for airbag only restraint in dynamic sled environment.

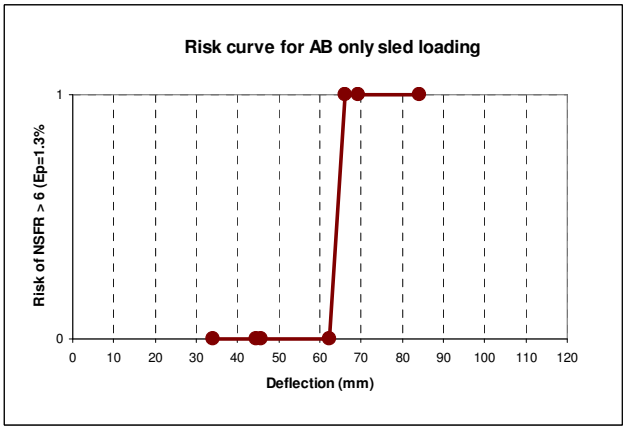

Figure 13. Example of risk curve for airbag only restraint in dynamic sled environment.

2.4.3.1 Sternal deflection

Figure 14 shows injury curves and risk curves established based on these simulations in terms of sternal deflection (X-component of the mid-sternum displacement relative to the spine in A-P direction) for a fragile subject. It can be observed that the injury curve and the risk curve vary from one loading type to another, the 6kN belt loading presenting the most

notable difference. The same observation can be made for a stronger subject (Figure 15). Based on these observations, it can be concluded that the sternal deflection is a loading-type dependent metric.

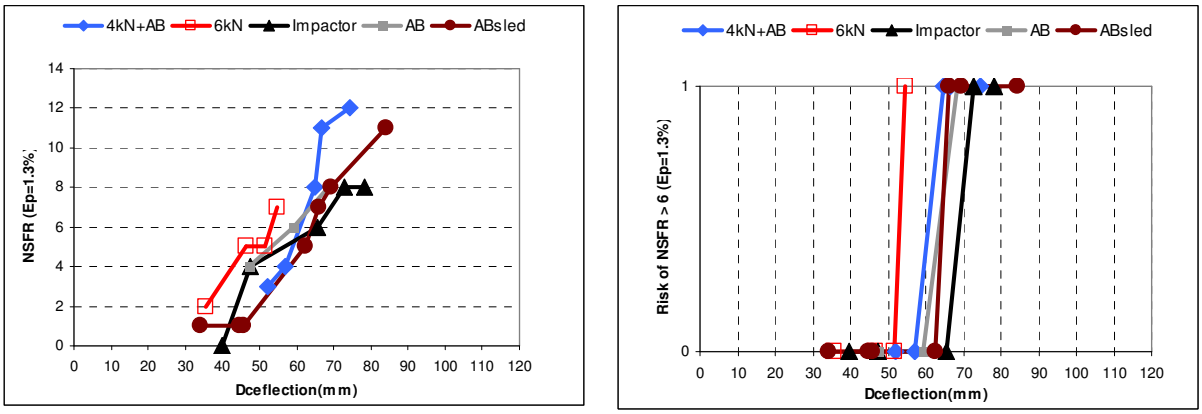

Figure 14. Injury curves (left) and risk curves of NFR>6 (right) with sternal deflection as injury criterion. Plastic strain failure threshold was fixed at 1.3%, representing a fragile subject.

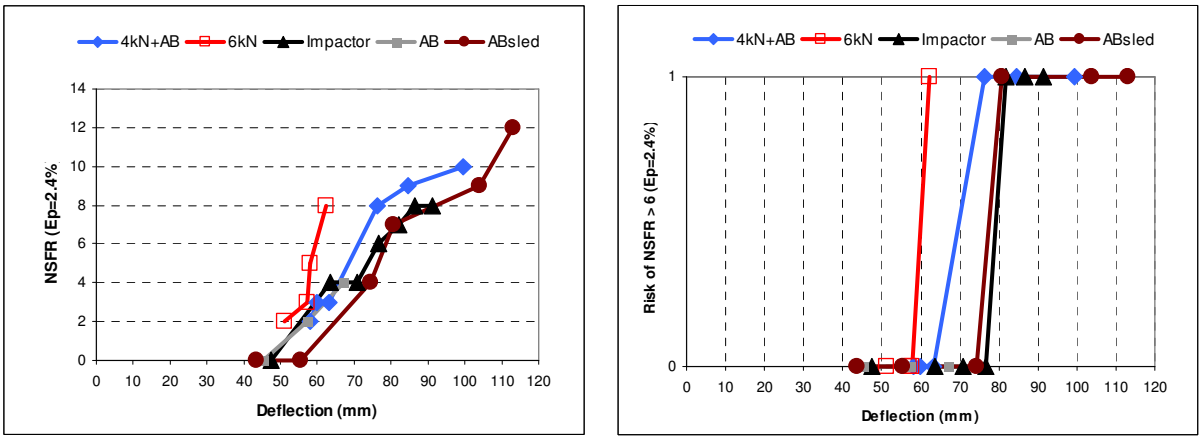

Figure 15. Injury curves (left) and risk curves of NFR>6 (right) with sternal deflection as injury criterion. Plastic strain failure threshold was fixed at 2.4%, representing a stronger subject.

2.4.3.2 Combined deflection – a new injury criterion candidate

Simulations with HUMOS2LAB model allow examining the ribcage deformation shape under different loading types. Figure 16 compares these deformation shapes. It can be observed that important buckling was associated with restraints containing a belt, and in particular with a belt only restraint.

Tests with cadavers also showed this type of thorax deformation shape under belt loading. Shaw et al. (2009) performed cadaver tests under airbag loading and belt loading. Chest bands were used to capture thoracic deformation shape. Figure 17 showed their observation relative to the difference of deformation shape under these two types of loading.

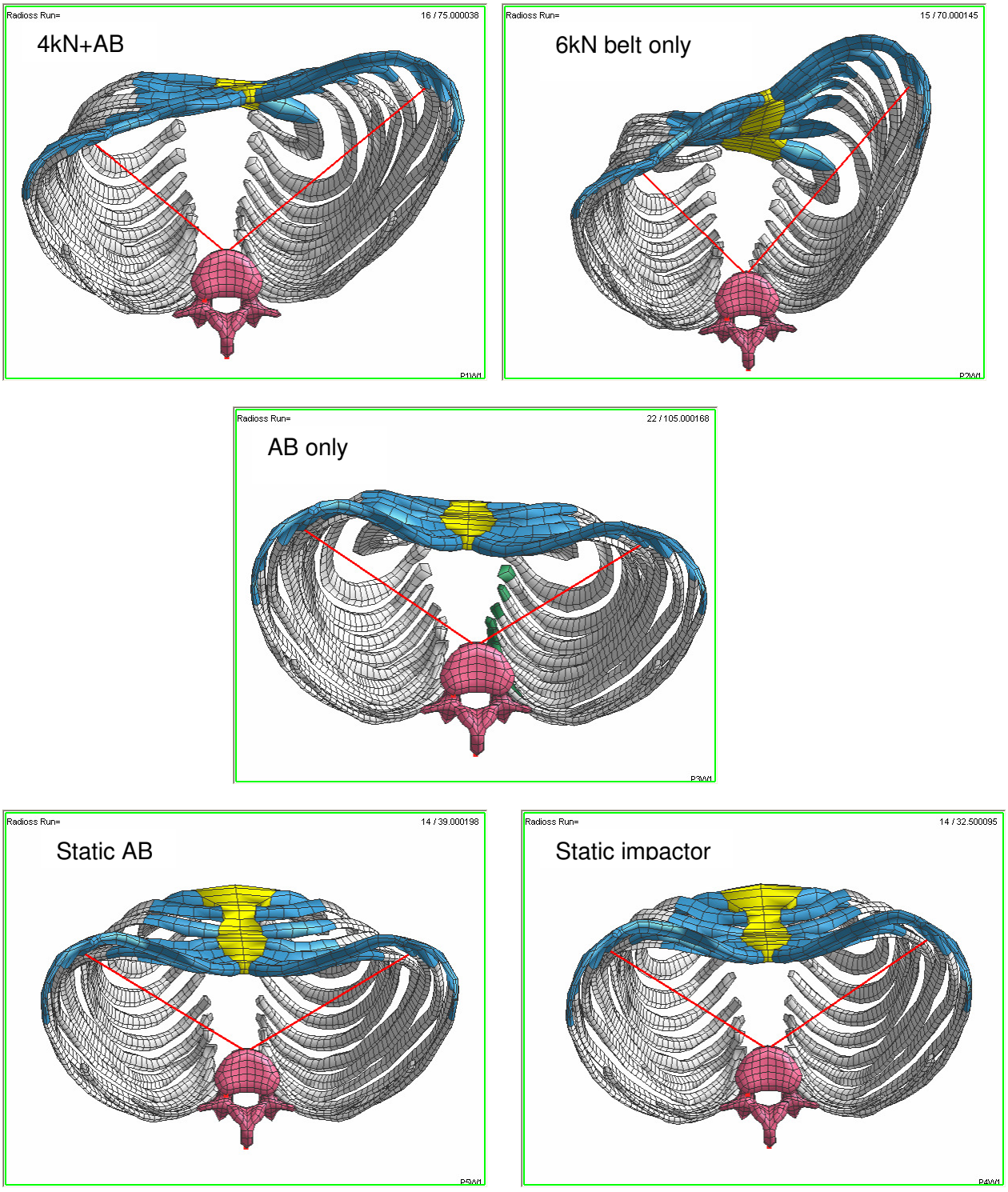

Figure 16. Ribcage deformation shape under different loading types based on the HUMOS2LAB simulations.

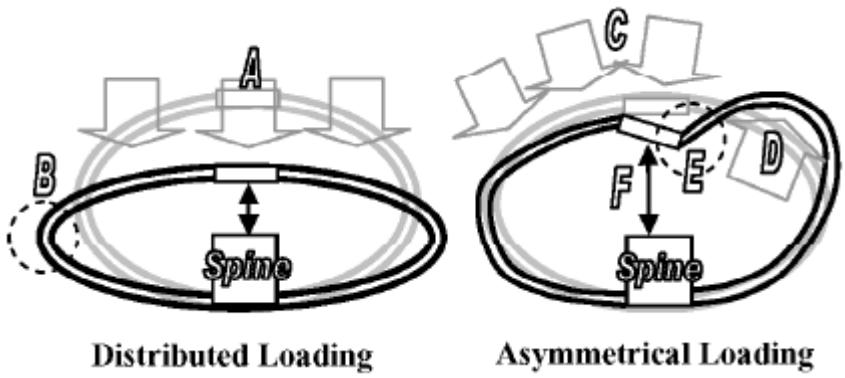

Figure 17. Comparison of ribcage deformation shape between distributed loading and asymmetrical loading based on PMHS tests (Shaw et al. 2009).

Based on these facts, a new injury criterion candidate, named as Combined Deflection and noted as Dc, was defined as below:

$$Dc = Ds + Cf \times \left[(dD - Lc) + \left|(dD - Lc)\right|\right]$$

Where:

Ds represents the sternal deflection (the X-component of the mid-sternum displacement relative to the spine in A-P direction). This deflection reflects the amplitude of the symmetric part of the ribcage deflection.

dD, named as differential deflection, is the difference between right and left deflections of lower ribcage measured at the joint between the 7th ribs and the cartilage (the X-components in A-P direction).

Lc, named as characteristic length, serves to amplify the differentiation effect of the term “dD – Lc” between different types of asymmetric loadings.

Cf, named as contribution factor, is a coefficient to weigh the contribution of the differential deflection to the Dc.

The Dc was calculated for each simulation performed with HUMOS2LAB model, Lc being fixed at 24 mm, and Cf at 0.15. These values were chosen to give the best result in terms of independency for the various loading types. Figure 18 shows injury curves and risk curves corresponding to different loading types for a fragile subject, and Figure 19 shows similar results for a stronger subject.

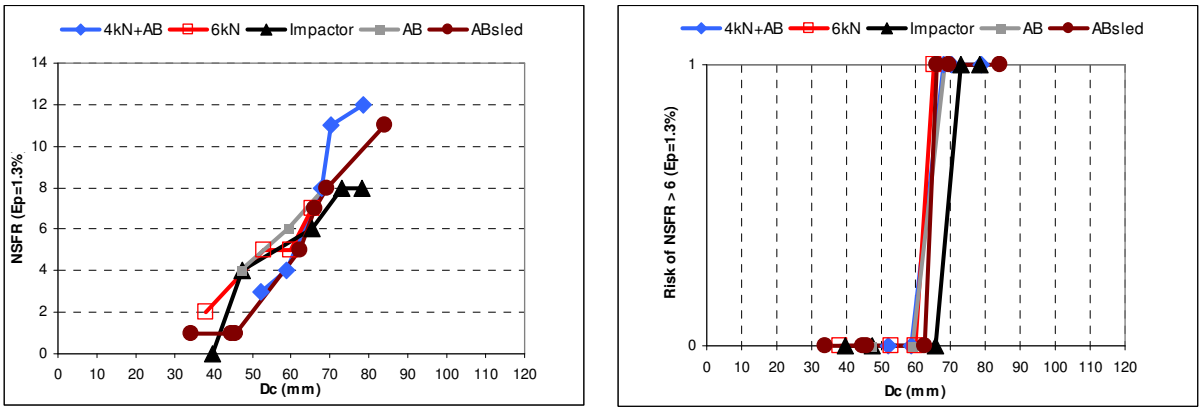

Figure 18. Injury curves (left) and risk curves of NFR > 6 (right) with Dc as injury criterion. Plastic strain failure threshold was fixed at 1.3%, representing a fragile subject.

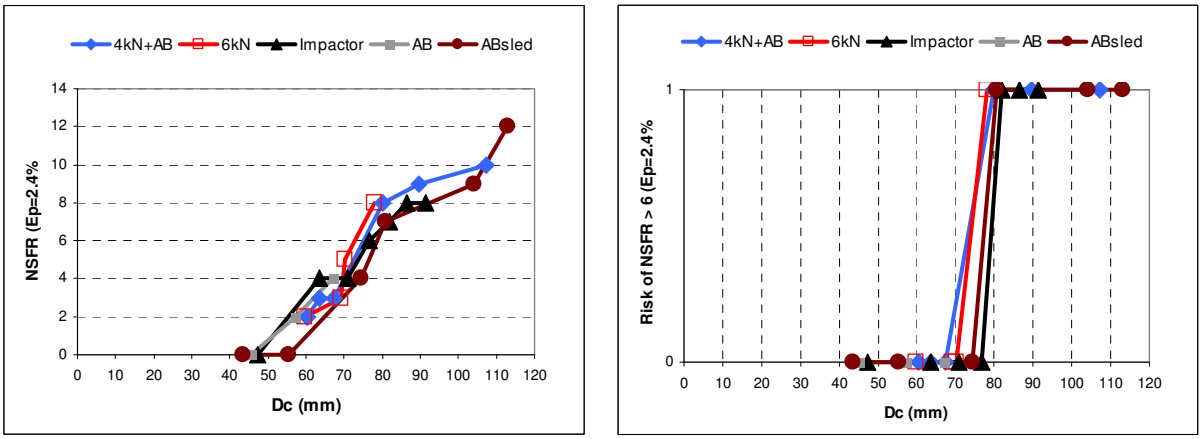

Figure 19. Injury curves (left) and risk curves of NFR > 6 (right) with Dc as injury criterion. Plastic strain failure threshold was fixed at 2.4%, representing a stronger subject.

It can be observed that:

- Injury curve does not change significantly from one loading type to another.
- Risk curves of NSFR > 6 are reasonably close, especially when only sled tests are considered.
- Closeness between injury curves, but also between risk curves is much better with combined deflection than with sternal deflection.
- Above observations are true both for a fragile subject (strain threshold at 1.3%) and also for a stronger subject (strain threshold at 2.4%).

2.5 A strain-based injury criterion - NFR

In Chapter 3, it was suggested that rib fractures can be explained by excessive strain level and that the bending is the main component leading to high strain level. This mechanism of rib fractures suggests that a strain (curvature)-based injury criterion is possible to evaluate rib fracture risk.

A first idea may be to use the maximum peak strain to predict rib fracture risk. However, based on our simulations, we found that the maximum peak strain of ribs does not correlate with the number of fractured ribs. Following is an example to illustrate this phenomenon.

First, let's compare two simulations of sled tests, performed under identical crash conditions (a 50km/h 0° frontal sled test): Simulation A corresponding to a 6kN shoulder load limiting belt only restraint, and Simulation B corresponding to a combined restraint with a 4 kN shoulder load limiting belt plus a driver airbag. Figure 20 show rib fractures for Simulation A and Simulation B. Elements in blue colour are those whose plastic strain went beyond the failure threshold fixed at 3%. The maximum peak strain is higher in Simulation A than in Simulation B. We can observe that there are eight fractured ribs in Simulation A and three fractured ribs in Simulation B. So, for the subject with a 3% plastic strain as failure threshold, higher peak strain means also more fractured ribs.

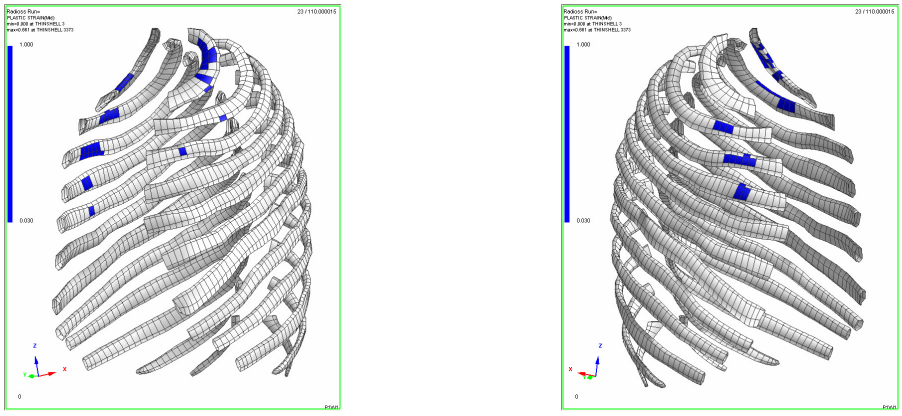

(a) Simulation A: LL6kN belt only

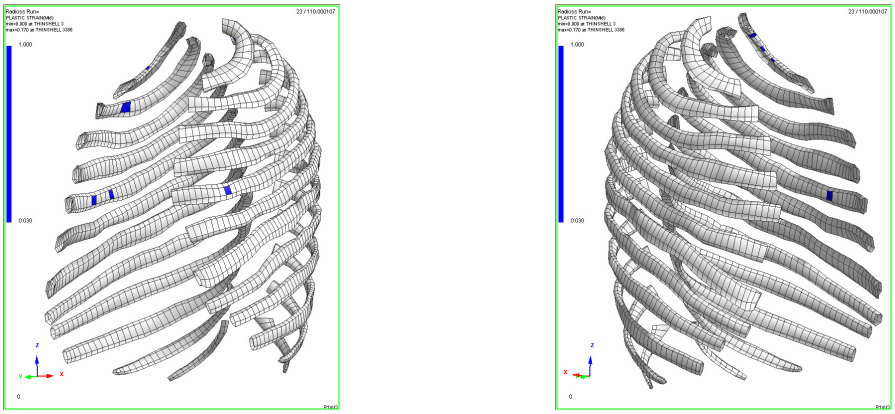

(b) Simulation B: LL4kN+AB

Figure 20. Rib fractures (blue elements) with plastic failure strain at 3%: (a) corresponding to a 6kN shoulder load limiter belt only restraint, and (b) corresponding to a 4kN shoulder load limiter belt plus airbag restraint.

Now let's examine the same simulations but with a more fragile subject (the failure strain fixed at 1.8%). The maximum peak strain is higher in Simulation A than in Simulation B. We can observe that there are eight fractured ribs in Simulation A and twelve fractured ribs in Simulation B. So, for the subject with a 1.8% plastic strain as failure threshold, higher peak strain does not mean more fractured ribs.

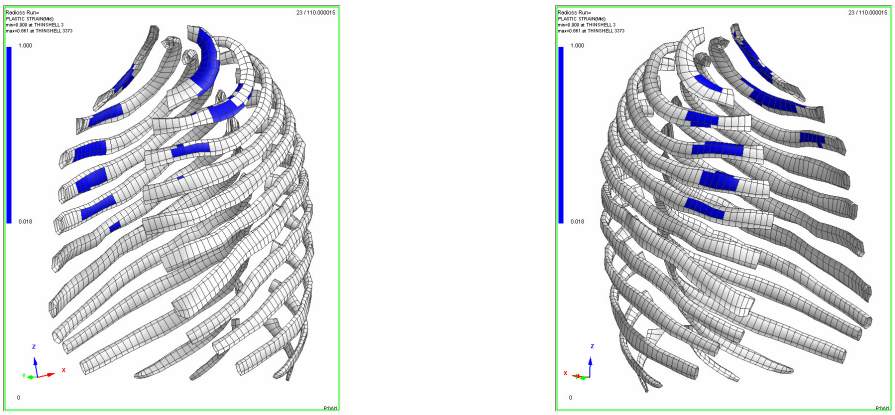

(a) Simulation A: LL6kN belt only

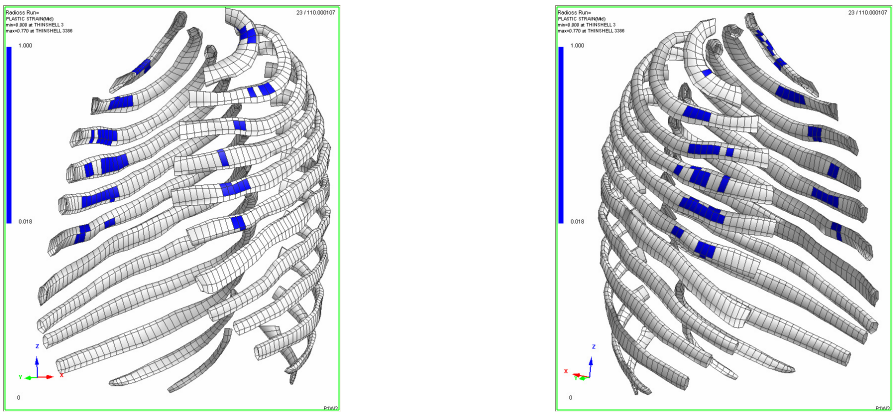

(b) Simulation B: LL4kN+AB

Figure 21. Rib fractures (blue elements) with plastic failure strain at 1.8%: (a) corresponding to a 6kN shoulder load limiter belt only restraint, and (b) corresponding to a 4kN shoulder load limiter belt plus airbag restraint.

Based on above elements, we propose to use the number of fractured ribs (NFR) as a global injury criterion. On the one hand, this number intrinsically reflects the injury level of ribs, and on the other hand, it can be determined by strain measurement of each rib. However, a mechanical dummy does not mimic rib fractures. Besides, a mechanical dummy, as THOR and H-III, do not have the same number of ribs as the human. So one may wonder how it is possible to apply such a criterion on a dummy.

Figure 22 illustrates a possible approach to use this criterion. The key point is to determine, for a given dummy, a strain threshold. For each rib of the dummy, once its maximal peak strain reaches the threshold, the rib will be considered as fractured. In this way, we can determine the number of fractured ribs for the dummy in question for each test. But what is the best way to determine the strain threshold? To do this, a three-step approach can be used. First, PMHS-dummy matched tests should be gathered, where we know rib fracture

outcome of all PMHS tests, and where the strain distribution of each rib is measured. Then, the NFR-PMHS should be plotted versus the NFR-dummy determined by supposing a strain failure threshold. Finally, we should vary this strain failure threshold until the best correlation is founded. This strain threshold will be the threshold for this specific dummy. For another dummy, we can apply the same method to identify its proper strain threshold.

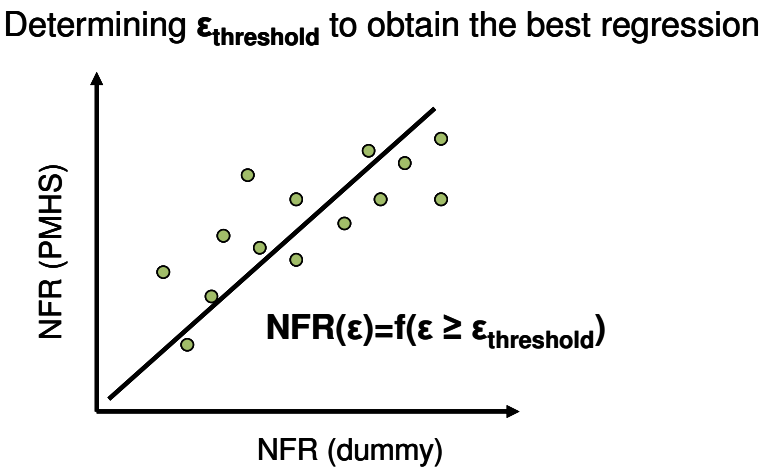

Figure 22. Scheme of a possible approach to apply the NFR as an injury criterion to dummies.

Once the strain threshold determined, the NFR can be measured easily and becomes an injury criterion just as sternal deflection. It can be used to discriminate two restraints as showed in Figure 23a, or to evaluate the injury risk by constructing risk curves (Figure 23b). For example, a NFR of 1 may indicate that the risk of AIS>=3 is 20%. A NFR of 4 may indicate that the risk of AIS>=3 is 50%. However, it is important to keep in mind that NFR(dummy) is equivalent to the number of ribs exceeding the strain threshold, which will be lower for the dummy than the PMHS because the dummy ribs won't fail and cause other ribs to be subjected to greater strain. Furthermore, it should be remembered that current THOR dummy has sevens ribs while human has 12. So, NFR(dummy) should be considered as an global indicator reflecting the severity of ribcage deformation.

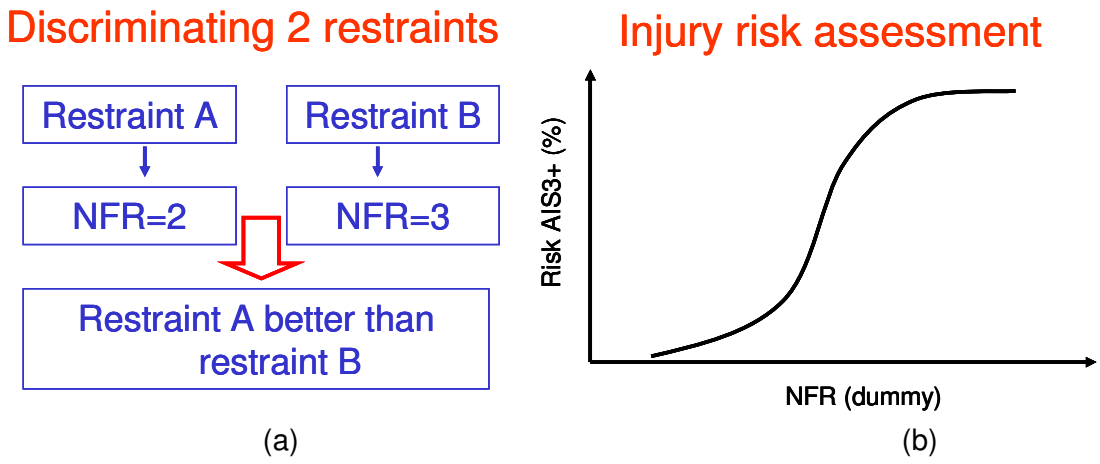

Figure 23. Scheme illustrating how the NFR can be used to discriminate different restraints (a) and to assess injury risk (b).

In order for the NFR to work on a mechanical dummy, a reasonable correlation between the NFR-PMHS and the NFR-Dummy should exist. This probably urges that the dummy should be able to capture ribcage strain distribution in a similar way than human bodies. And this similitude should be true for different types of loading and its tendency should follow the same trend than human bodies versus impact severity. This implies a large amount of PMHS tests duplication with the dummy equipped with strain gauges. But for a feasibility study, a demonstrator with a dummy model may be efficient. It is sufficient to duplicate simulation matrix, presented above for the HUMOS2LAB model, with the dummy model.

2.6 Discussion

2.6.1 Further validation of HUMOS2LAB model

As mentioned in Section 2.4.1 “Simulation matrix”, the baseline HUMOS2LAB model was modified to strengthen clavicle-ribs 1 complex under shoulder belt loading. It was with this modified HUMOS2LAB model that simulation matrix was carried out. We have not performed a new round of validation for this modified version. On one hand, we did not expect that this local modification significantly alters the appropriateness of the model to represent the thorax; on the other hand, carrying a new round validation would ask more resources and delay the core activities of task 2.3: identifying injury mechanism and relevant global injury criteria. However, in order to consolidate our findings and to gain further confidence in the model when applying to belt loadings (e.g. studies into load limiters settings etc), the modified HUMOS2LAB model was further evaluated by using additional experimental data.

2.6.1.1 Validation versus Gold standard PMHS tests

Shaw et al performed (2009) frontal PMHS sled tests under Gold standard configuration. In these tests, main motion of subjects was forward displacement of upper torso restrained by a shoulder belt, while lower limbs and pelvis underwent only very limited motion. Multi point deflections of the thorax, shoulder belt loading and upper torso displacements were recorded. These measurements constitute a good set of data to evaluate the HUMOS2LAB model. Figure 24 compare HUMOS2LAB model response to corridors derived of these experimental tests by Lebarbée et al. in the frame work of an ISO informal group on frontal impact biomechanical requirement. It is to be noted that the right clavicle under the compression of the shoulder belt ruptured in the HUMOS2LAB model. In order to know the influence of clavicle fracture on the thorax response, a simulation with stiffer clavicle material law was run. This simulation did not result in clavicle fracture. Response of both simulations was showed in Figure 24.

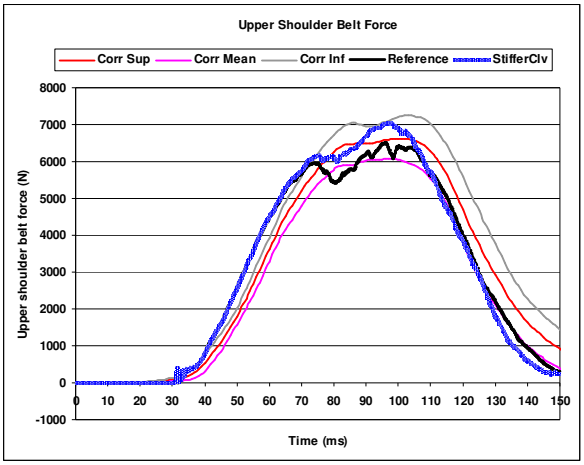

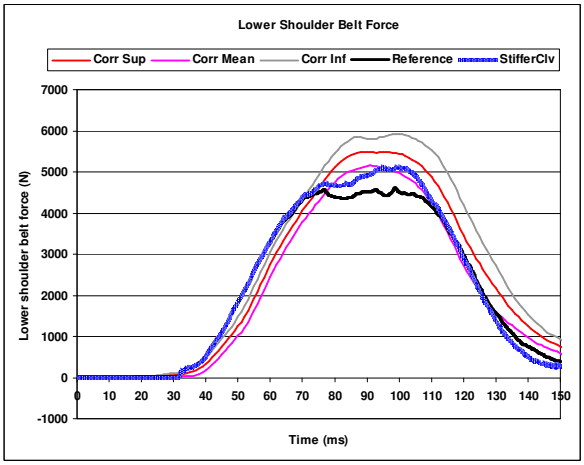

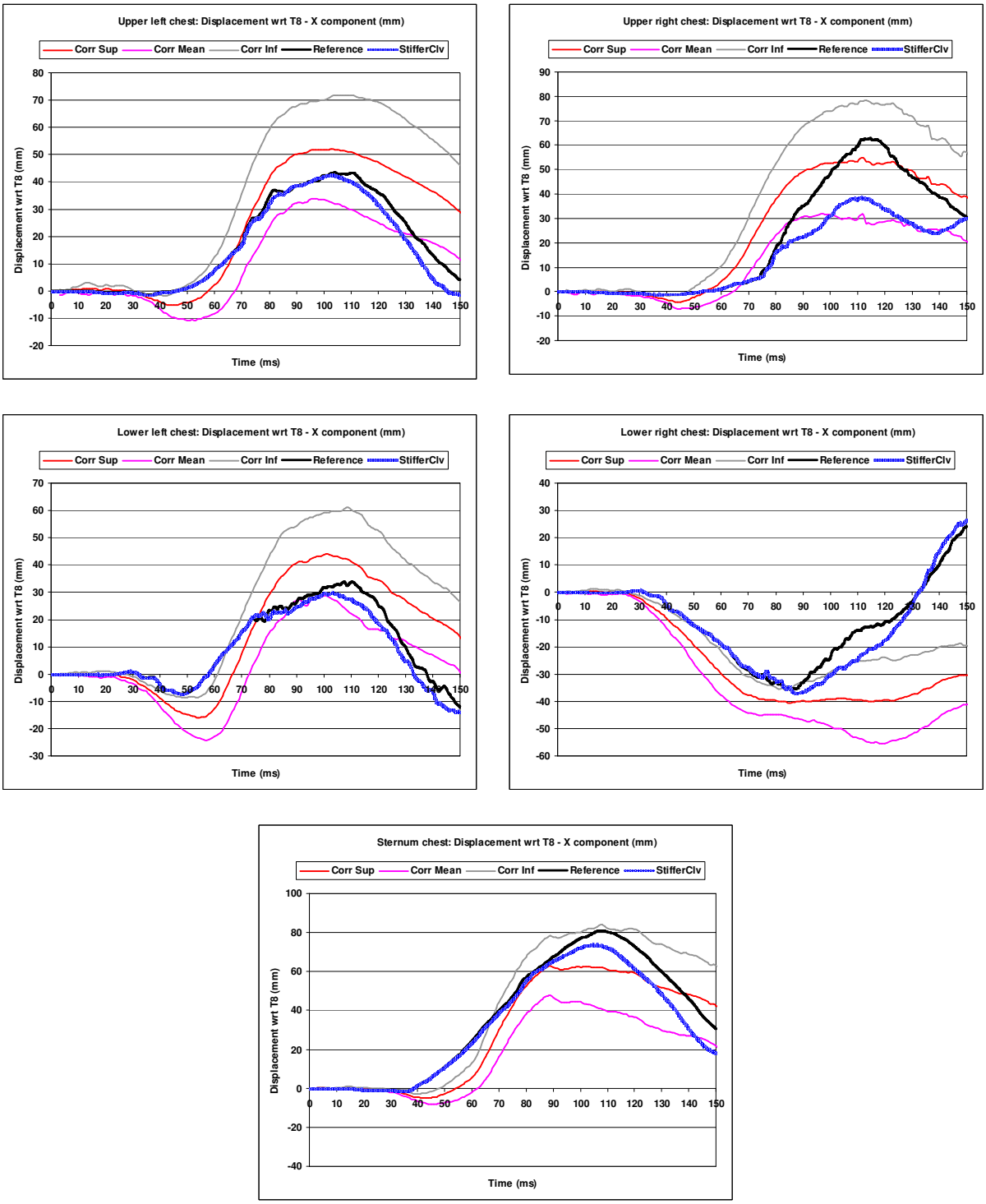

Figure 24. Comparison of HUMOS2LAB model responses to corridors based on sled tests with belt only restrained cadavers performed by Shaw et al. 2009. The corridors were derived by Lebarbée et al in the framework of ISO WG5. Two simulation results correspond to cases with clavicle fracture (Reference) and without clavicle fracture (StifferClv).

It can be observed that model responses match reasonably well with corridor, and buckling out of lower right chest was captured by the model. Clavicle fracture does not change

significantly the validation level of the HUMOS2LAB model: its influence was limited mainly to upper right chest deflection, near right clavicle.

2.6.1.2 Full ribcage strain profile validation versus shoulder belt PMHS tests

CEESAR performed frontal subsystem cadaver tests under shoulder belt restraint. Figure ** illustrates the setup of these tests. The main interest of these tests lies in measurements of rib strain profile of all ribs (apart from floating ribs). This set of data allows evaluating the relevance of a model, far beyond the global response validation. Figures ** shows strain profile comparison between HUMOS2LAB model and experimental measurements of two PMHS tests: ten lines of figures corresponding to ten pairs of ribs, respectively. This comparison was composed of four components:

- Column 1 compares RMS (Root Mean Square of strain, refer to Section 3.2.3 for its definition), which is an indicator of global strain level of the rib considered, and is proportional to deformation energy absorbed by the rib under pure bending conditions.
- Column 2 compares average normalized strain profile of each rib. The strain gauge measurement was normalized by RMS, and was averaged in the time interval between 10% and 99% of RMS max. Signal after rib fracture was not considered.
- Colomn 3 compares normalized strain profile at the instance where RMS max was reached. Signal after rib fracture was not considered.

- Colomn 4 compares strain profile without normalization at the instance where RMS max was reached. Signal after rib fracture was not considered.

Following remarks should be noted when examining this comparison:

- RMS is influenced by anthropometry and mechanical properties of subjects tested. So this comparison should be examined with precaution: there is no normalization of results. This is true also for column 3 and column 4.
- The average normalized strain profile should be privileged: It characterizes the best the strain profile for a given type of loading since results were normalized and averaged.
- Ribs 1 and 10 were only instrumented with few gauges in PMHS tests, so precision should be considered with precaution.
- Positive strain means rib under traction.

It can be observed that, in general, model responses match reasonably well with PMHS data, despite of some important differences in some locations of ribcage.

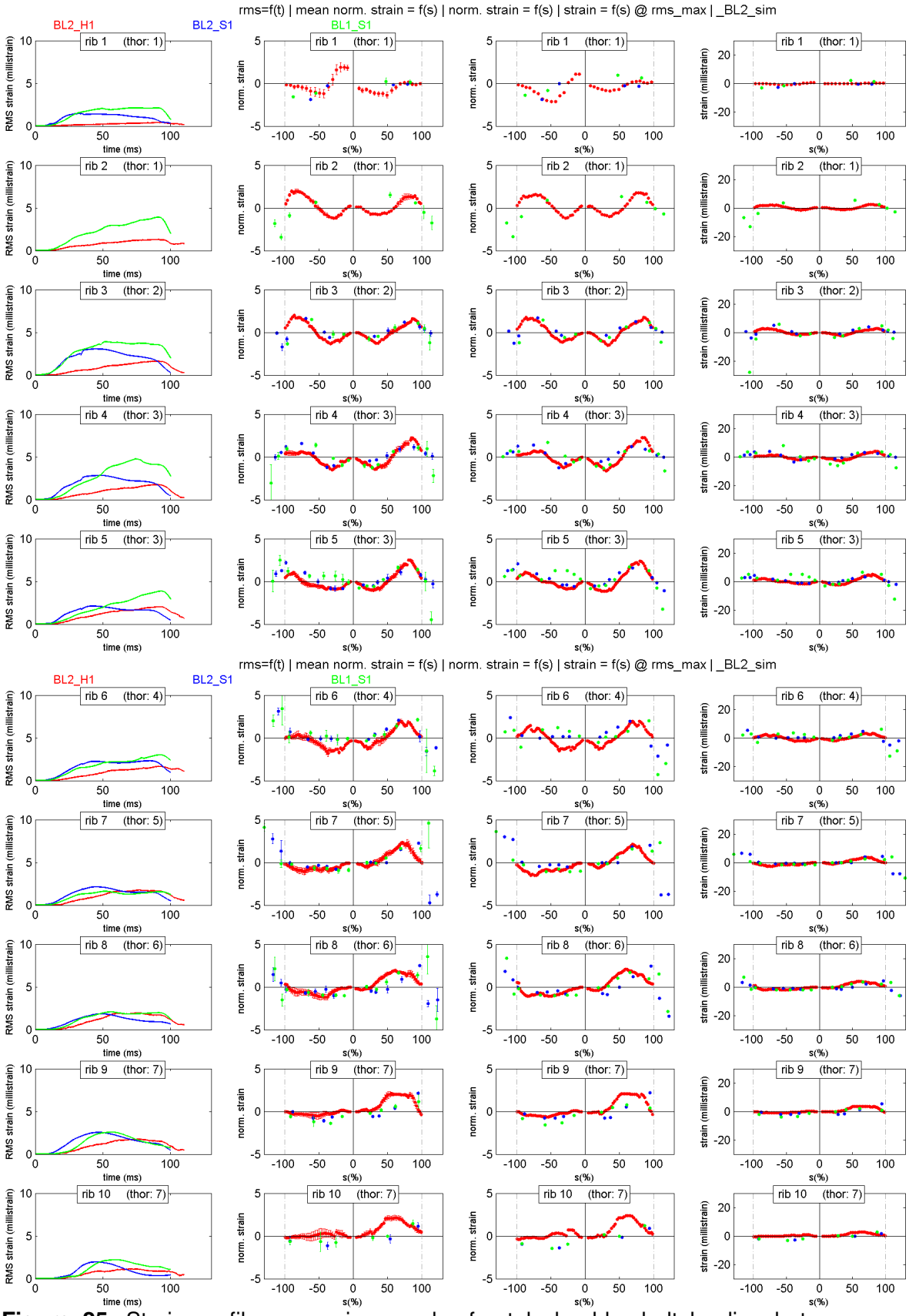

Figure 25. Strain profile comparison under frontal shoulder belt loading between model response (red color) and two PMHS tests.

2.6.1.3 More full ribcage strain profile validation cases

The above approach was extended to more configurations where full ribcage strain profile was measured. These configurations are:

- LAB Impactor tests at 0°
- LAB airbag tests at 0°

Brief description of these tests can be found in Section 2.2 “Validation database”. Figures ** and ** show strain profile comparison between HUMOS2LAB model and experimental measurements. Remarks in the above section relative to strain profile comparison are to be followed.

It can be observed that, in general, model responses match reasonably well with PMHS data, despite of some important differences in some locations of ribcage.

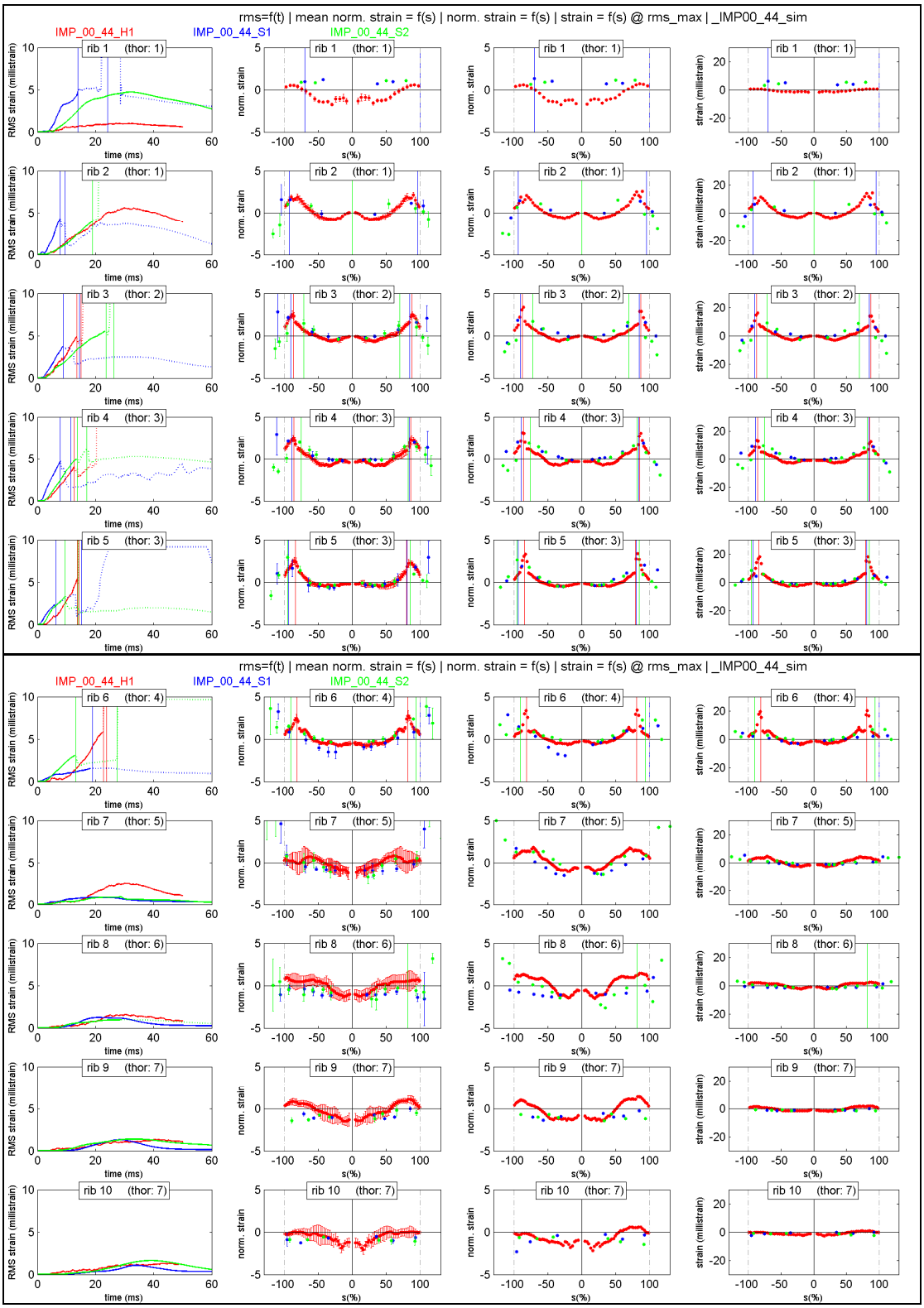

Figure 26: Impactor 0° strain profile comparison between model response (red color) and two PMHS tests. Vertical continue lines mark rib fracture positions. For RMS curves, the part after rib fracture is plotted in dot lines, and were not considered to calculate strain profile.

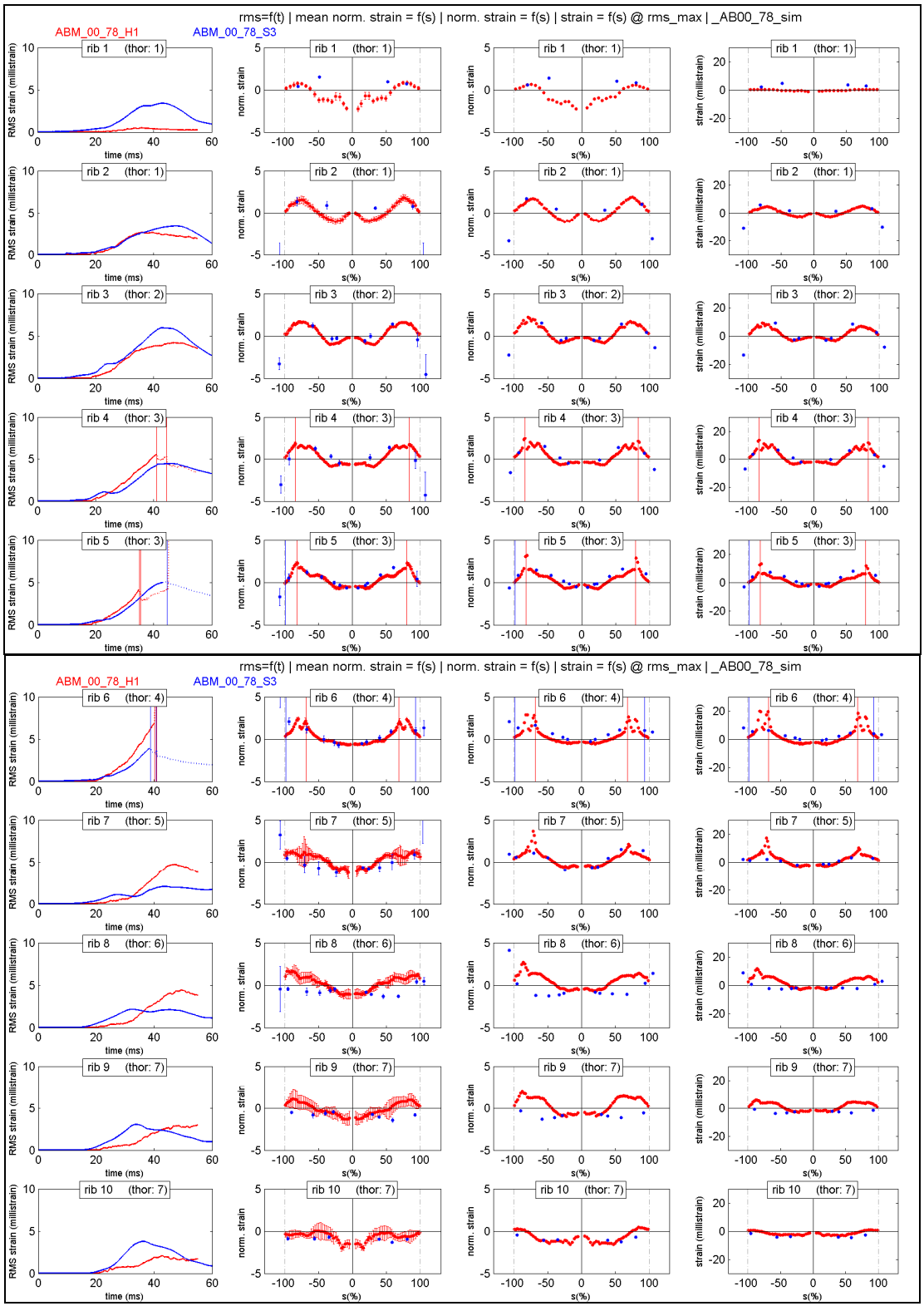

Figure 27: Airbag 0° strain profile comparision between model response (red color) and corresponding PMHS test. Vertical continue lines mark rib fracture positions. For RMS curves, the part after rib fracture is plotted in dot lines, and were not considered to calculate strain profile.

2.6.1.4 General remarks on HUMOS2LAB model validation

The HUMOS2LAB model used in this study was further evaluated in terms of gross motion under Gold standard configuration which is similar to real loading condition in frontal impact. Moreover, full strain profile mapping of rib cage of the model was compared to PMHS data under three types of frontal impact loading: shoulder belt, impactor and airbag. The general convergence observed between the model responses and the experimental data supports a reasonable level of relevance for the model to represent human body responses under impact.

2.6.2 Effects of rib fracture modeling mode

In the HUMOS2LAB model, rib fractures are simulated by deleting shell elements representing cortical bone of ribs, once their plastic failure thresholds are reached. With a mechanical dummy, it is unrealistic to imagine, at the time being, a fracturable ribcage. So, it is natural to ask if the Dc would work on a mechanical dummy. To investigate this question, simulations were run without deleting shell elements that reached the failure threshold. It is easy to understand that such an approach is more dummy-like but neglects in some extent the domino effects of rib fractures.

Restraint-dependency of sternal deflection as an injury criterion can be observed in Figure 28 (for a fragile subject) and Figure 29 (for a stronger subject).

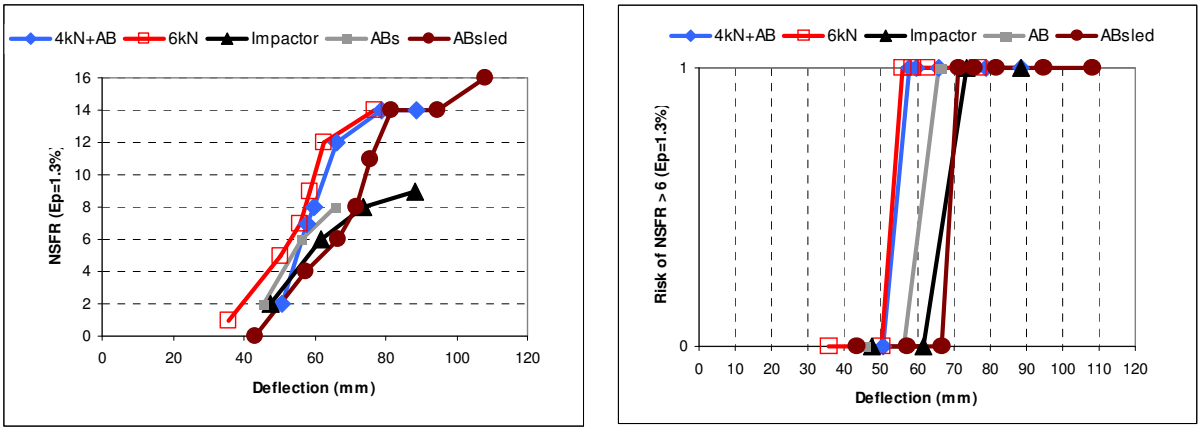

Figure 28: Injury curves (left) and risk curves of NFR>6 (right) with sternal deflection as injury criterion, based on simulation without element deleting. Plastic strain failure threshold was fixed at 1.3%, representing a fragile subject.

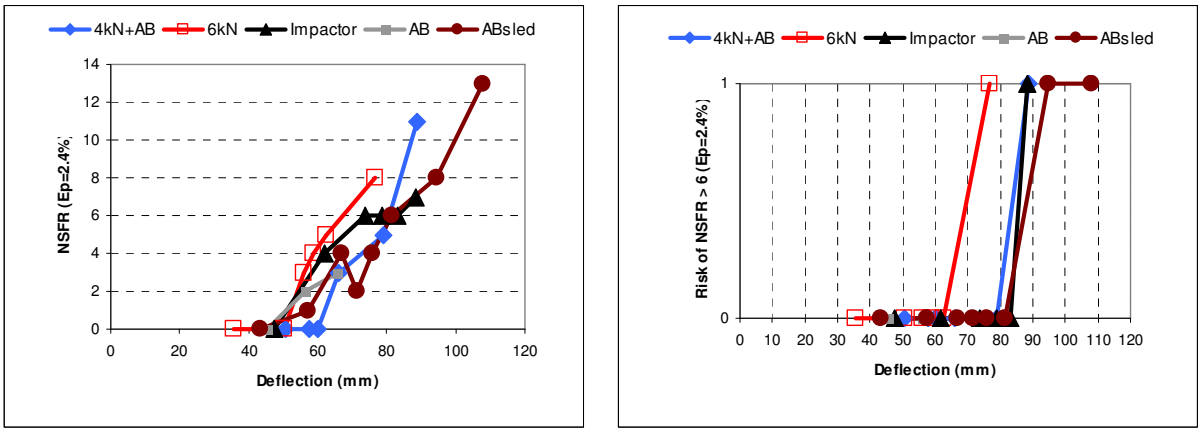

Figure 29: Injury curves (left) and risk curves of NFR>6 (right) with sternal deflection as injury criterion, based on simulation without element deleting. Plastic strain failure threshold was fixed at 2.4%, representing a stronger subject.

Injury curves and risk curves in terms of Dc are given in Figure 30 for a fragile subject and in Figure 31 for a stronger subject. It can be observed that restraint-dependency is considerable for fragile subject, but is not significant for stronger subject, especially when only restraints in dynamic sled environment are taken into account. Although a more significant restraint-dependency was observed with this modified HUMOS2LAB model, the Dc remains globally better than the sternal deflection, and presents only a moderate restraint-dependency when examining the overlook of injury curves corresponding to sled-related loading types.

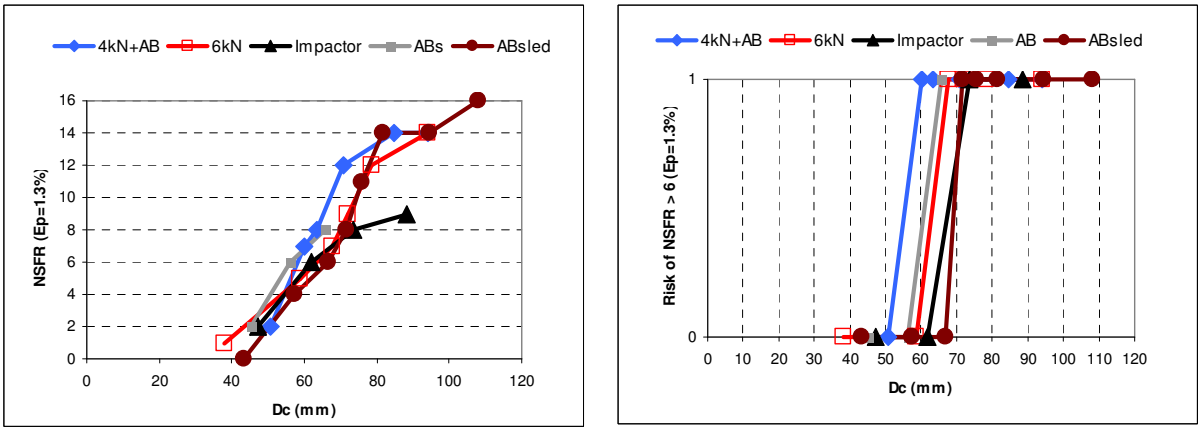

Figure 30 Injury curves (left) and risk curves of NFR>6 (right) with Dc as injury criterion, based on simulation without element deleting. Plastic strain failure threshold was fixed at 1.3%, representing a fragile subject.

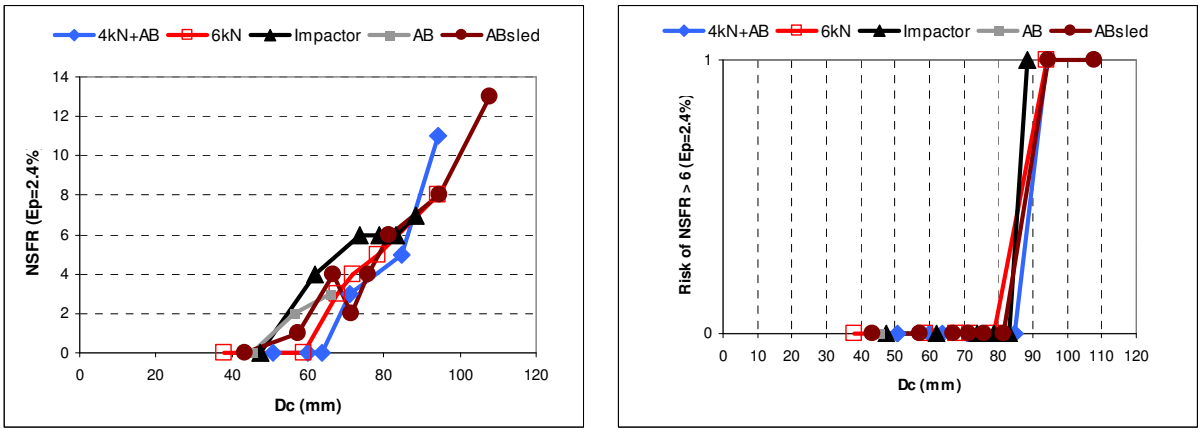

Figure 31 Injury curves (left) and risk curves of NFR>6 (right) with Dc as injury criterion, based on simulation without element deleting. Plastic strain failure threshold was fixed at 2.4%, representing a stronger subject.

2.6.3 Applicability of Dc to dummies

One important question is whether the Dc can be applied to mechanical dummies.

In Figure 33, THOR geometry and HUMOS2LAB geometry are compared. It can be noted that the two lower thoracic deflection measurements correspond well to the deflection measured at Ribs 7 of HUMOS2LAB model. The two upper deflection measurements can be used to approximate the mi-sternum deflection.

Petitjean et al. (2002) performed THOR and H-III sled tests (Figure 32). For the THOR dummy, they found a 47 mm differential deflection for the 6 kN belt only restraint and a 37 mm differential deflection for the 4kN+AB restraints. Even for the H-III dummy, they found also the existence of differential deflection: 15 mm with the 6kN restraint and 8 mm with the 4kN+AB restraint.

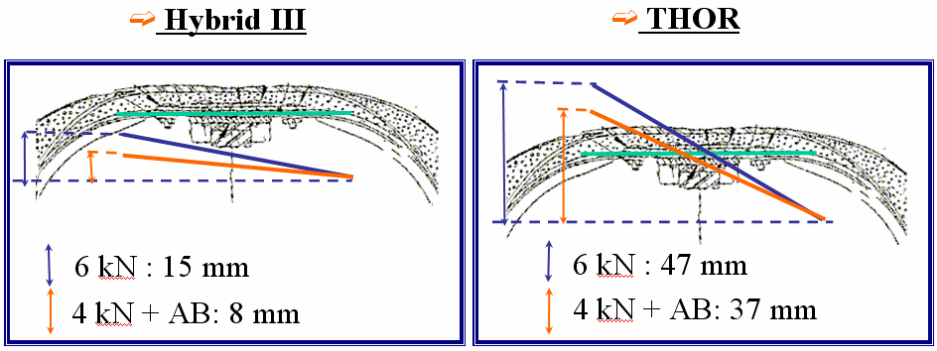

Figure 32: THOR and Hybrid III allow to capture differential deflection at lower thorax level in sled tests with shoulder belt or with combined shoulder plus airbag restraint (Petitjean et al. 2002).

So, by principle, the combined deflection can be calculated with current THOR dummy. However, it is unknown if the criterion measured with the dummy remain valid, i.e. keep being not sensitive to loading types, as it is the case with HUMOS2 LAB model.

To verify this, the most direct method is to assembly matched cadaver-THOR tests and to construct risk curves for different types of loading. However, current available tests with cadavers and THOR are not available to the THORAX project to perform such a work.

An alternative is to use a model of THOR dummy to duplicate simulations performed with HUMOS2LAB. However, such a model is not available for this project.

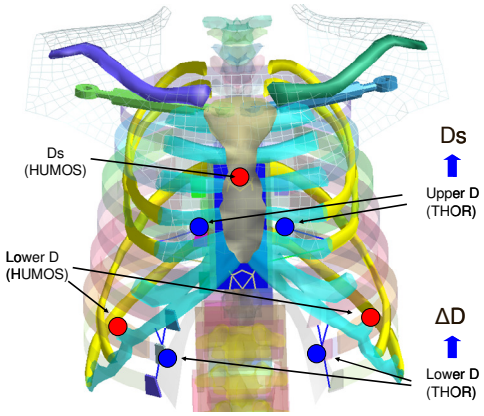

Figure 33: Comparison of the THOR dummy (NHTSA THOR FE model) geometry to the HUMOS2LAB model.

2.6.4 Choices of Lc and Cf

Lc and Cf are two parameters which determine how the differential deflection of lower thorax should contribute to the combined deflection. In the above results and discussions, Lc was fixed at 12 mm and Cf at 0.3 for both fragile and resistant subjects. However, there is no reason that these parameters should be the same between fragile and resistant subjects. By using population-oriented Lc and Cf, the restraint-independency of the Dc can be further improved. Regarding the application of Dc on a mechanical dummy, it is obvious that specific Lc and Cf should be determined.

2.6.5 Limitations of the study

Findings and recommendations reported by the study were based on HBM simulations. They are results of a series of exploring activities, which were made possible by exploiting advantages of HBM approach. Results are more indicative than confirmative. They should be checked in particular with respect to experimental data when they become available.

2.7 Conclusions

A human body model, the HUMOS2LAB, was evaluated with respect to four types of biomechanical data: 1) global force and deflection-based corridors, 2) rib strain profile, 3) spacial repartition of rib fractures and 4) ribcage damage evolution versus loading severity, under different loading types and regarding different impaction direction. The convergence between the model responses and the experimental data supports a reasonable level of relevance for the model to represent human body responses under impact.

A series of simulations using the HUMOS2LAB model were performed, forming a “virtual” PMHS tests database. Five loading types were covered by this database: 3 points shoulder-lap belt restraint, 3 points shoulder-lap belt + airbag restraint, and airbag only restraint in

dynamic sled test environment, airbag and cylinder impactor loading in static environment. For each simulation, rib fractures outcome was established and different metric of ribcage deflection were recorded.

Based on these “virtual” PMHS tests, excessive strain, mainly generated by bending, was identified as mechanism of rib fractures.

It was found that maximum peak strain of ribs does not predict numbers of fractured ribs correctly. It was suggested to directly use the NFR (Numbers of Fractured Ribs) as a global injury criterion. A scheme to use the NFR on a mechanical dummy, where ribs always remain in elastic stat, is proposed. The NFR offers potential to be a universal injury criterion – restraint-independent, impact direction-independent and suitable for evaluating different levels of injuries.

A more usual metric, named as Combined Deflection and noted as Dc, is also proposed. This metric is a global deflection-based predictor for serious injury (more than six fractured ribs). Injury curve and risk curve constructed with this criterion do not vary significantly from one loading type to another. It has potential to candidate as a restraint-independent injury predictor.

Both the above mentioned criteria have been reported to the THORAX team and have been considered in the demonstrator THOR dummy. For the Combined Delfection criterion multiple point chest deflection measurement device (3D-ITRRAC) was developped. For the evaluation of the NFR criterion the chest cage of the demonstrator was instrumented with a suitable numbers of strain gages.

3 Human Body Model studies into stiffness requirements for the rib cage: A parametric study on thoracic response and combined deflection criterion

3.1 Introduction

The current criteria to calculate the risk of thoracic injuries during frontal impacts is based on the central chest deflection (UNECE (2007)). The THOR-NT central chest deflection is calculated from the compact rotary unit (CRUX) measures. The CRUX is designed to sense the three dimensional displacement, relative to the lower part of the spine box, of four distinct points of the ribcage. Assuming that injury can be predicted by local ribcage deflections, or related parameters, it will then be a condition for THOR-NT, or any other anthropometric test device (ATD), to achieve a biofidelic force-deflection thoracic response. The designs of the ATD ribcages were based on results from pendulum tests. These tests reflect the force-deflection behavior under conditions rarely seen in common frontal accidents. Typically the thorax is loaded trough a lap and diagonal seat belt and an airbag.

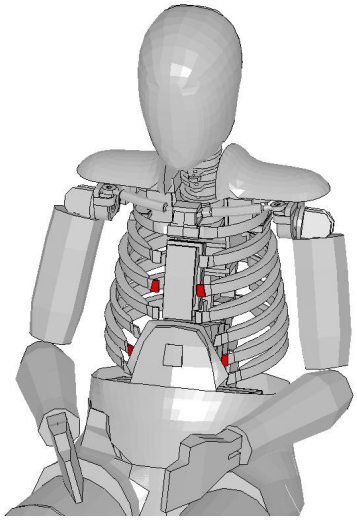

Figure 34. CRUX points on THOR-NT, displayed without jacket

The current report describes the work carried out in the THORAX project and was carried out at Chalmers University of Technology.

3.2 Objectives

The objective of this study was to use a human body model (HBM) to:

- Investigate the influence of the ribcage stiffness on the kinematic response of the ribcage and particularly on the calculated combined deflection criterion (DC),
- Clarify the contribution of the thoracic organs and tissue properties on the overall thoracic response in realistic frontal loading with modern restraint systems, and
- Support the ATD design by providing information on the thoracic stiffness and its sensitivity to modern restraint systems.

To fulfill the objectives the following approach was adopted:

- The HBM used, the Total HUman Model for Safety (THUMS), was modified and validated against three different PMHS tests (Appendix B).
- Then a parametric study on the influence of different ribcage stiffness on the kinematic response of the ribcage was carried out. The different ribcage stiffness values were achieved by modifications on material properties of different thoracic organs and tissues.

The main objective of this parametric study was to gain an understanding of the contribution of different thoracic tissues to the thoracic response to impact. Such new knowledge could be used in the design of new ATD. To address these purposes, the material properties of different tissues were modified in the THUMS. Then, the different THUMS states were tested on the table top and/or the sled test environments.

One more objective was to determine the influence of stiffness distribution on the calculation of the combined deflection criterion.

3.3 Methods

3.3.1 Calculation of effective stiffness and combined deflection criterion

The resultant effective stiffness and the combined deflection components were calculated. The effective stiffness was only calculated for the table top tests, it is defined as the slope of the linear regression of the force – chest deflection curve between 0 and 46 mm. It is expressed in force relative deformation, as expressed as deformation relative initial chest depth (N/%). The initial chest depth of 230 mm were used.

The combined deflection criterion, noted as DC, is defined by Song (2010) as:

$$DC = Ds + Cf \times \left[(dD - Lc) + \left|(dD - Lc)\right|\right] \quad (1)$$

Where:

Ds represents the sternal deflection (the X component of the mid-sternum displacement relative to the vertebrae T8).

dD, named as differential deflection, is the difference between right and left deflections of lower ribcage measured at the joint between the 7th ribs and the cartilage (the X-components relative to L1).

Lc, named as characteristic length, serves to amplify the differentiation effect of the term “dD – LC” between different types of asymmetric loadings.

Cf, named as contribution factor, is a coefficient to weigh the contribution of the differential deflection to the Dc.

At this moment there are not enough simulations to define the DC coefficients applicable to THUMS. Therefore, the HUMOS2LAB coefficients for DC calculation were chosen also for DC calculation using THUMS: Lc=24 mm and Cf=0.15

3.3.2 Modifications to the HBM – Weak and ATD-like states

The states generated by changes on different parameters were divided into two groups. One was for those modifications where the stiffness of individual tissues was reduced in 50%.

This group aimed to find the organs that reduced the ribcage stiffness the most. It is known that THOR has a stiffer response compared to PMHS as described in Shaw et al. (2002), Yaguchi et al. (2008) and Crandall (2008). It is therefore of importance to know which tissues are contributing the most to the ribcage stiffness, both in terms of total stiffness as well as coupling between regions of the ribcage, in THUMS. It is also of interest to know the effect on the model of the modifications introduced on an ATD. That is why the second group included states that made THUMS more ATD like. These groups were defined in order to study the effect on the chest when simplifications to THUMS were introduced. The different states are described on the following two sections:

3.3.2.1 Weak states

WEAK CARTILAGE – The cartilage elastic modulus and yield stress were reduced by 50%. The objective is to investigate the cartilage importance in ribcage coupling. It is also of interest to investigate the effect of a weaker cartilage on the bulging out behavior of THUMS.

WEAK STERNUM – The sternum cortical bone elastic modulus and yield stress were reduced by 50%. The objective is to investigate the sternum importance in ribcage coupling. It is also of interest to investigate the effect of a weaker sternum on the bulging out behavior of THUMS. This bulging out behavior is important for the calculation of the combined deflection criterion since it will influence the differential deflection, as defined in (1).

WEAK INTERCOSTAL MUSCLES – The elastic modulus of the intercostals muscles was reduced by 50%. THOR has no structure resembling the intercostals muscles. Therefore, the stiffness of the intercostals muscles in THUMS was reduced in order to investigate their contribution to ribcage coupling. Complete removal was not performed since the thoracic internal organs present in THUMS would be allowed to flow outside the ribcage in the absence of intercostals muscles.

WEAK COSTOVERTEBRAL LIGAMENTS – The elastic modulus of the trusses representing the costovertebral ligaments was reduced by 50%. This change is intended to determine if the costovertebral ligaments allow larger rib rotations while weak. Larger rib rotations could lead to a larger chest deflection measurement, but without increasing the compression on the ribcage.

WEAK RIBS – The elastic modulus and yield stress of the rib cortical bone was reduced by 50%. Ribs are considered to be the most important load path on the ribcage and it is therefore of interest to quantify their influence on the thoracic stiffness.

3.3.2.2 ATD-like states

STIFFER RIBS – The elastic modulus and yield stress of the rib cortical bone was increased by 50%. THOR's ribs are stiffer than those of humans. The objective of simulating this state is to investigate its effect on chest stiffness and deflection.

SHORTETR CARTILAGE – A shown in Figure 35, THOR ribs end much closer to the sternum than the ribs in THUMS. The rib bones in THUMS, from the 2nd to the 8th, were extended so that they ended at the same distance from the sagittal plane as the ribs in THOR. Cartilage was made proportionally shorter.

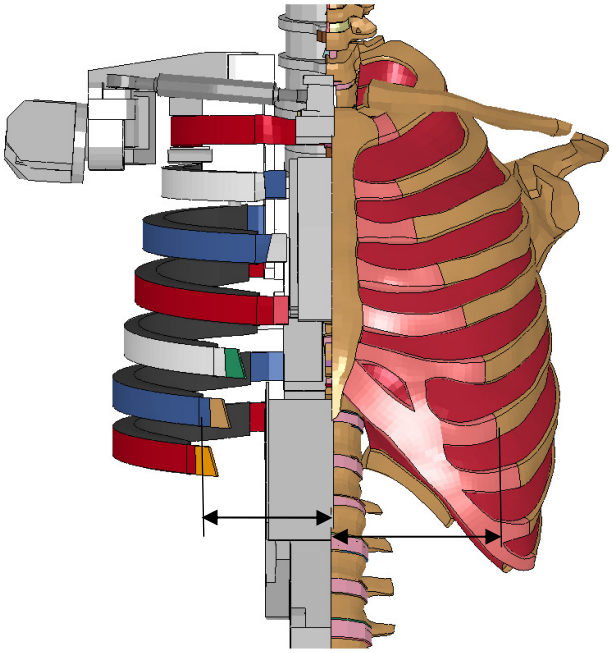

Figure 35. THOR (left) and THUMS (right) ribcage. The bony part of the ribs in THUMS ends further away from the sagittal plane compared to THOR.

DIVIDED STERNUM – The elastic modulus of the first rib cortical bone was increased 100%. The sternum was divided in two parts, as in Figure 36, by reducing the elastic modulus of a row of elements by 90%. These modifications are intended to represent the design of the THOR in this region. THOR's first rib and clavicles are attached to the upper sternum and this assembly is coupled to the mid sternum trough the bib.

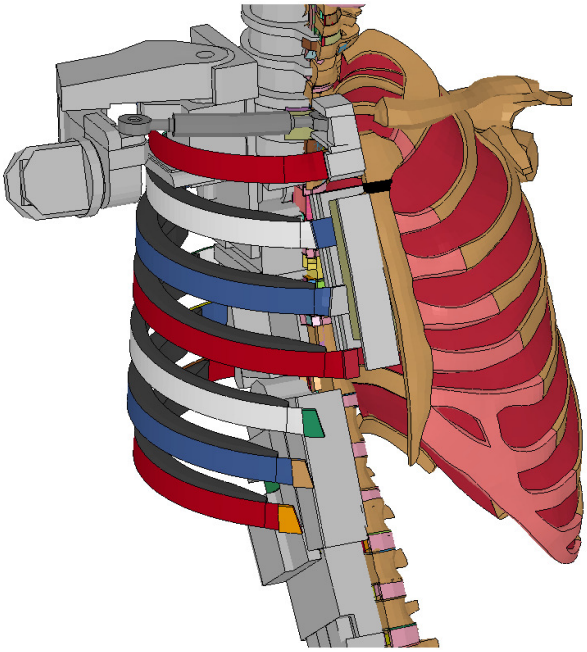

Figure 36. THOR (left) and THUMS (right) ribcage. The thick black line on the sternum indicates the elements that were modified.

80% INTERNAL ORGAN'S MASS ON SPINE: The mass of the thoracic and abdominal internal organs was reduced by approximately 80%. The mass was added to the thoracic and lumbar vertebra instead. The other mechanical properties of the internal organs remained the same, i.e. it contributed to support the rib cage. This has the objective to assess the contribution of the inertial loading of the internal organs on the ribcage deformation.

STIFFER RIBCAGE and NO INTERNAL ORGANS: The internal organs were removed completely and their total mass was added to the spine. To avoid the ribcage from bottoming out, the whole ribcage was made stiffer. The elastic modulus for the cortical rib and sternal bones, and the rib cartilage was increased by 150%. The costovertebral ligaments elastic modulus was increased by 900% to avoid excessive rib rotation.

HORIZONTAL CLAVICLE: The clavicle in THUMS was modified by changing the clavicle position so that the upper face in the clavicle became horizontal and its distal end coincided with the acromion as in '
Figure 37. These changes made the clavicle resemble that of the THOR. The clavicle was modeled as a rigid body. The seat belt was repositioned on the chest in order to fit the new geometry generated by the changes in the clavicle.

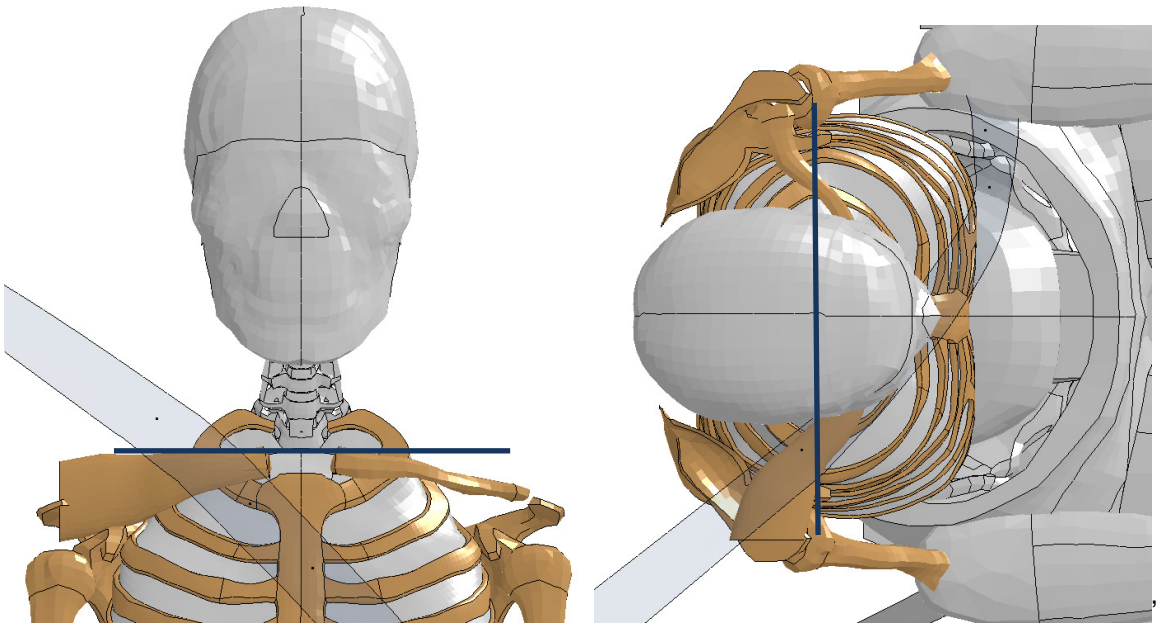

Figure 37. Horizontal clavicle state. The right clavicle in THUMS shows the modified clavicle, while the left corresponds to the original position.

3.4 Results

In this chapter the results for the parametric study are presented. The first section is devoted to the contribution of different tissues on the thoracic effective stiffness. This part of the parametric study was only performed on the table top tests since measuring the force applied on the ribcage during the sled test was not possible. The second section presents the displacements in the sled tests for the different states and the third section presents the combined deflection components and the influence of different tissue properties on these components, both for the table top and the sled tests. A comparison between the sled tests and the table top test when using the simulated belt will also be presented.

3.4.1 Effective Stiffness

The table top set up and the intact state for the thorax were used as a baseline for the stiffness parametric study. These values are summarized in Table 4 andTable 5 for both weak and ATD-like states. The normalized effective stiffness values are also displayed in these tables. The effective stiffness for the intact configuration was considered as the reference value for normalization for each of the four load cases.

When loaded by the hub, the load built up in the chest was much lower than for any other load case. For distributed load the chest responded with a load more than four times as high for given deformation. For the weak states, the state weak ribs in combination with the hub load case produced the lowest effective stiffness whereas the weak sternum state produced the highest when the distributed load was applied.

Table 4. Effective stiffness for different states under the four load cases on the table top test

STATE	Effective stiffness [N/%]			
	HUB	BELT	DOUBLE BELT	DISTRIBUTED
Intact	3670	11554	14041	16457
Weak cartilage	3482	11333	13941	16334
Weak sternum	3535	11228	13973	16525
Weak Intercostals	3223	10760	12942	14662
Weak cv ligaments	3631	11308	14000	16308
Weak ribs	3086	10636	12837	15224
Stiffer ribs	4062	12072	14846	17240
Shorter cartilage	4035	11997	14163	16203
Divided sternum	3682	11380	14035	16491
80% Mass on spine	3374	10818	13009	14830
Stiffer ribcage-no internal organs	4526	12654	15620	16977

Table 5. Normalized effective stiffness for different states under the four load cases on the table top test, the norm is the intact state for the respective load case

STATE	Normalized effective stiffness [%]			
	HUB	BELT	DOUBLE BELT	DISTRIBUTED
Intact	100	100	100	100
Weak cartilage	95	98	99	99
Weak sternum	96	97	100	100
Weak Intercostals	88	93	92	89
Weak cv ligaments	99	98	100	99
Weak ribs	84	92	91	93
Stiffer ribs	111	104	106	105
Shorter cartilage	110	104	101	98
Divided sternum	100	98	100	100
80% Mass on spine	92	94	93	90
Stiffer ribcage-no internal organs	123	110	111	103

Notably, the chest response to hub loading was 1.23 times that of an intact HBM when the internal organs in the thorax were removed and the ribcage made stiffer.

3.4.2 Combined deflection criterion

The present results are reported as defined in Section 3.3.2. The value dD corresponds to the value at the costochondral joints Figure 38. Measurement points for the differential deflection. The yellow markings show the positions used in the estimations of the dD; the rectangle for the CRUX and the yellow circle for the costochondral joints. The black dot indicates the location of the point where sternal deflection was measured.

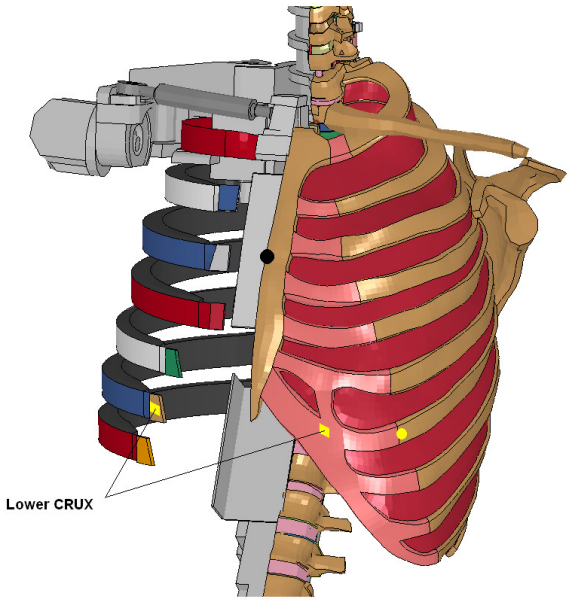

Figure 38. Measurement points for the differential deflection. The yellow markings show the positions used in the estimations of the dD; the rectangle for the CRUX and the yellow circle for the costochondral joints. The black dot indicates the location of the point where sternal deflection was measured.

3.4.2.1 Table top tests

In the following sections, the thoracic response in form of ribcage deflection is presented. All values were measured at the instant when the energy of the state was equal to the energy at 20% chest deflection for the respective INTACT state. All energies were computed as the integral of the table top normal force-chest deflection curve. This allowed comparing the different states to each other under the same load case. In the following four sections, the displacements on the coronal plane and the chest deflection are presented for each load case in the table top tests.

As expected, only the belt load case presented a significant differential deflection. All other load cases produced differential deflections of less than a millimeter. Therefore, the differential deflection was only reported for the belt load case (Table 8). With no differential deflection, the combined deflection criterion will be equal to the sternal deflection.

3.4.2.1.1 Hub

The displacement pattern and compression values are presented on Figure 39 and Figure 40 for the hub load case. The maximum sternal deflection is also reported on Table 6, as well as the normalized value having the INTACT state as reference.

Clearly the maximum compressions occur in the positions lateral of the sternum measurement point. It is also clear that the compressions in the region of the two lower and proximal points are similar to the compression of the sternum. Independent of states, the hub load produces downward displacements of the chest anterior.

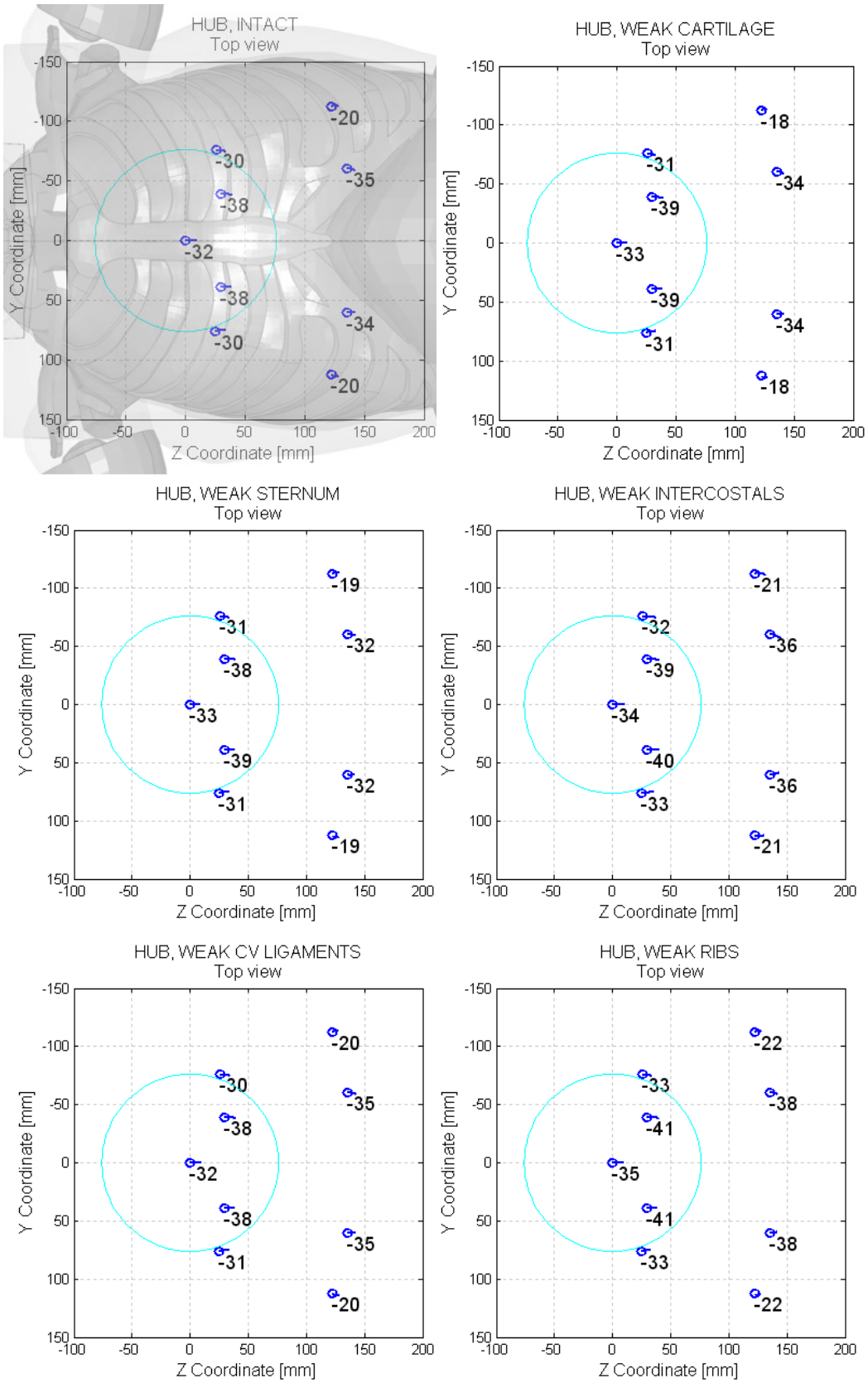

Figure 39. Displacements in the coronal plane and chest compression, numbers provided in the plots, for the HUB load case and weak states.

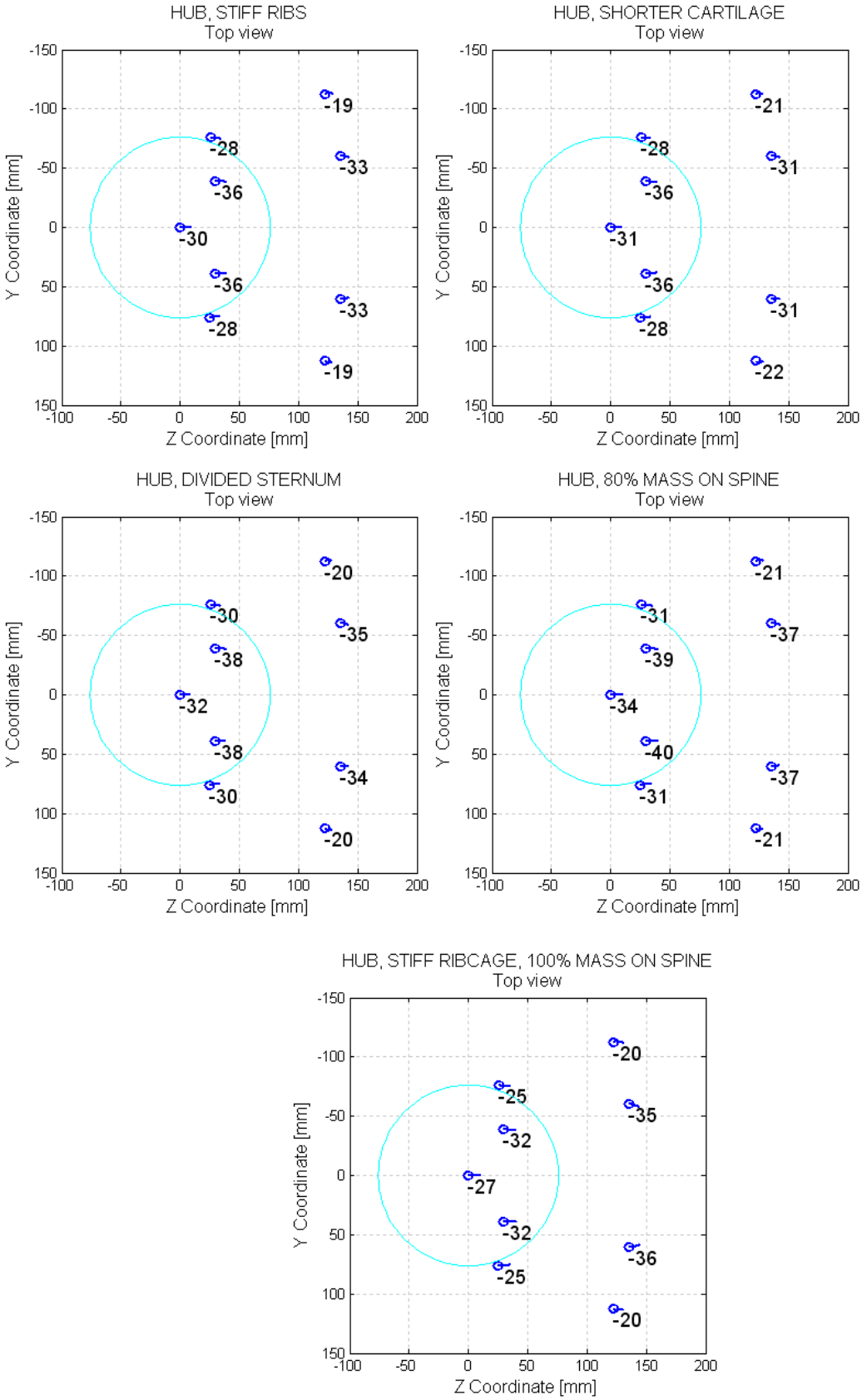

Figure 40. Coronal pane displacements and chest compression, HUB load, ATD-like states

Table 6. Sternal deflection for the hub load case

HUB, STATE	Sternal deflection [mm]	Normalized value wrt the INTACT state [%]
Intact	32	100
Weak cartilage	33	103
Weak sternum	33	103
Weak Intercostals	34	106
Weak cv ligaments	32	100
Weak ribs	35	109
Stiffer ribs	30	94
Shorter cartilage	31	97
Divided sternum	32	100
80% Mass on spine	34	106
Stiffer ribcage-no internal organs	27	84

3.4.2.1.2 Single belt

The displacement pattern and compression values are presented in Figure 41 and Figure 42 for the single belt load case. The maximum sternal deflection is also reported on Table 7, as well as the normalized value having the INTACT state as reference. On Table 8, the differential deflection is presented and the combined deflection is presented on

Table 9.

For all week-states, peak compressions of the chest were in a position lateral of the belt. For the ATD-states, peak compressions of the chest occurred underneath the belt when the cartilage was made shorter.

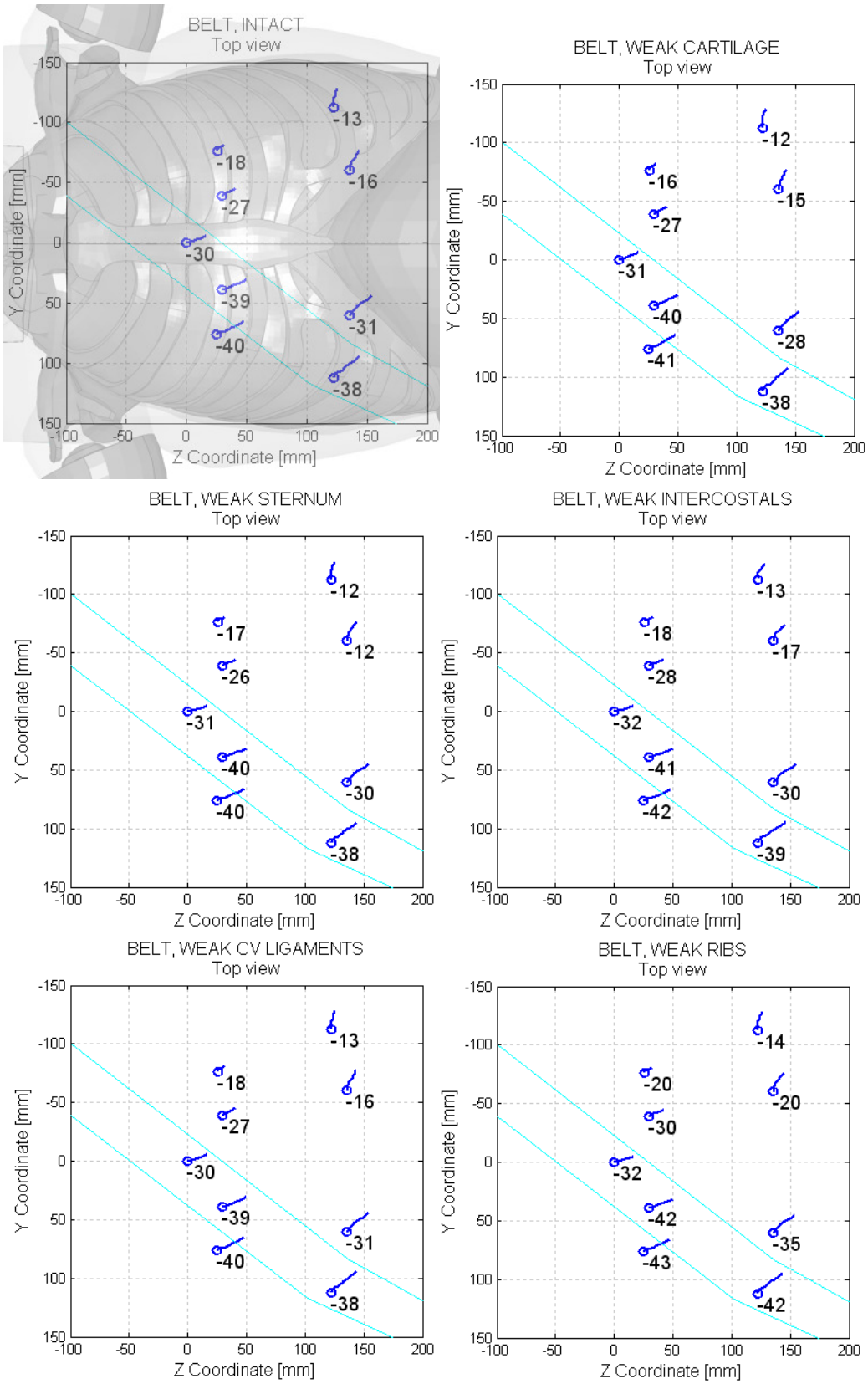

Figure 41. Displacements in the coronal plane and chest compression for the BELT load case and weak states

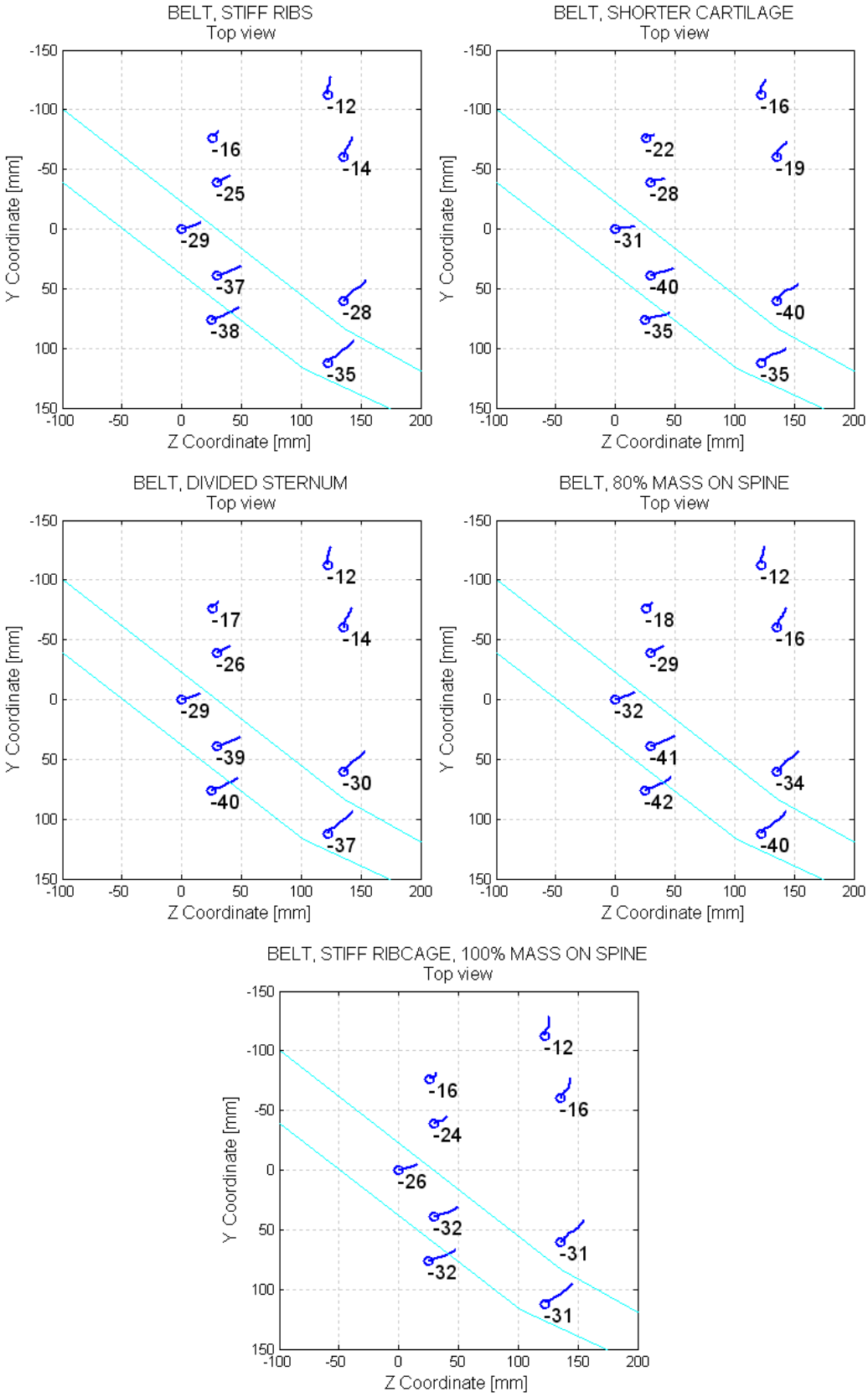

Figure 42. Displacements in the coronal plane and chest compression for the BELT load case and ATD-like states

Table 7. Sternal deflection (DS) under the BELT load case

BELT, STATE	Sternal deflection [mm]	Normalized value wrt the INTACT state [%]
Intact	30	100
Weak cartilage	31	103
Weak sternum	31	103
Weak Intercostals	32	107
Weak cv ligaments	30	100
Weak ribs	32	107
Stiffer ribs	29	97
Shorter cartilage	31	103
Divided sternum	29	97
80% Mass on spine	32	107
Stiffer ribcage-no internal organs	26	87

Table 8. Differential deflection (dD) calculated at the costochondral joints (CC)

BELT, STATE	Differential deflection [mm]	Normalized value wrt the INTACT state [%]
Intact	25	100
Weak cartilage	27	108
Weak sternum	26	104
Weak Intercostals	27	108
Weak cv ligaments	25	100
Weak ribs	27	108
Stiffer ribs	23	92
Shorter cartilage	19	76
Divided sternum	25	100
80% Mass on spine	28	112
Stiffer ribcage-no internal organs	19	76

Table 9. Combined deflection (DC) under the BELT load case

BELT, STATE	Combined deflection [mm]	Normalized value wrt the INTACT state [%]
Intact	31	100
Weak cartilage	31	100
Weak sternum	32	103
Weak Intercostals	33	106
Weak cv ligaments	31	100
Weak ribs	33	106
Stiffer ribs	29	94
Shorter cartilage	31	100
Divided sternum	30	97
80% Mass on spine	33	106
Stiffer ribcage-no internal organs	26	84

3.4.2.1.3 Double diagonal belt

For the diagonal belt load in the table top test, the displacement pattern and compression values are presented on Figure 43 and Figure 44. The maximum sternal deflection is also reported on Table 10, as well as the normalized value having the INTACT state as reference.

For the stiffer ribcage and the inertia of the soft organs added to the spine, the chest compressed less except the lower middle region (Figure 44).

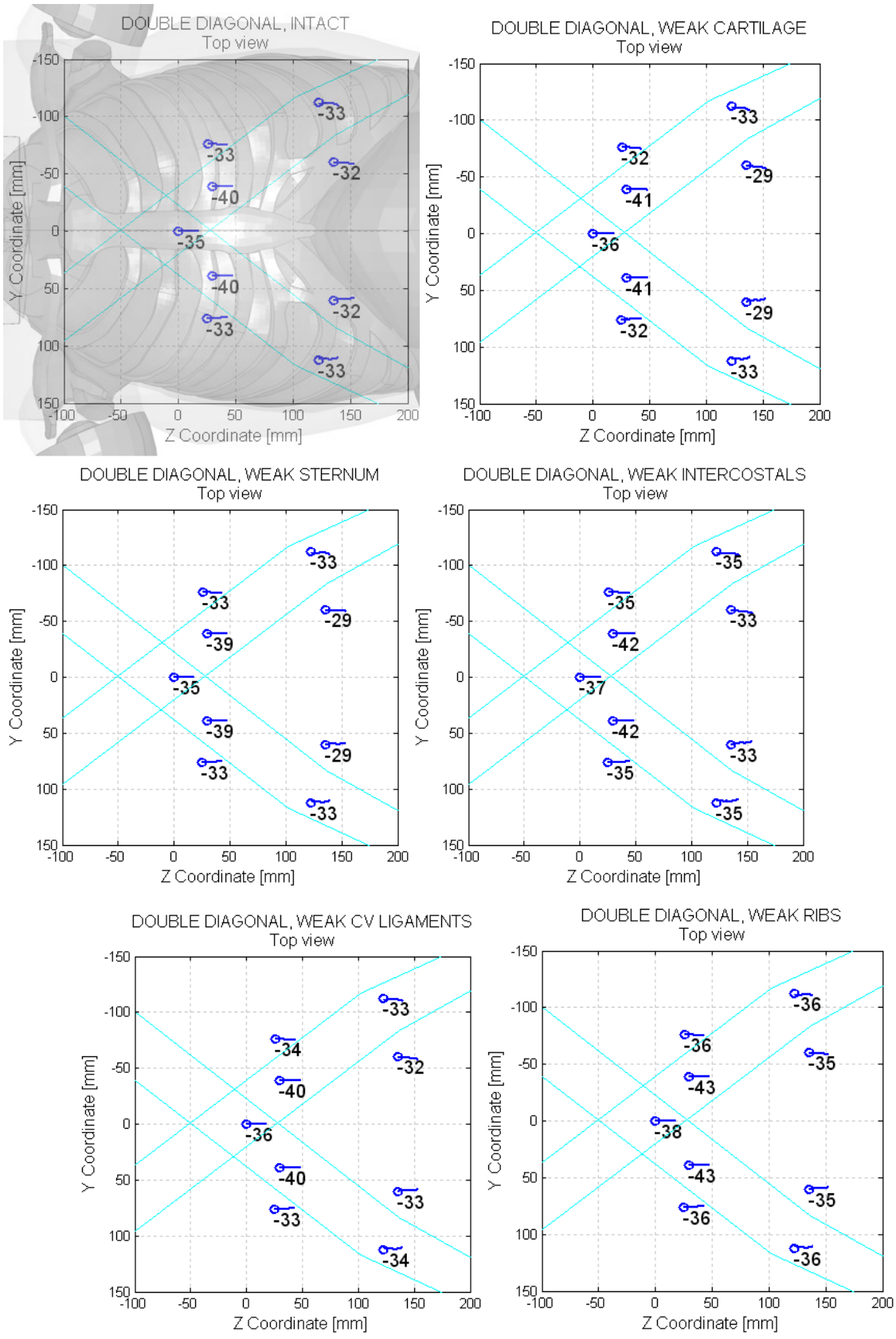

Figure 43. Displacements in the coronal plane and chest compression for the DOUBLE BELT load case and weak states

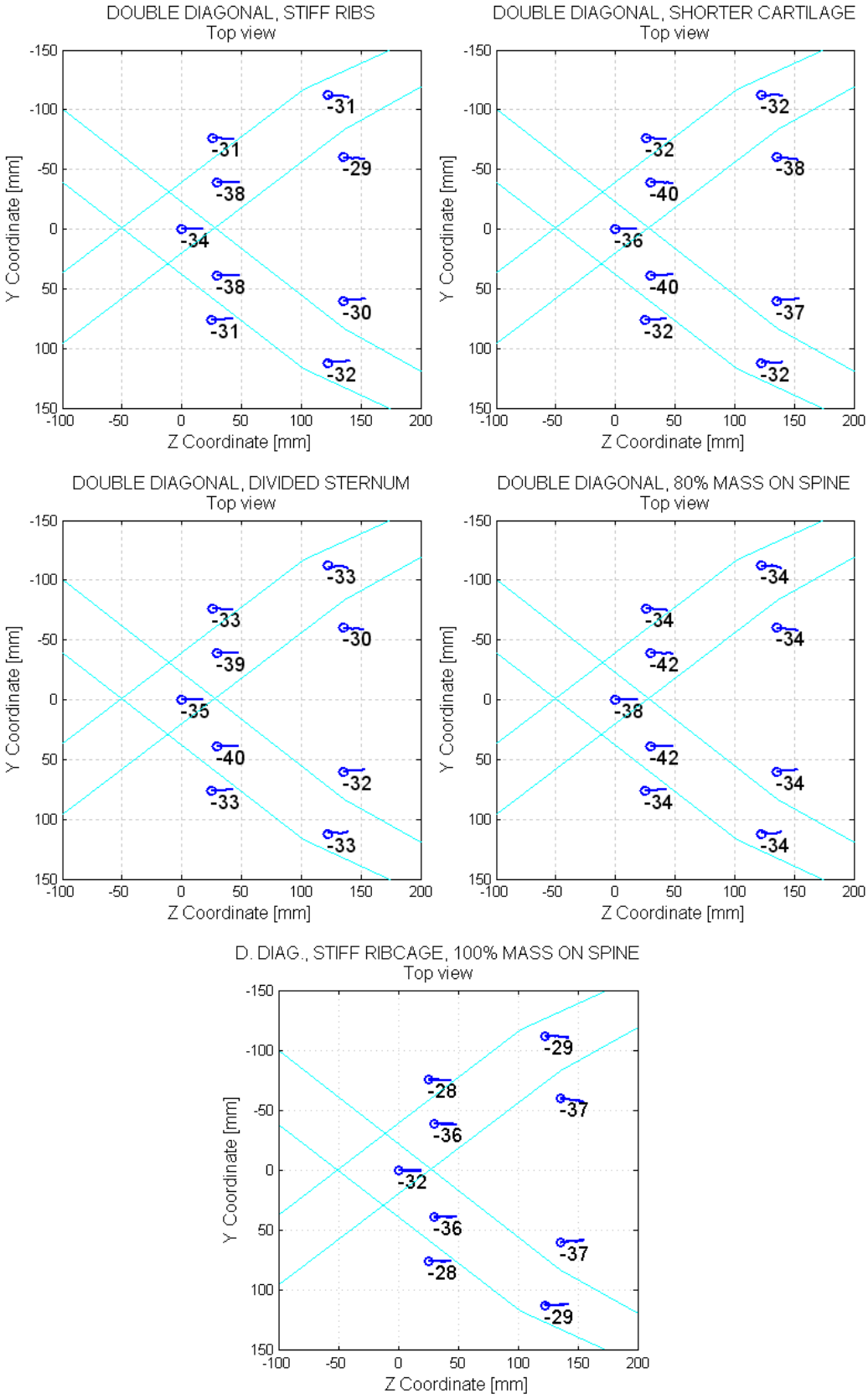

Figure 44. Displacements and chest compression for the DOUBLEBELT load case and ATD-like states

Table 10. Double diagonal belt

DOUBLE BELT, STATE	Sternal deflection [mm]	Normalized value wrt the INTACT state [%]
Intact	35	100
Weak cartilage	36	103
Weak sternum	35	100
Weak Intercostals	37	106
Weak cv ligaments	36	103
Weak ribs	38	109
Stiffer ribs	34	97
Shorter cartilage	36	103
Divided sternum	35	100
80% Mass on spine	38	109
Stiffer ribcage-no internal organs	32	91

3.4.2.1.4 Distributed load

The displacement pattern and compression values for the distributed load case are presented on Figure 45 and Figure 46. The maximum sternal deflection is also reported in Table 11, as well as the normalized value using the INTACT state as the reference.

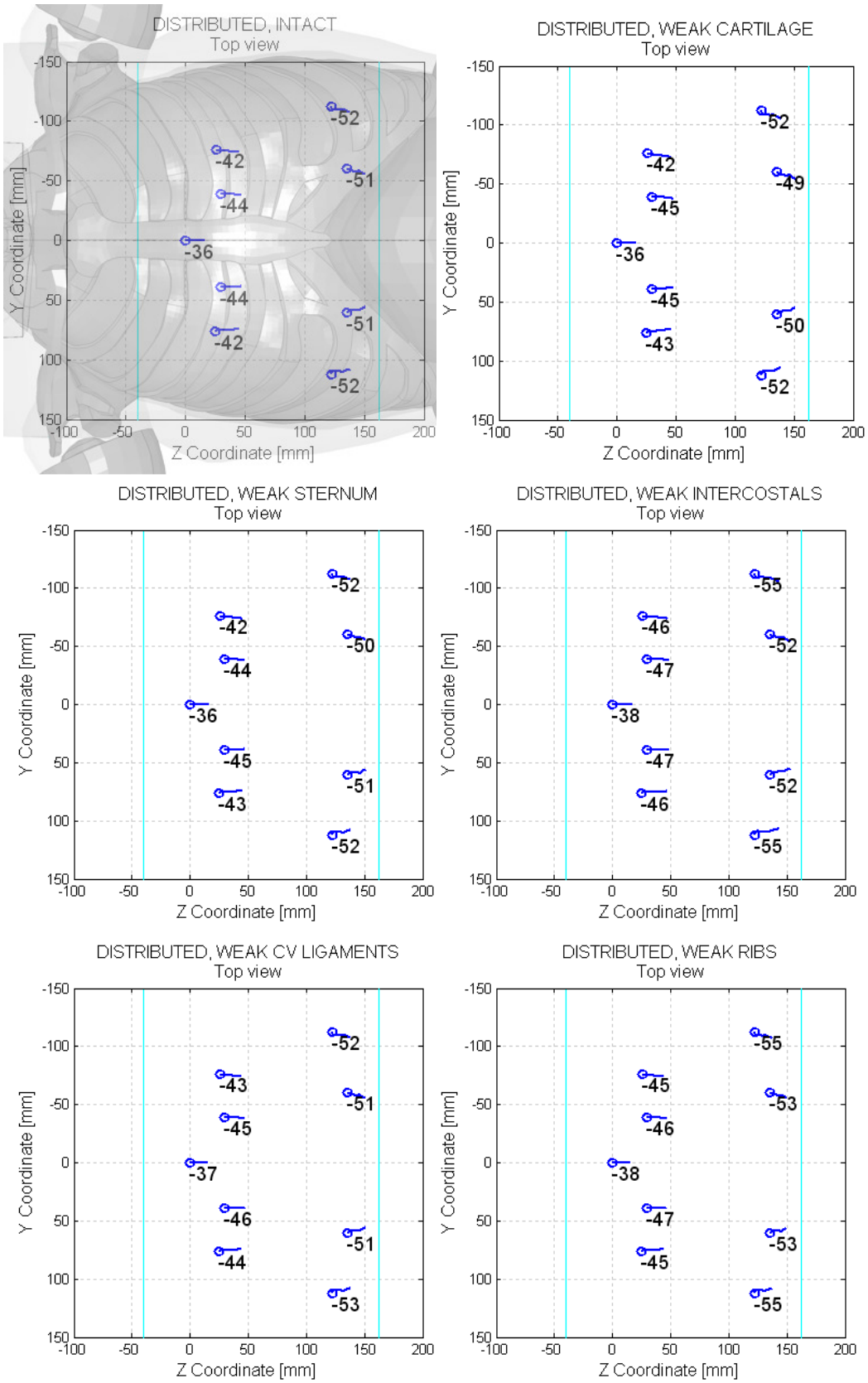

Figure 45. Displacements and chest compression for the DISTRIBUTED load case and weak states

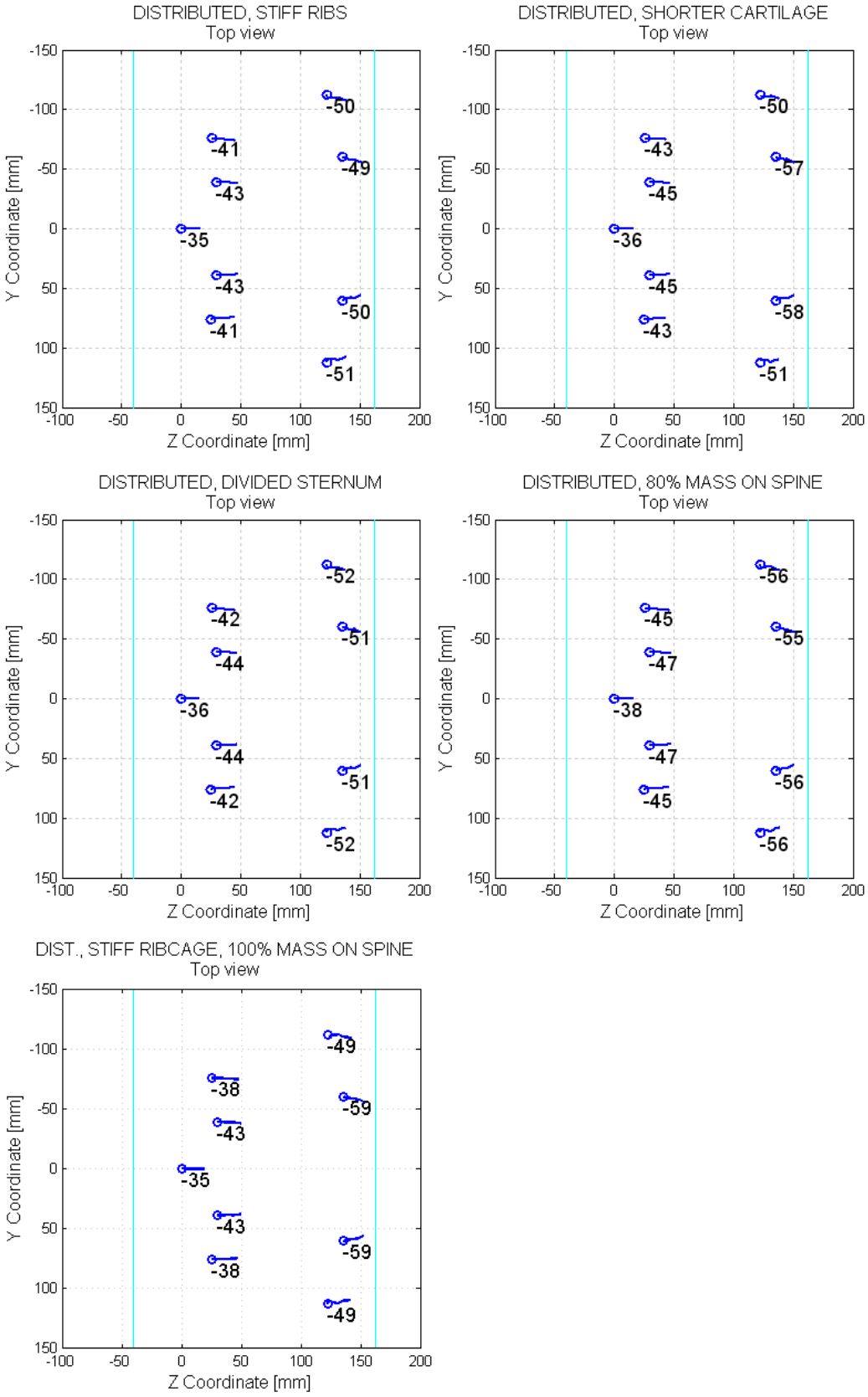

Figure 46. Displacements and chest compression for the DISTRIBUTED load case and ATD-like states

Table 11. distributed load

DISTRIBUTED LOAD, STATE	Sternal deflection [mm]	Normalized value wrt the INTACT state [%]
Intact	36	100
Weak cartilage	36	100
Weak sternum	36	100
Weak Intercostals	38	106
Weak cv ligaments	37	103
Weak ribs	38	106
Stiffer ribs	35	97
Shorter cartilage	36	100
Divided sternum	36	100
80% Mass on spine	38	106
Stiffer ribcage-no internal organs	35	97

3.4.2.1.5 Sternal and differential deflections on table top tests

Table 12 summarizes the sternal deflections as a function of load and states. Clearly the sternum compression changed more when the thorax properties were changed when loaded by the hub as compared to the other loads. Table 13 presents the differential deflections. It can be noted that additional rib cage stiffness produces a better coupling between the mid-to-lower sections and the upper section of the ribcage. It can also be noted that cartilage and rib length clearly influence the coupling between the right and left thorax regions (as indicated by dD).

Table 12. Sternal deflection on table top tests

	Sternal deflections [mm]				Normalized deflections of the sternum			
	HUB	BELT	XBELT	BAND	HUB	BELT	XBELT	BAND
Intact	31.8	30.3	35.2	35.9	1.00	1.00	1.00	1.00
Weak cartilage	32.6	30.5	35.8	36.1	1.03	1.01	1.02	1.01
Weak sternum	33.0	30.9	35.2	36.2	1.04	1.02	1.00	1.01
Weak Intercostals	33.7	31.8	37.0	38.2	1.06	1.05	1.05	1.07
Weak cv ligaments	32.2	30.4	35.7	36.7	1.01	1.00	1.01	1.02
Weak ribs	35.0	32.4	37.7	37.8	1.10	1.07	1.07	1.05
Stiffer ribs	30.0	28.8	33.7	34.7	0.94	0.95	0.96	0.97
Shorter cartilage	30.6	31.1	35.5	36.4	0.96	1.03	1.01	1.02
Divided sternum	31.7	29.5	34.9	35.8	1.00	0.97	0.99	1.00
80% Mass on spine	33.6	32.2	37.8	38.0	1.06	1.06	1.07	1.06
Stiffer ribcage-no internal organs	27.3	26.0	32.4	34.7	0.86	0.86	0.92	0.97

Table 13. Differences on chest deflection

	Difference between 4th and 7th rib level deflections [mm]	dD [mm]
	HUB	BELT
Intact	10	25
Weak cartilage	13	26
Weak sternum	12	26
Weak Intercostals	11.5	26
Weak cv ligaments	10.5	25
Weak ribs	11	28
Stiffer ribs	7	23
Shorter cartilage	6.5	19
Divided sternum	10	25
80% Mass on spine	10	28
Stiffer ribcage-no internal organs	5	19

3.4.2.2 Sled tests

The response of the ribcage during the GS sled test, using the different HBM states, was evaluated by computing the combined deflection criterion factors (i.e. sternal deflection and differential deflection) and the combined deflection criterion as defined in Section 3.2.3. The values for these parameters are showed in

Table 14 at the time of maximum combined deflection as computed using the costochondral joint data. In

Table 15 the maximum values of each factor are displayed. All maximum values for DC and its factors are reported before 100 ms. After 100 ms there is some unrealistic interaction between the abdomen and the lower ribs, therefore the data was only reported up to that time.

The head and T8 longitudinal displacements wrt the buck coordinate system are displayed on Figure 47 for the weak states, and on Figure 48 for the ATD-like states. Figure 49 shows the location of the nine points tracked on the ribcage. The displacement and compression of these points during the sled tests appear in Figure 50 and Figure 51 for the different states. During the THUMS validation in the sled test, all chest points were referred to the coordinate system on T8. Since the combined deflection criterion uses the coordinate system on T8 to measure the sternal deflection and a coordinate system on L1 to calculate the differential deflection, the same references were used to create the figures describing the displacement on the coronal plane and the deflection. The upper chest points and the sternum were tracked with respect to the coordinate system on T8. The lower chest points were tracked with respect to the coordinate system fixed on L1.

Clearly the thorax properties, ribcage stiffness, soft organ mass transferred to the spine, and clavicle bone shape have an influence on the head and T8 displacements (Figure 48).

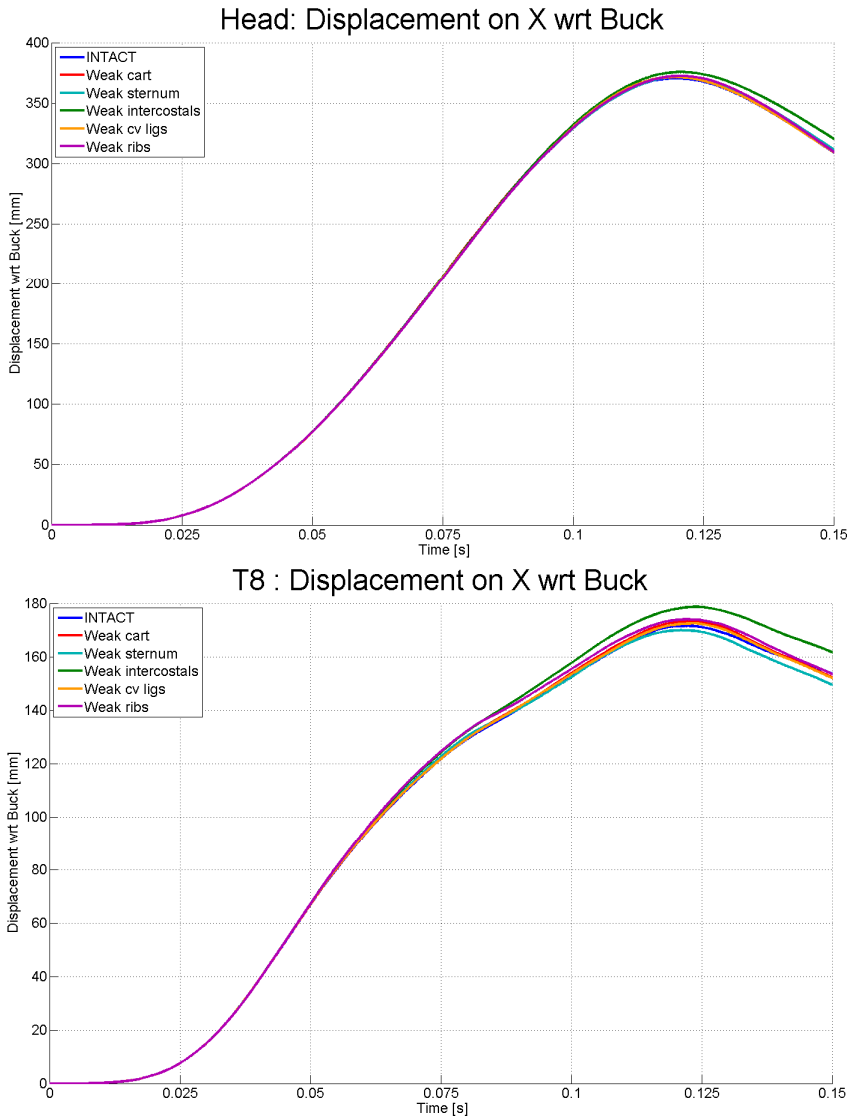

Figure 47. Head and T8 longitudinal displacements wrt buck for the weak states

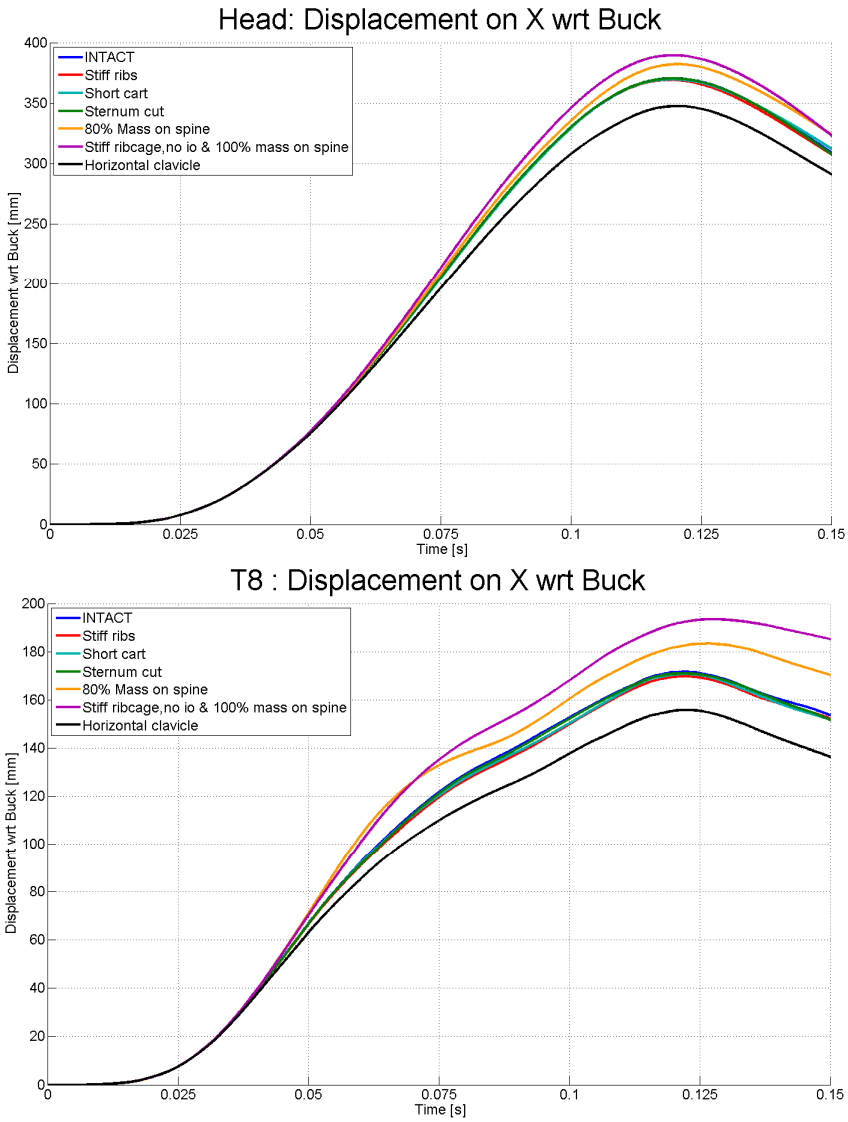

Figure 48. Head and T8 longitudinal displacements wrt buck for the ATD-like states

Table 14. Sternal, differential, and combined deflections (Ds, dD and DC) computed at the costochondral (CC) joint at time of maximum DC.

CASE	Sternal deflection [mm] at maximum DC	Differential deflection [mm] at maximum DC	Max DC [mm]	% max DC	t for max DC[s]
Intact	53	35	56	100	0.081
Weak cartilage	54	38	58	104	0.083
Weak sternum	58	41	63	113	0.081
Weak Intercostals	56	49	63	112	0.081
Weak cv ligaments	54	36	57	102	0.082
Weak ribs	59	40	63	113	0.083
Stiffer ribs	48	39	53	94	0.077
Shorter cartilage	51	13	51	92	0.088
Divided sternum	53	34	56	100	0.081
80% Mass on spine	57	40	62	110	0.078
Stiffer ribcage-no internal organs	62	6	62	111	0.081
Clavicle	55	30	56	100	0.087

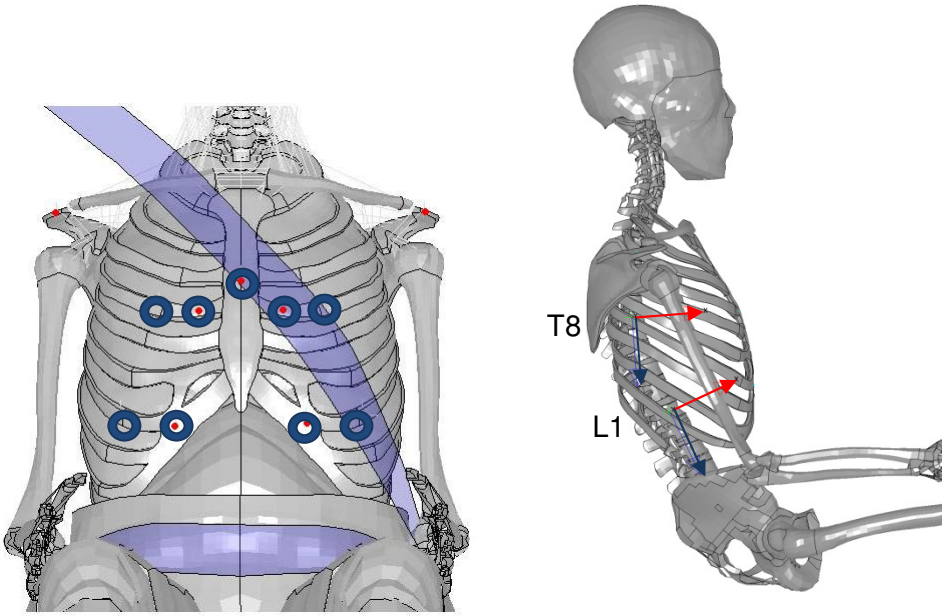

Figure 49. Tracked points and coordinate systems location during the sled tests.

It is apparent that shorter cartilage produces a different deformation pattern as compared to that of the intact model (Figure 51). It can also be noted that design changes to the clavicle had a large effect on the deformation pattern; it appear to shield the upper right torso (the belted side).

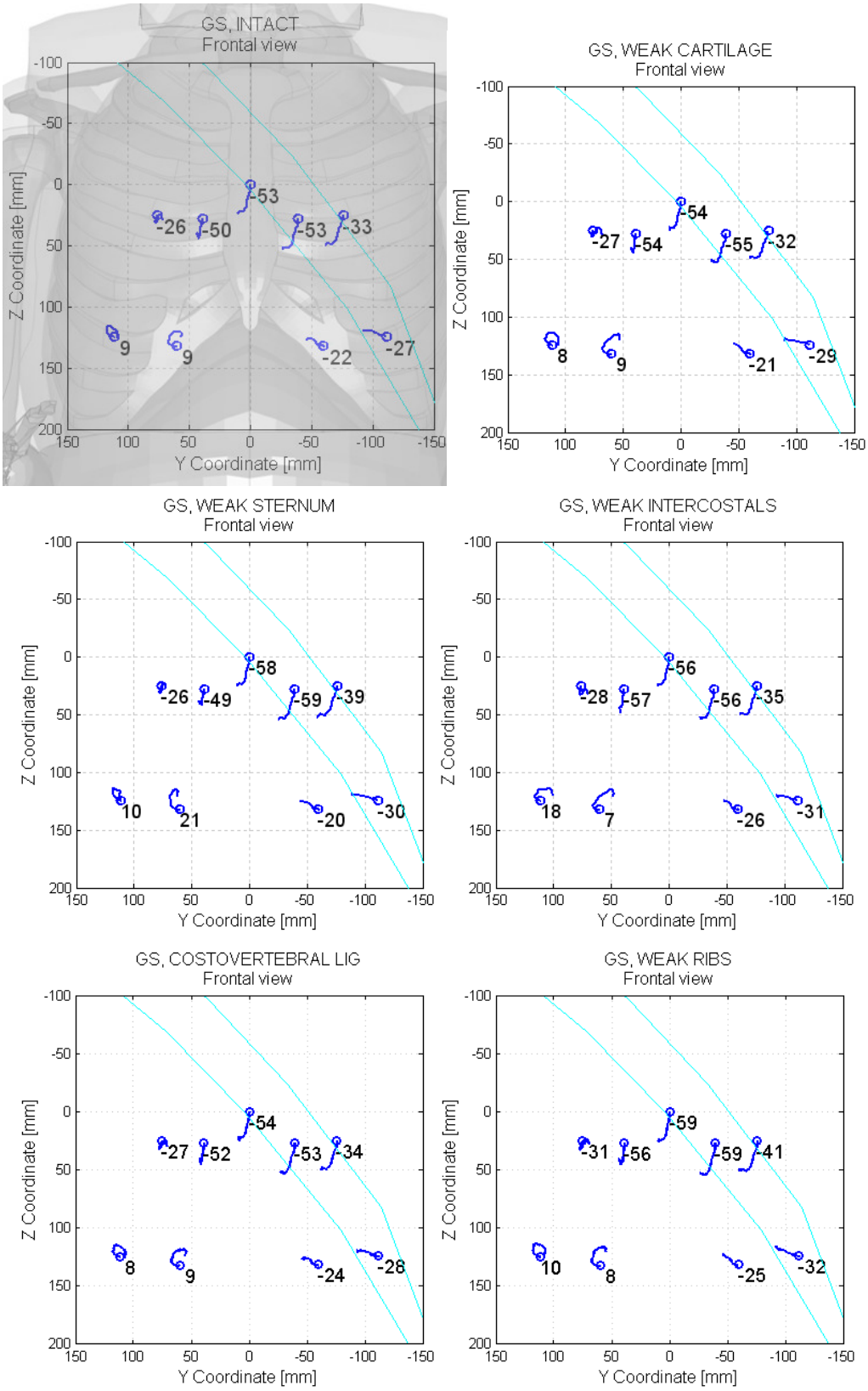

Figure 50. Chest displacements at time of maximum DC for the weak states under the sled test

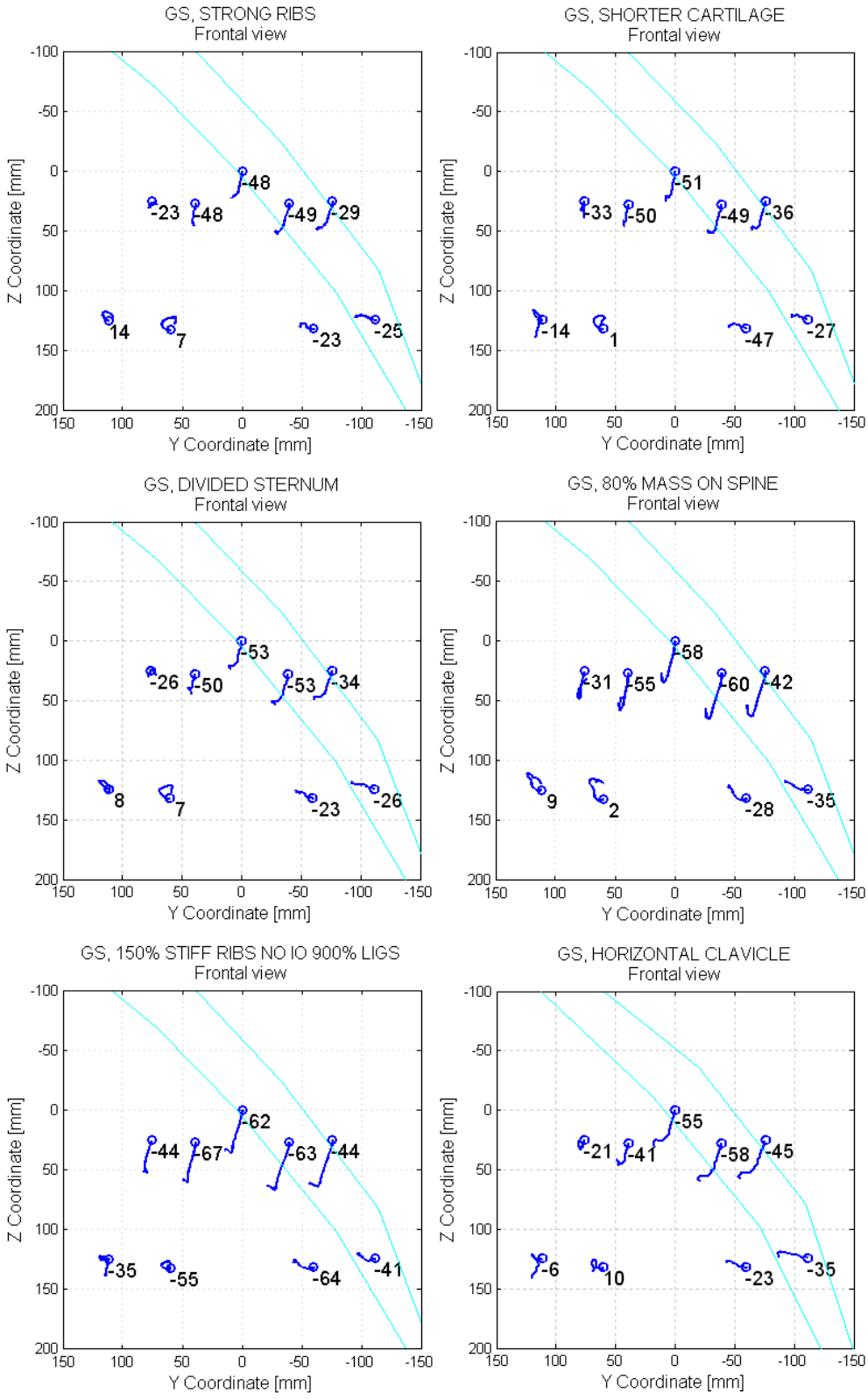

Figure 51. Chest displacements at time of maximum DC for the ATD-like states under the sled test

The compression during time for the sternum and both of the costochondral joints at the 7th rib level are displayed in Figure 52 and Figure 53 for all the weak states. The difference between left and right compressions at the costochondral joints constitutes the differential deflection term in the combined deflection definition and it is reported in Figure 54. Figure 55 shows the difference on deflection between the left and right costochondral joint at the 4th rib level.

Peak sternum displacemnets varied from approximately 54 to 58 mm (Figure 52). Peak bulge out, which only occurred on the right side of the chest, varied from 24 to 32 mm while the compression, on the left side of the chest, only varied between -20 and -24 mm at the time when the peak bulge out appeared (Figure 53).

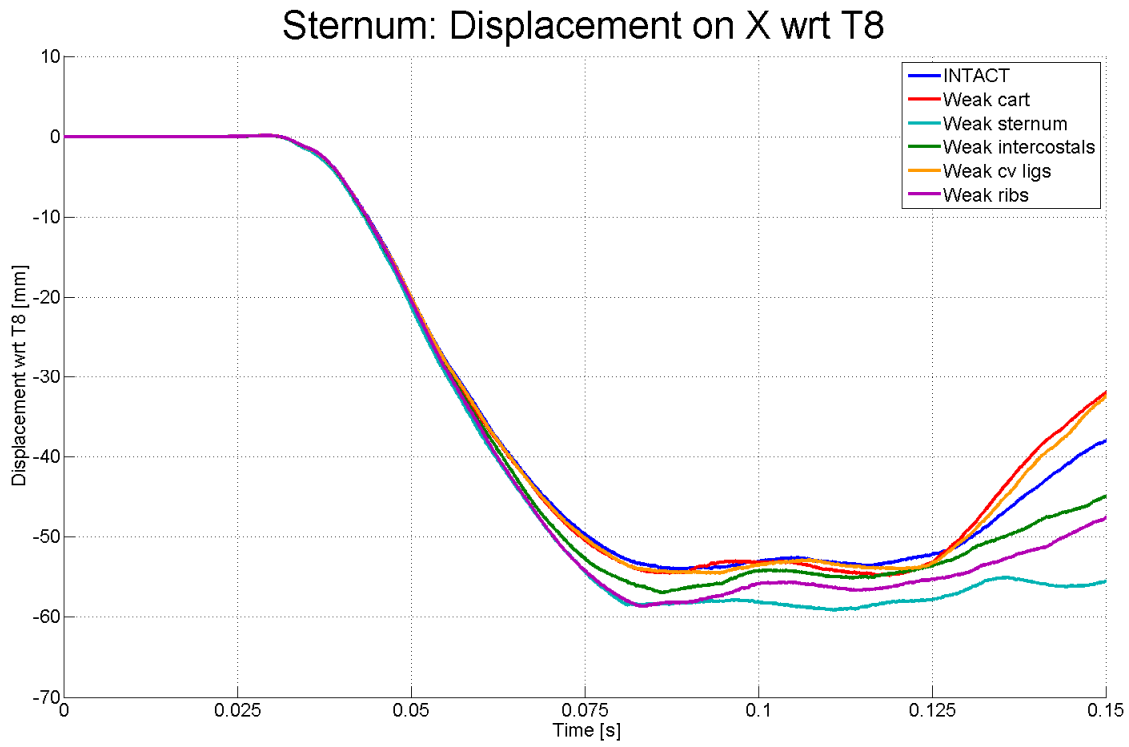

Figure 52. Sternal compression against time in the sled test wrt T8 for the weak states

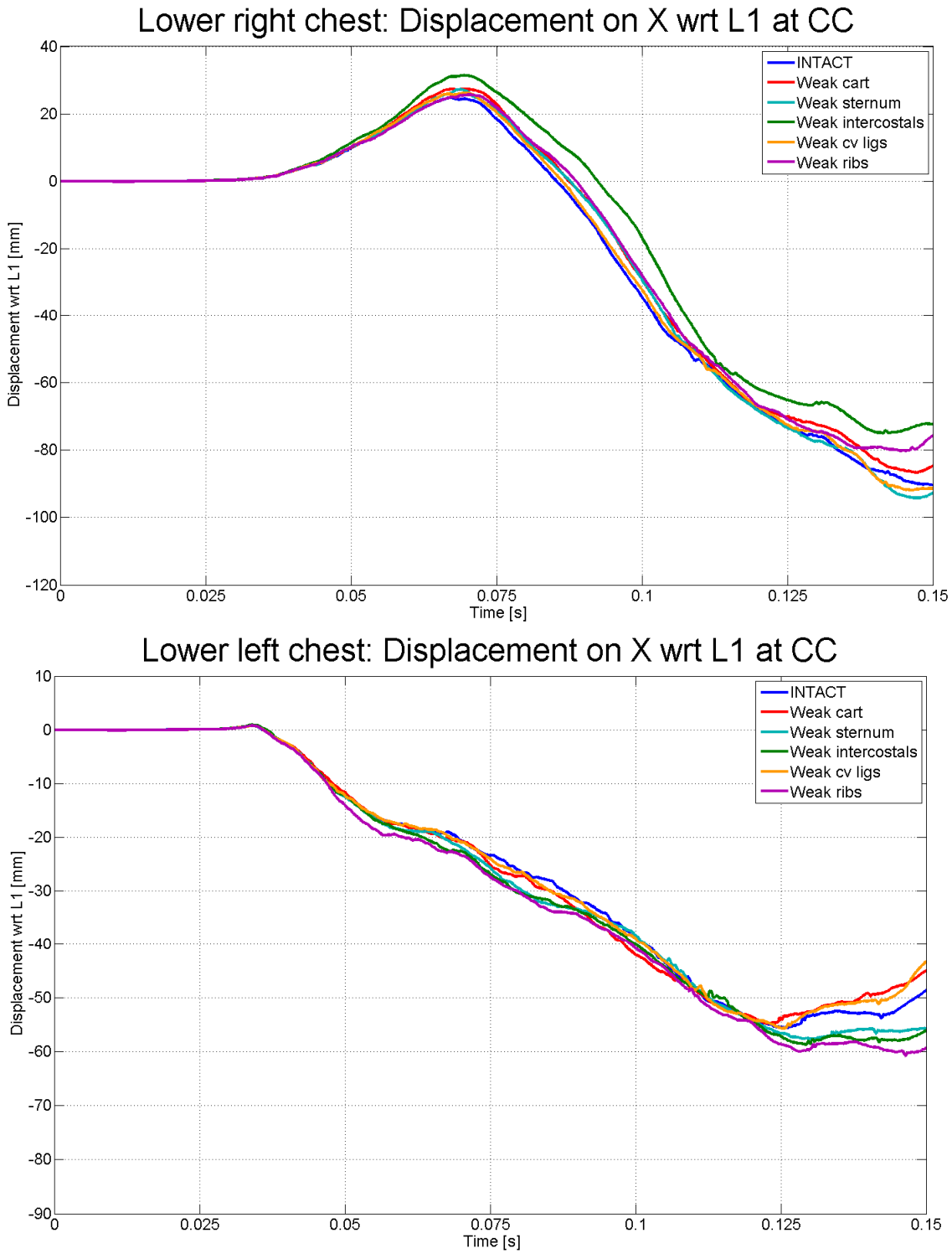

Figure 53. Right and left compressions against time for the weak states during the sled tests wrt L1

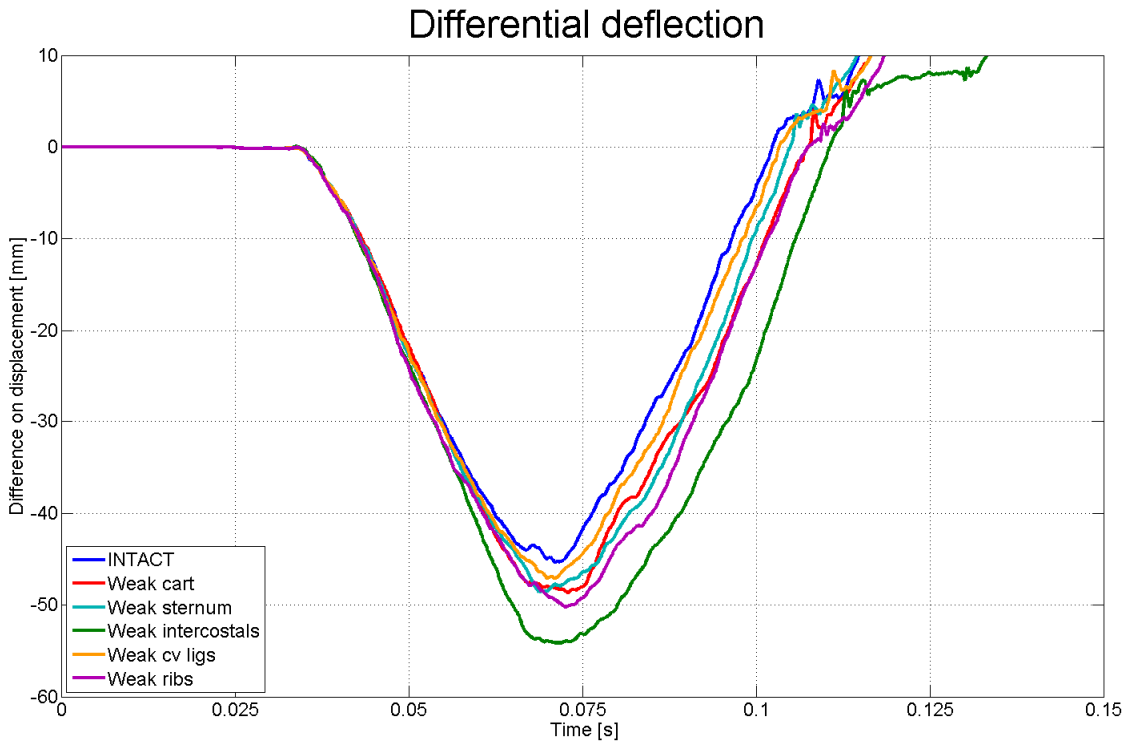

Figure 54. Differential deflection for the weak states during the sled tests

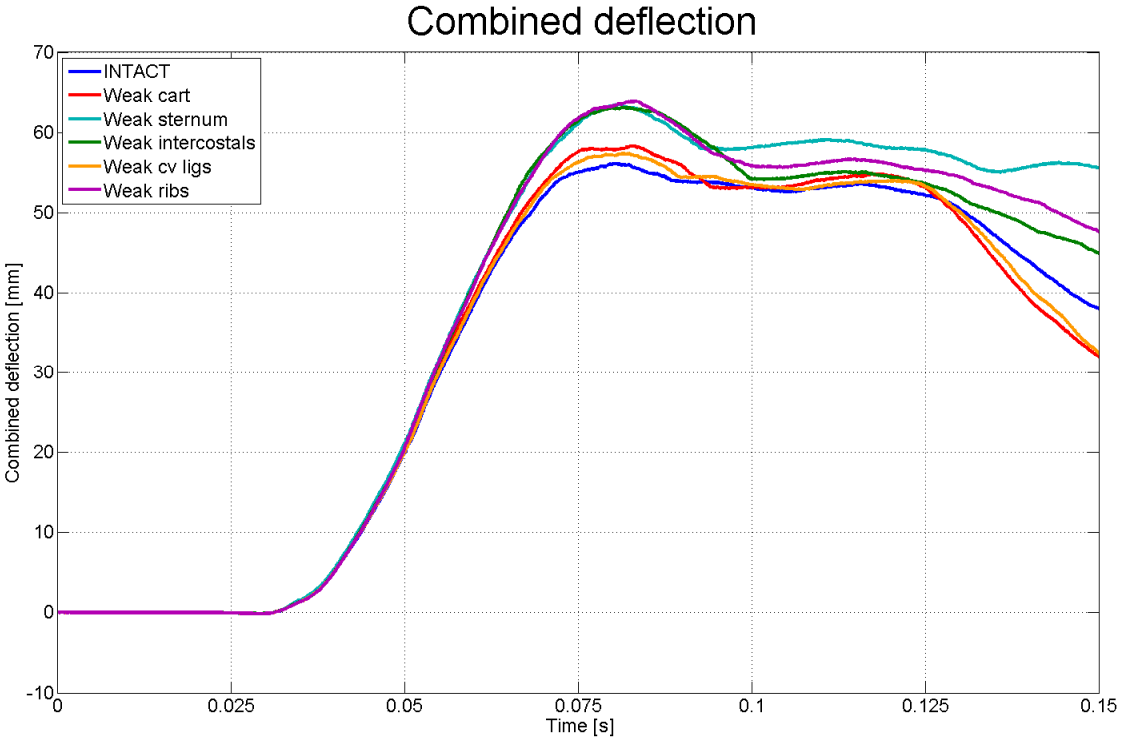

Figure 55. Combined deflection for the weak states during the sled tests

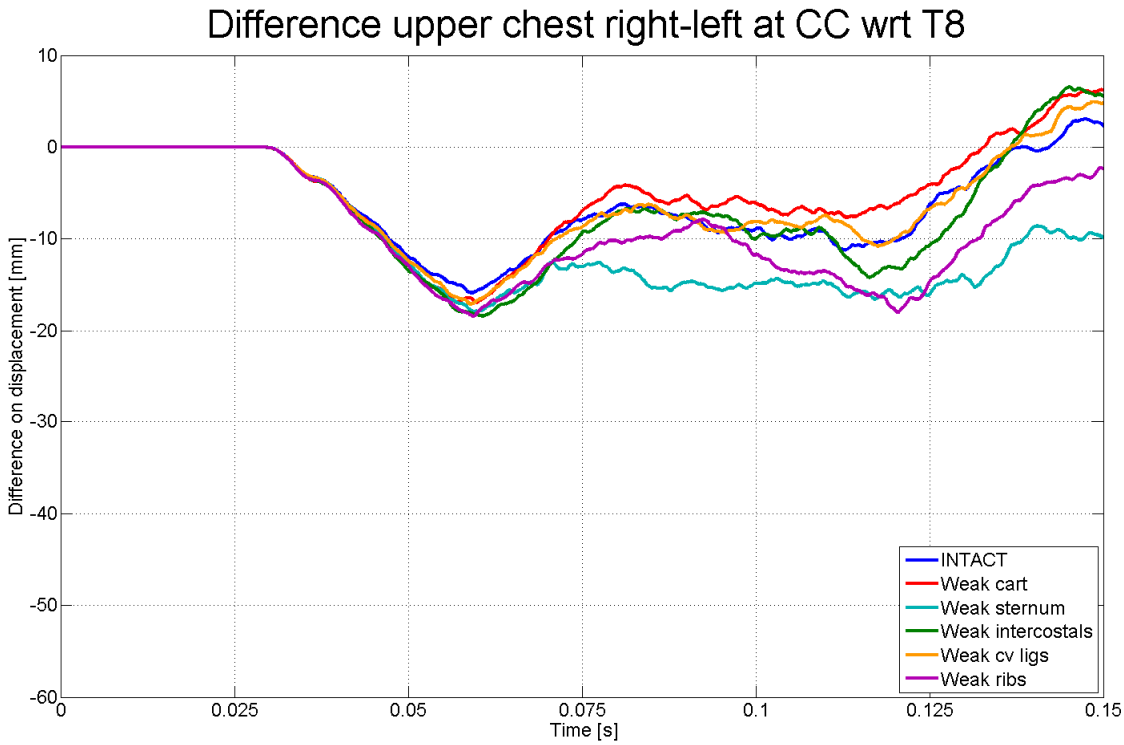

Figure 56. Difference in deflection between left and right costochondral joints at the 4th rib level for the weak states under the sled test

The compression during time for the sternum and both of the costochondral joints at the 7th rib level are displayed in Figure 57 and Figure 58 for all the ATD-like states. The difference between left and right compressions at the costochondral joints constitutes the differential deflection term in the combined deflection definition and it is reported in Figure 59. Figure 61 shows the difference on deflection between the left and right costochondral joint at the 4th rib level.

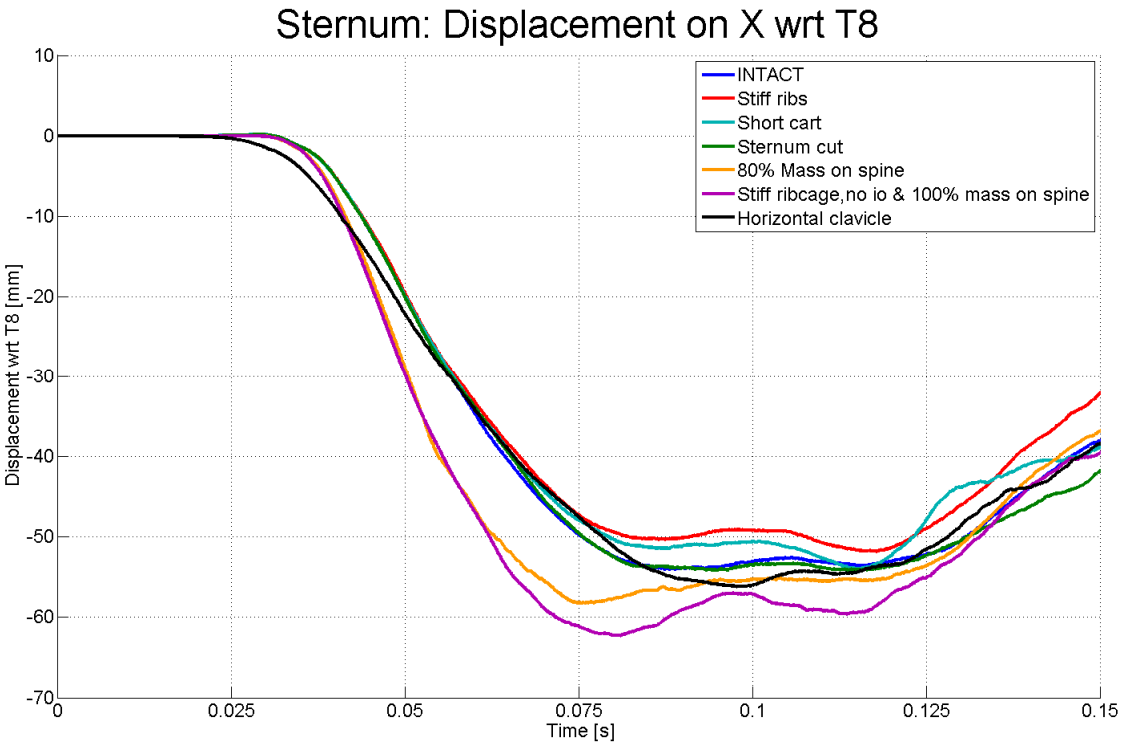

Figure 57. Sternal compression against time in the sled test wrt T8 for the ATD-like states

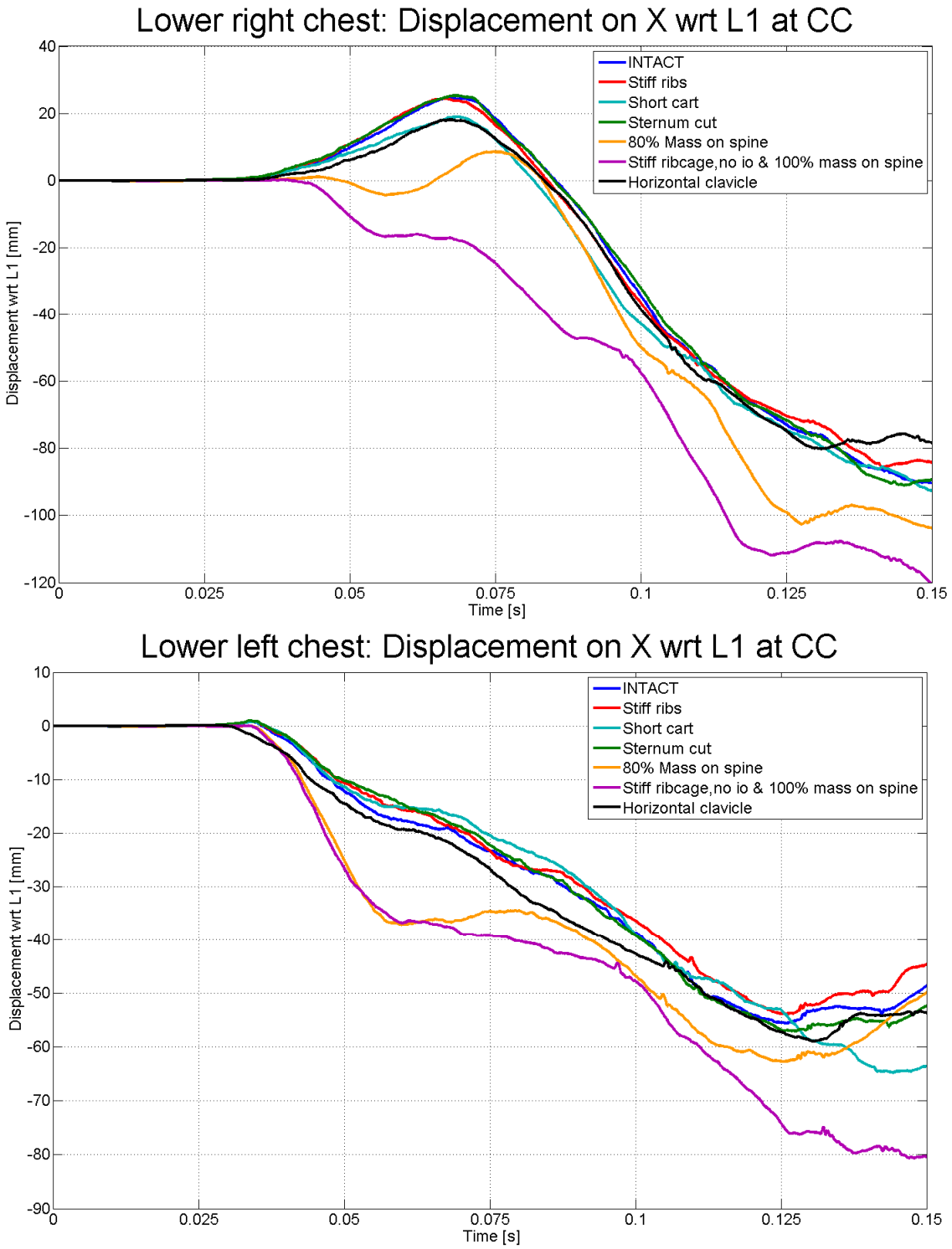

Figure 58. Right and left compressions against time for the ATD-like states during the sled tests wrt L1

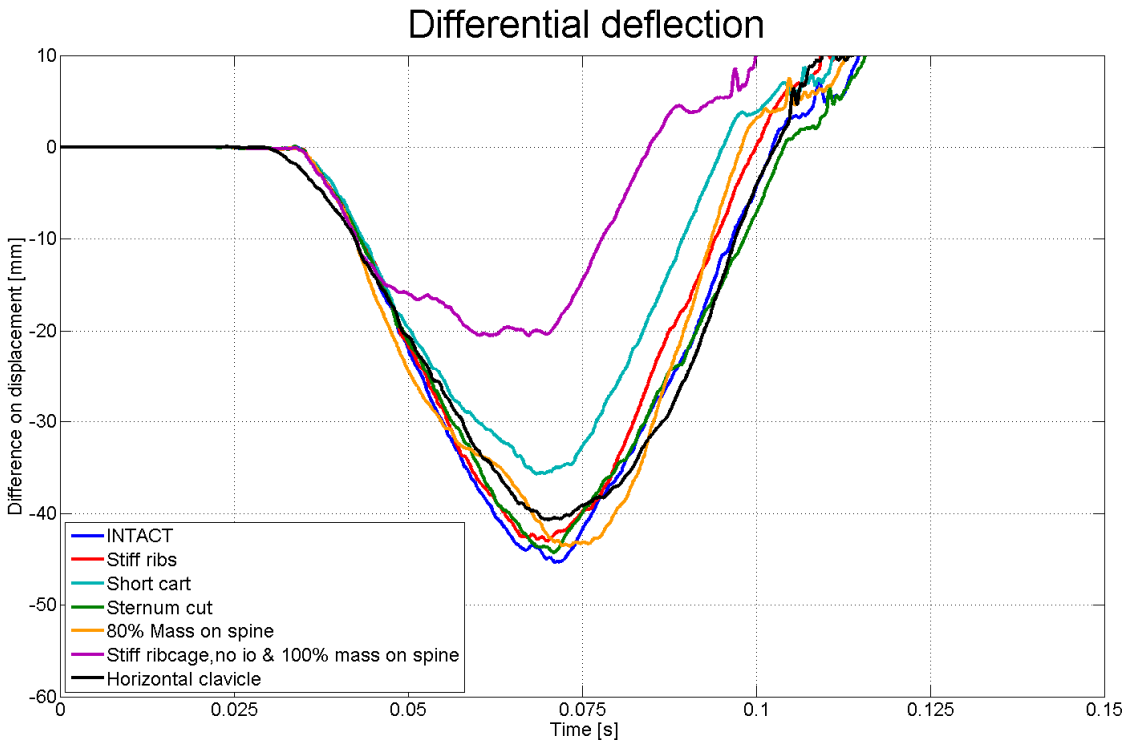

Figure 59. Differential deflection for the ATD-like states during the sled tests

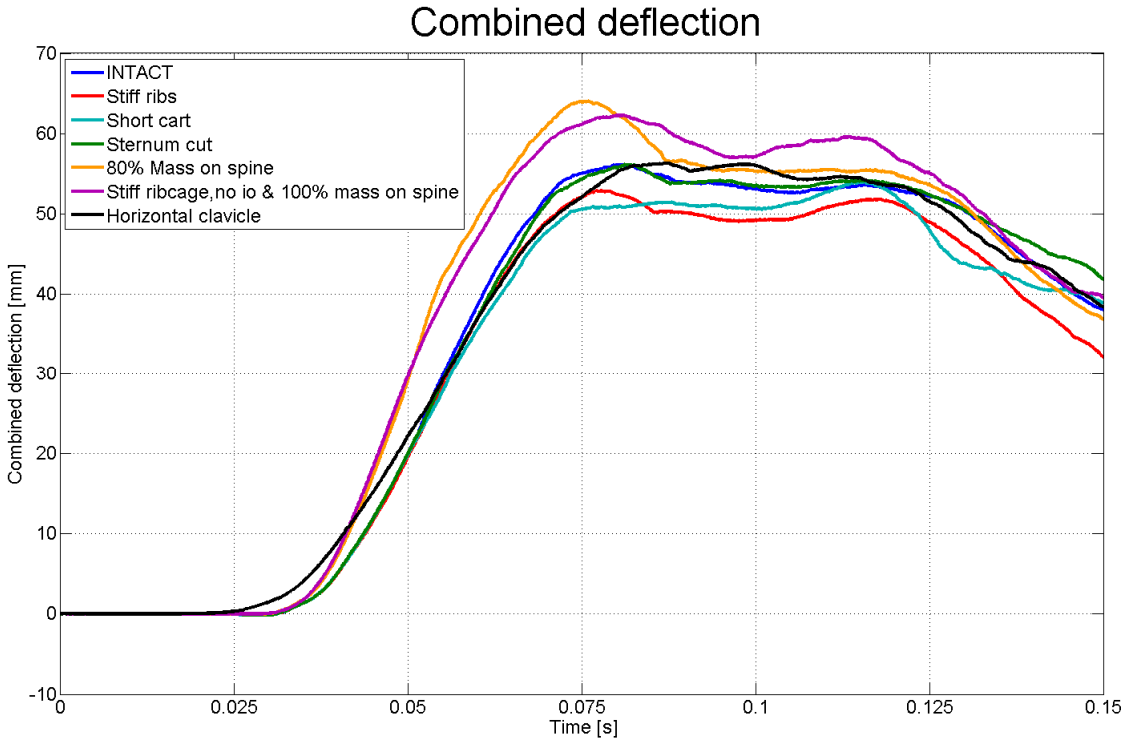

Figure 60. Combined deflection for the ATD-like states during the sled tests

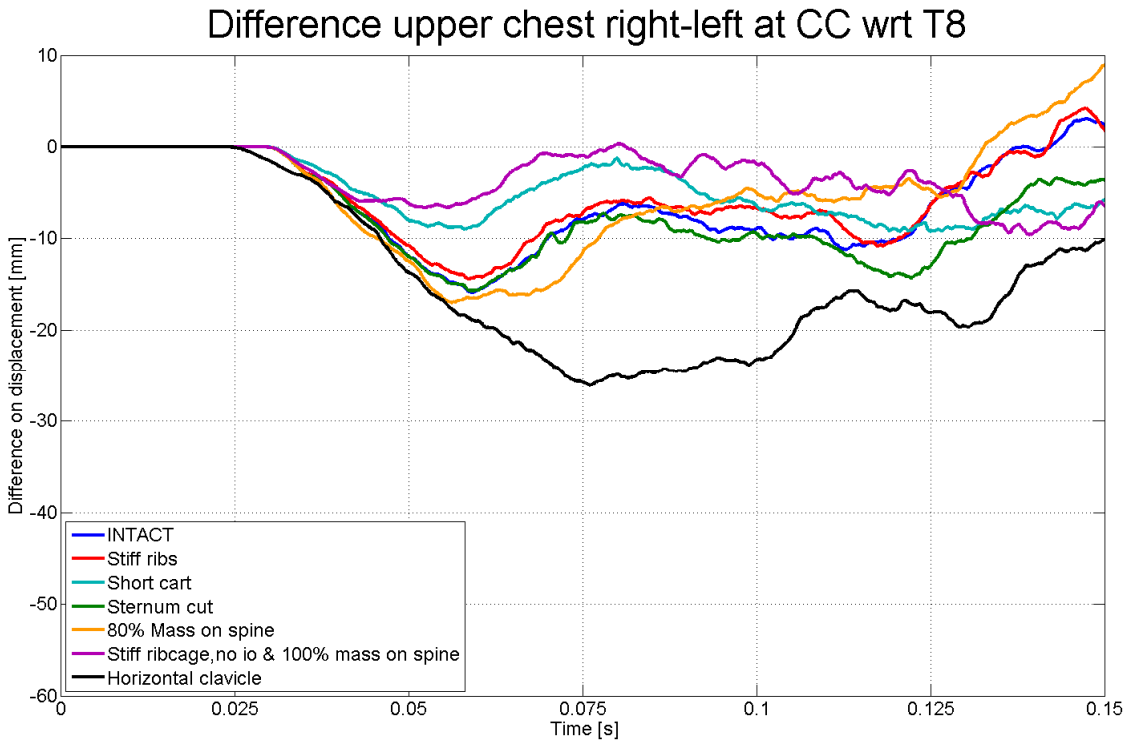

Figure 61. Difference in deflection between left and right costochondral joints at the 4th rib level for the ATD-like states under the sled test

Table 15. Maximum values and timing for sternal deflection, differential deflection and combined deflection

CASE	DS		dD		DC	
	Max DS [mm]	t at max DS[s]	Max dD [mm]	t at max dD[s]	Max DC [mm]	t at max DC[s]
Intact	54	0.088	45	0.071	56	0.081
Weak cartilage	54	0.087	49	0.073	58	0.083
Weak sternum	59	0.083	49	0.070	63	0.081
Weak Intercostals	57	0.086	54	0.071	63	0.081
Weak cv ligaments	55	0.094	47	0.071	57	0.082
Weak ribs	59	0.084	50	0.073	63	0.083
Stiffer ribs	50	0.088	43	0.070	53	0.077
Shorter cartilage	51	0.088	36	0.069	51	0.088
Divided sternum	54	0.095	44	0.071	56	0.081
80% Mass on spine	57	0.079	41	0.072	62	0.078
Stiffer ribcage-no internal organs	62	0.081	21	0.067	62	0.081
Clavicle	56	0.098	41	0.070	56	0.087

3.4.3 Coupling and stiffness

A complementary way to visualize the stiffness and coupling results for the hub and sled tests is introduced in Figure 62 to Figure 65. The distributed and double diagonal belt load cases are not included since they apply a distributed and symmetric load on the ribcage and therefore the coupling within the ribcage cannot be measured. The following figures summarize the results that appear on Table 12 to

Table 15. The normalized stiffness, displayed on the ordinate, was calculated as the inverse of the sternal deflection for the table top and the sled tests, and then normalized with respect to the value for the intact state for each load case. The normalized coupling is plotted on the abscissa and it refers either to the lateral or vertical coupling, these values were also normalized with respect to the intact state value for the respective load case. The lateral coupling refers to the difference in compression between right and left costochondral joints on the 7th rib level. The vertical coupling was obtained from the difference in compression between the 4th and 7th costochondral joints.

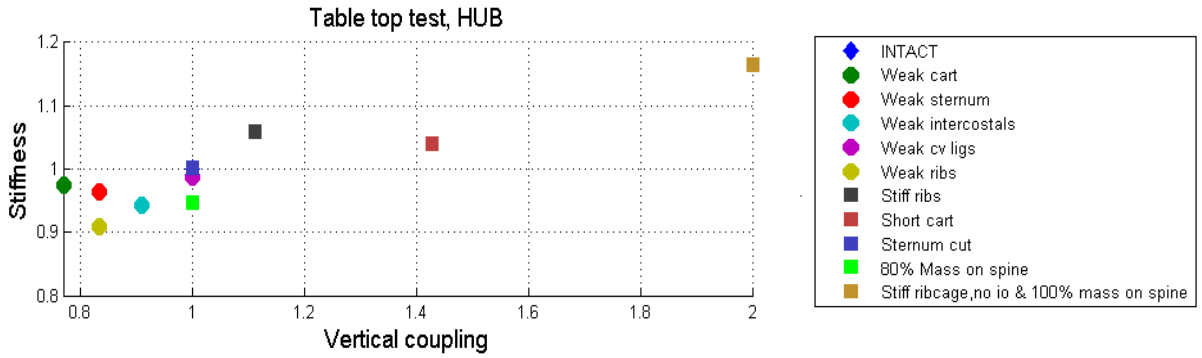

Figure 62. Stiffness and vertical coupling for all states in the table top hub load case

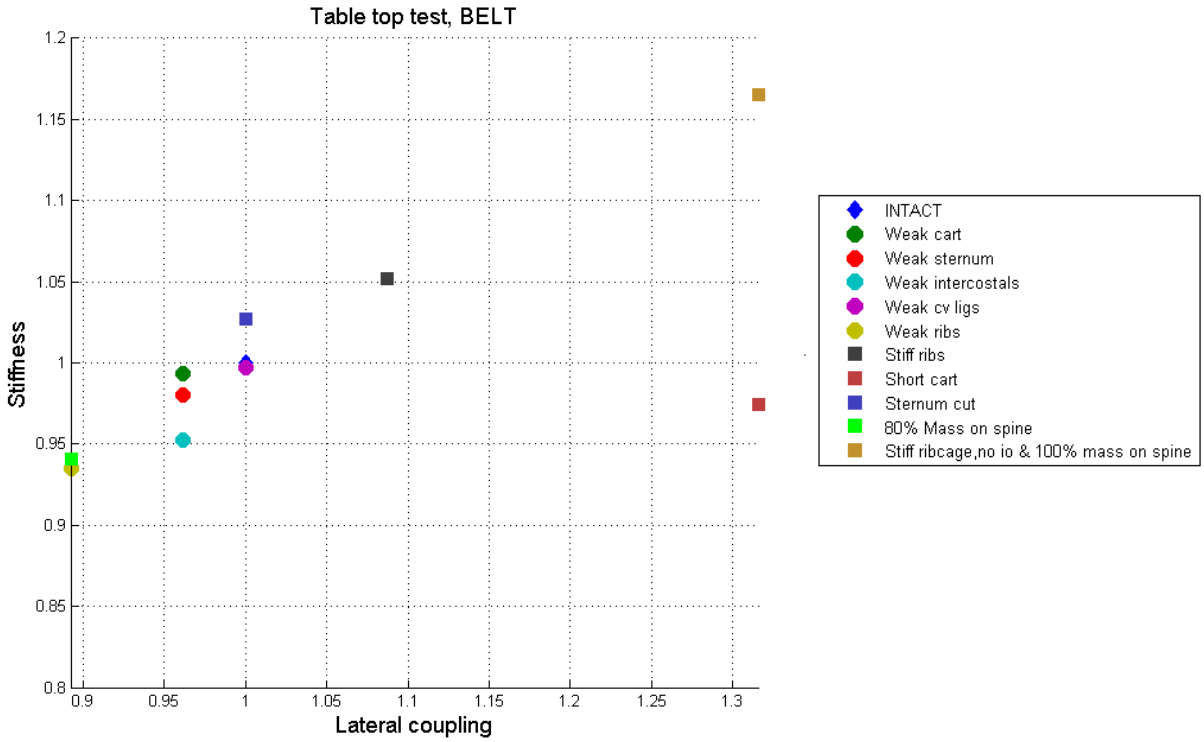

Figure 63. Stiffness and lateral coupling for all states in the table top belt load case

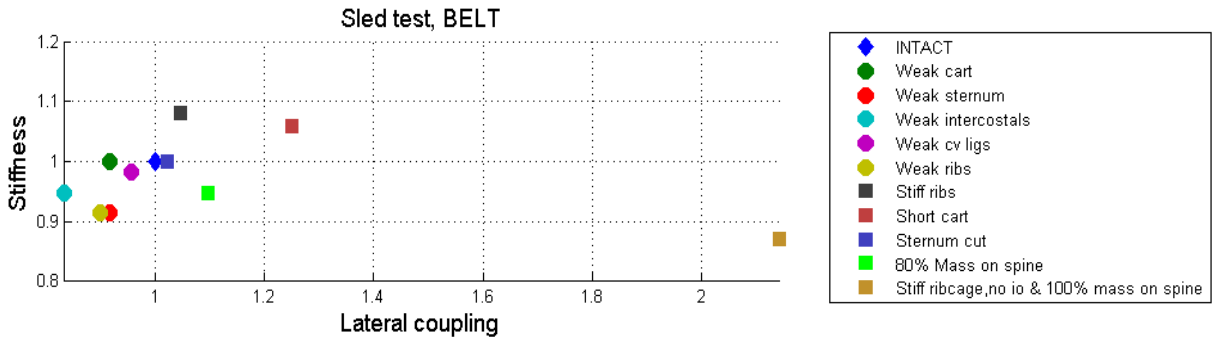

Figure 64. Stiffness and lateral coupling for all states in the sled test

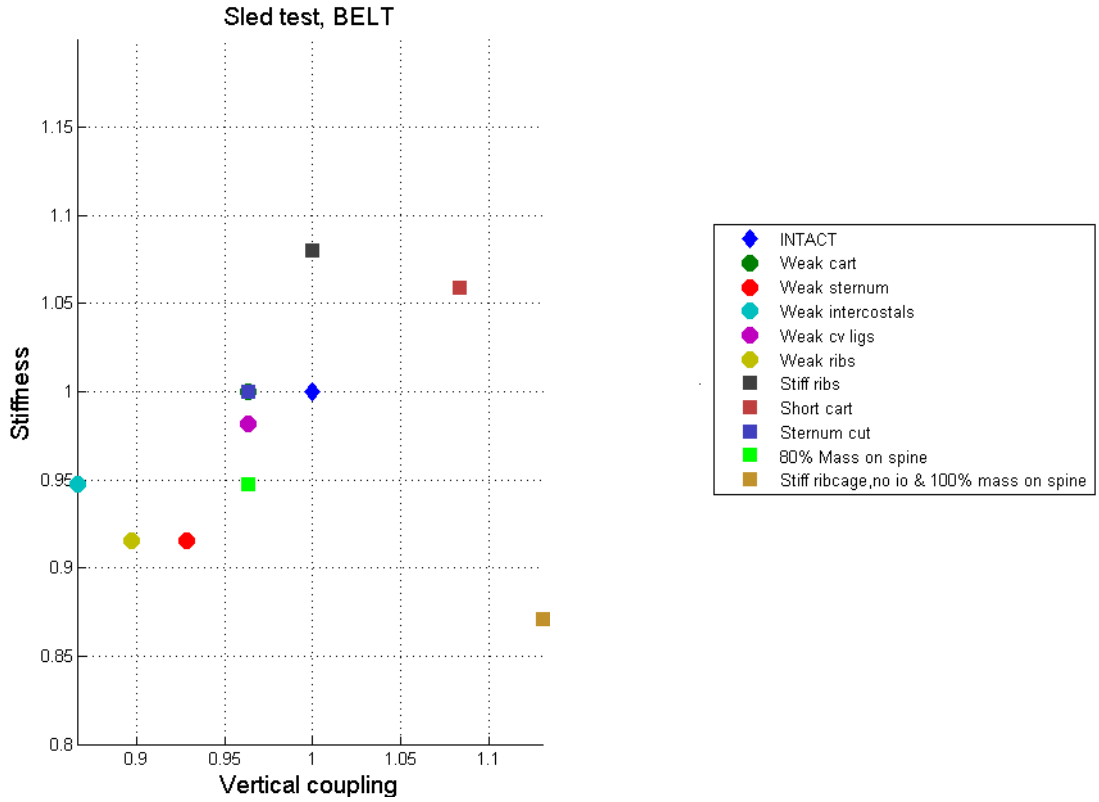

Figure 65. Stiffness and vertical coupling for all states in the sled test

All previous figures show an inverse relation between the stiffness and coupling, both in table top and sled tests. There are some states with a relation stiffness-coupling that lies outside the region where all other states are. There are also states that present opposite behavior between the sled and table to tests, as the 80% mass on spine state in Figure 63 and Figure 64. These responses will be discussed on the following sections.

3.5 Discussion

The influence of each state on the combined deflection criterion is described in the following Sections. There are two main differences between the table top and the sled tests, these are 1) inertial loading of internal organs and 2) the back is free to move in the sled test. Peak sternal deflection for the table top tests was deliberately limited to around 30 mm while it was

around 50 mm for the sled tests. The reason for that difference was that THUMS was not able to properly simulate sternal deflections for much larger sternal deflections than 30 mm in the table top tests; especially when the double diagonal belt and distributed load cases were simulated.

Sternal deflection values and the effective stiffness are not identical because they were measured at different locations. The sternal deflection was measured as the displacement along the x-axis of a point on the sternum with respect to L1. For the effective stiffness calculations, the chest compression was used. This compression was measured as the change in length of an extensometer attached to the different loading devices and includes the skin and soft tissues. Despite different measuring techniques, the trends obtained from both these parameters were similar.

3.5.1 Weak states

3.5.1.1 Weak cartilage

All table top tests using the HBM with weaker rib cartilage presented more compression on almost all points located under the corresponding loading device, as in Figure 39 and Figure 40. The weaker rib cartilage produces a less coupled ribcage and that likely explains why the chest compression is localized to the area under the loading devices. The reduced coupling of the ribcage explains also the smaller compressions on the unbelted side of the single belt load case and the increase in differential deflection on the single belt load case, as seen in Table 8.
The weaker cartilage also increased the “s” shape of the cartilage under the distributed, diagonal and double diagonal load cases as in Figure 66. The weak cartilage state generated the largest difference on compressions between the 4th and 7th rib levels during the hub load case, as in Table 13.

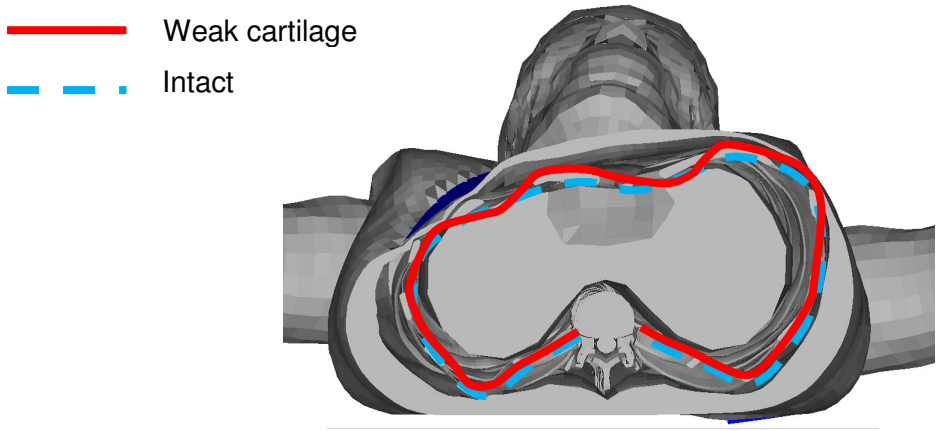

Figure 66. Cross section at the 7th rib level under diagonal belt load. The red line represents the cross section profile with a weak cartilage and the blue dotted line the intact state

In addition, the sternal deflections, as recorded in the table top tests, increased the most for the hub load case when cartilage was made weaker. This case suffered also the largest decrease in effective stiffness. The other three thorax states presented very similar values on sternal deflection and effective stiffness.
In the sled tests, the lower right point on the chest presented a larger bulge out compared to the intact state and the lower left side a larger deflection. As a consequence, the differential deflection value increased for this state as reported in Table 13. This suggested a coupling

reduction, as in the table top test. The sternal deflection increased for this state around 1%. As a result of this increase in differential and sternal deflections, the combined deflection increased in 4%. The displacements on the coronal plane were similar to those of the intact state with the exception of the points on the 7th rib level; which had larger displacement amplitude on the weak cartilage state.

In summary, introducing a weak cartilage in the THUMS rib cage decreased the ribcage coupling both on the craniocaudal and lateral axes. The effect of the cartilage changes was less for the distributed loads whereas larger for the localized loads.

3.5.1.2 Weak sternum

The state with a weak sternum showed higher compressions than the intact state in all load cases and in all points just underneath the loading devices, as depicted in Figure 67. The points not directly underneath the loading devices consistently showed less compression than in the intact state. This indicates a loss in coupling within the ribcage. The differential deflection in the belt load case increased 4%, as expected for a less coupled structure. The difference between the 4th and 7th rib level deflections under the hub load case increased and that increment was the second largest among the weak states, as in Table 8.

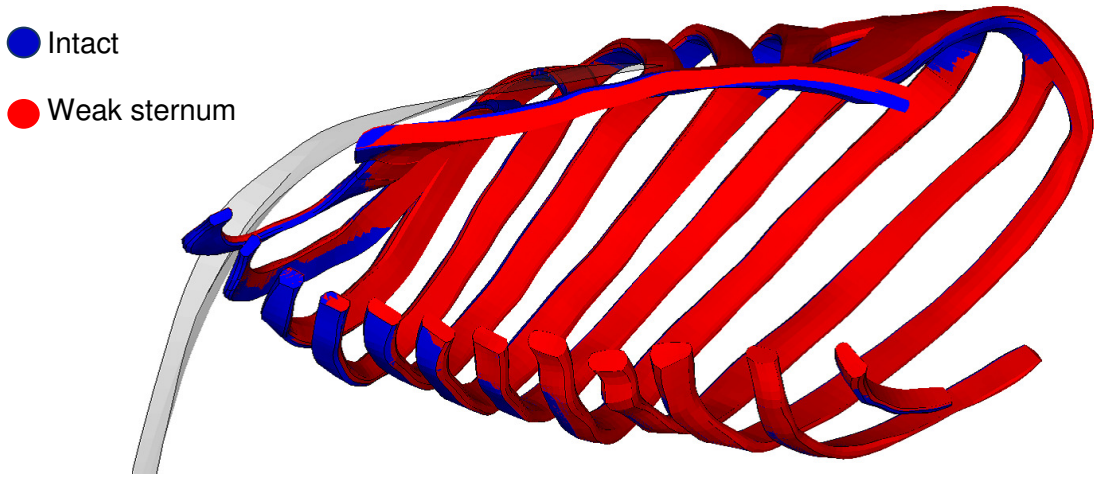

Figure 67. Mid sagittal view comparing the ribcage displacements between the intact and weak sternum states for the belt load case.

The sternal deflection and effective stiffness for the double diagonal belt and the distributed load cases remained unchanged for this state. The sternal deflection increased between 2 and 4% and the effective stiffness decreased 3 and 4% for the localized load cases.

The weak sternum state generated one of the largest sternal deflections on the sled test, with an increment of 9%. This state also presented a moderate increase in the differential deflection and thus an increase in the combined deflection of 13%. The displacements in the coronal plane was similar to that for the intact state, the difference was on the 7th rib level, where the displacement along the craniocaudal axis showed larger amplitude.

In summary, the weak sternum state decreased the ribcage stiffness but this had only an effect on the localized loads in the table top tests. This state decreased the ribcage coupling in both the lateral and craniocaudal directions.

3.5.1.3 Weak intercostal muscles

A 50% reduction on the elastic modulus of the intercostal muscles generated the second weakest response. This change caused loss of between 7 to 12% in stiffness as estimated in the different table top load cases. The sternal compression increased about 6% for all load cases on the table top. In this state and in contrast with the two previous, all points on the ribcage deflected more than in the intact state. The differential deflection increased 4% for the belt load case. The difference between 4th and 7th rib levels suffered the third largest increment.

As for the sled test, THUMS with weak intercostals presented a 6% larger sternal deflection. A larger deflection than the intact state was also measured on the lower left chest, whereas the largest expansion among all states was reached by this state on the lower right chest, as in Figure 53. The differential deflection for this state was the largest among all weak states and this state experienced a 13% larger combined deflection value. The differences on the coronal plane displacements are mainly concentrated on the lower right side of the ribcage. In Figure 50 it is possible to observe the larger amplitude of displacements on the craniocaudal and lateral axes.

In THUMS, the weaker intercostal muscles reduced the chest stiffness and increased the sternal deflection. This state also presented the largest differential deflection, suggesting less coupling on the ribcage. The differential deflection in the sled test increased because the belted side suffered one of the largest deflections and the unbelted side presented the largest bulge out. An explanation for this is that the weak intercostal muscles made the 7th rib level more sensitive to localized loads by transferring less load to the neighboring ribs.

3.5.1.4 Weak costovertebral ligaments

The weak costovertebral ligaments state had no large effect on the effective stiffness or the sternal deflections. The largest effective stiffness drop was 2% for the belt load case. The sternal deflection increased 2% for the distributed load case. The deflections for all points on the ribcage were very similar to the intact state; especially for the hub and belt load cases, refer to Figure 39 and Figure 41. The differential deflection on the belt load case for the table top remained unchanged and a marginal increase was measured for the difference between deflections on the 4th and 7th rib levels as in Table 8.

3.5.1.5 Weak ribs

The weak ribs state had the weakest response for all load cases in the table top test, with exception for the distributed load case. The stiffness reduction varied from 16% for the hub load case to 7% for the distributed load case. The sternal deflection increased 10% for the hub load case and 7% for all other cases. The deflections increased on all tracked points of the ribcage, as in Figure 39 to Figure 45. The differential deflection for the belt load case increased the most compared to all other states. The difference between 4th and 7th rib levels for the hub load case presented a 10% increase, as in Table 13.

On the sled tests, the weak ribs state generated the largest sternal deflection and second largest differential deflection. The increment in differential deflection was a consequence of a larger deflection on the lower left chest point, the one under the belt. The unbelted side at the same level experienced almost no change compared to the intact state, as in Figure 53. The lower right chest displacements on the coronal plane had larger amplitude for this state compared to the intact sate. The DC value increased 13% and it was among the largest increments.

For THUMS, this state generated the weakest response on the sled and table top tests, with exception for the distributed case. The weak ribs state differential deflections were among the largest on the sled and table top tests. Since the ribs are the main load paths, the differential deflection increment reflects a weaker load bearing structure rather than a coupling loss.

3.5.1.6 Weak states summary

The whole body kinematics during the sled test was barely affected by the modifications introduced on the weak states. The head and T8 longitudinal displacements were similar between these states. The intercostal muscles state was the one that produced responses that deviated the most as compared to the intact response, with an increase of about 6% on the T8 longitudinal displacement, as shown in Figure 47.

The states that decreased the effective stiffness the most were the weak ribs and weak intercostals. Both states reduced the stiffness in all load cases. On the other hand, the weak sternum and weak rib cartilage states reduced the stiffness mainly on the localized loads, the hub and belt. This result could be used to tune the response of an ATD or HBM to localized and distributed loads. For example, assume that a model is too stiff for distributed loads but has a correct response for localized loads. This model can be made more humanlike by making the ribs weaker. This change will decrease the stiffness for all type of loads and as such improve the model response to distributed loads. A stiffer sternum and/or rib cartilage will then return the stiffness response to localized loads to an adequate level.

The two states with the largest differential deflection on the table top and sled tests were the weak ribs and weak intercostals muscles. The weak ribs presented the largest dD on the table top followed by the weak intercostals muscles, while the weak intercostals suffered the largest dD on the sled test. In THUMS, the weak intercostals muscles state was the most sensitive to the load imposed from inertia of the internal organs. The unbelted lower right chest site experienced the largest bulge out among all weak states, and the lower left site had one of the largest deflections. These two increments combined and gave the largest dD on the sled test. On the table top test, on contrary, the increment in dD was only due to the larger inward deflection on the belted side.

The simulations with THUMS on the table top tests showed that the hub load case was the most sensitive to the different weak states.

3.5.2 ATD-like states

The ATD-like states results should not be compared quantitatively since the changes among the states were of different nature and thus not comparable. The results will be presented with reference to the intact state.

3.5.2.1 Stiffer ribs

The stiffer ribs state increased the effective stiffness for all load cases in the table top test. The hub load case had the largest increase in effective stiffness. In accordance with a stiffer ribcage, all deflections measured on the chest were smaller than in the intact state. As for the differential deflection, refer to Table 13, it decreased for this state. The difference between deflections on the 4th and 7th rib levels also decreased.

In the sled test, the sternal deflection was 7% less and the differential deflection was 4% less than for the intact state. The displacements on the coronal plane were similar to those of the intact state.

The stiffer ribs made the ribcage stiffer. The reduction in differential deflections was a consequence of stiffening the ribcage. Since no structure that contributes to coupling was modified, the reduction should be due to increased stiffness and not considered as an increased coupling.

3.5.2.2 Shorter cartilage

The state with shorter cartilage deformed 4% less under the hub table top load case compared to the intact state and presented a 10% higher stiffness in that load case. This result was expected since the hub was engaging a larger bony region and less cartilage after the change was introduced. The distributed load case responded with 2% larger sternal deflection and 2% less stiffness than the intact state. This result was unexpected, since less cartilage and longer rib bone were thought to increase the ribcage stiffness. A possible explanation to this softer response is that the costochondral joints were pushing the rib cartilage and sternum inside the chest since the ribs end were pointing to the ribcage interior, as depicted on Figure 68. In contrast, the rib ends on the intact state were pointing outside the ribcage in the intact state. The belt and double belt cases showed a larger chest deflection, but an increase in stiffness. This apparent inconsistency in the results was a result of the position of the chest deflection measuring points. The sternal deflection was taken at the sternum bone, while the chest deflection to calculate the stiffness was taken on the respective loading device. The most important result for this state was the drastic decrease in differential deflection and even a reduction on the compression difference between the 4th and 7th rib levels during the hub table top load case, refer to Table 13. These results suggest a more coupled ribcage.

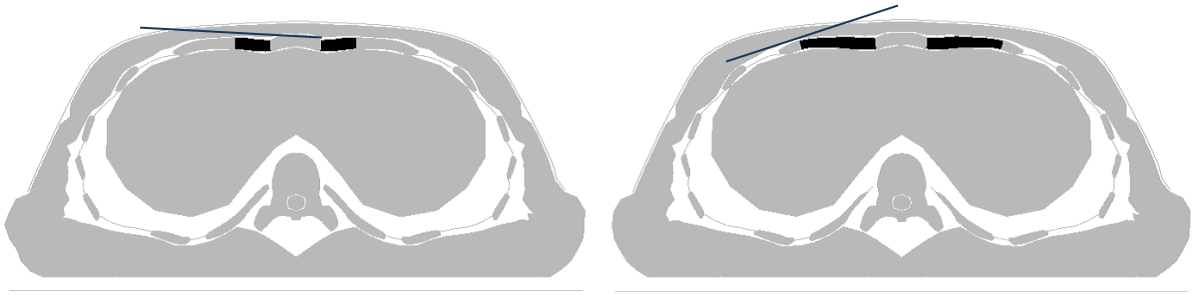

Figure 68. Transversal view at the 4th rib level of the deformed ribcage under the distributed load. Shorter cartilage state on left and intact on right. The rib cartilage is displayed in black and the line illustrates the rib tangent at the costochondral join.

On the sled test, the sternal deflection decreased around 6%. Note that the sudden increase in chest compression showed in Figure 57 at around 110 ms was discarded since at that time the ribcage and the abdominal organs presented an unrealistic contact. Therefore, all tabulated data for DC, DS, dD and displacements on the coronal plane for this state were taken at time 88 ms. Again, even more important than the decrease in sternal deflection, the decrease in ribcage differential deflections was more significant during this load case. Differential deflections on levels 4th and 7th decreased drastically; refer to Table 14. From Figure 58 it was seen that the right point on the 7th rib level, unbelted side, presented a maximum bulge out that was half of the intact state. On the same figure, but for the left side, the deflection was the smallest among all ATD-like states.

3.5.2.3 Divided sternum

A stiffer first rib and a separated sternum at the level of the first intercostal space only changed the response of the load cases that engaged the shoulder on the table top tests, i.e. single belt and double belt. The single belt state responded with 3% less sternal deflection, while the double diagonal belt presented a 1% reduction compared to the intact state. In both cases, the cut on the sternum acted as a hinge, refer to Figure 69, and as a result the compression decreased on the 7th rib level points; but the differential deflection remained the same. The fact that only the load cases that engaged the shoulders presented a change in sternal deflection suggests that the cut of the sternum reduced the coupling between the shoulder and the sternum. In other words, the gap on the sternum made that the clavicle moved posteriorly without pulling the sternum at the same extent as in the intact state. As for the stiffness, it was the same for all load cases on the table top except for the belt, where the stiffness dropped. This drop in stiffness despite a reduction in sternal deflection can be explained by the fact that for the stiffness calculation an external measurement was used while an internal measurement was used on the sternal deflection.

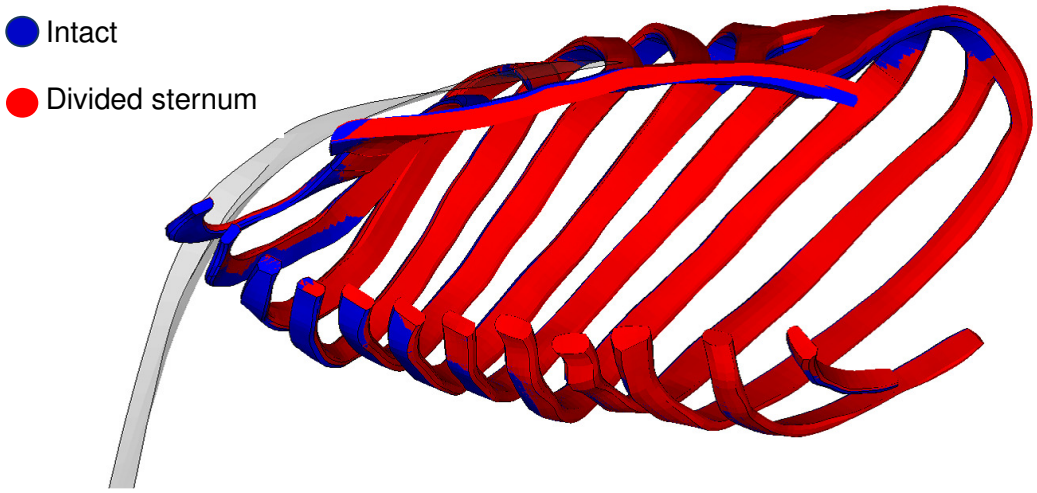

Figure 69. Mid sagittal view comparing the ribcage displacements between the intact and divided sternum states for the belt load case

The sternal deflection and differential deflections were very similar between this state and the intact during the sled tests. As on the table top tests, the deflection on the 7th rib level decreased; but the differential deflection remained practically unchanged. The maximum DC value was not altered for this state, compared with the intact as shown in Table 14.

3.5.2.4 Internal organs, 80% mass on spine

The losses in chest stiffness on the table top tests for this state were between 6 to 10%. The increase in sternal deflection was about 7% for all table top load cases. It is important to remind that the stiffness was calculated based on the exterior chest compression and the sternal deflection was measured on the skeleton. The differential deflection increased 12% for this state and the deflections were also larger on the points under the loader, as in Figure 42, suggesting a less coupled ribcage. There was a small change in the displacement pattern in the coronal plane. It presented slightly larger displacement in the craniocaudal direction.

In the sled tests the sternal compression was the second largest and it had the fastest compression rate, reaching the maximum compression earlier than for any other state (Figure 52). The left and right compressions at the 7th rib level are displayed in Figure 58, the left side compresses much more than any other state, particularly during the first 60 ms. The right side suffered compression and a small expansion, while all other states experienced expansion during the first 90 ms. As displayed in Figure 58, the differential deflection reached a value similar to that in the intact state, despite the very different responses experienced at the 7th rib level for these two states. The combined deflection value increased 14% with respect to the intact state. A factor that contributes to this larger DC value was the fact that the peak values for the differential deflection and the sternal compression coincide, while they were separated in time for about 15 ms for the other states.

The displacements in the coronal plane, showed in
Figure 51, had larger amplitude along the craniocaudal direction and different pattern compared to all previous states. The stiffness properties of the thoracic internal organs in this state remained, but they were 80% lighter. With these properties, the ribcage was unable to prevent the ribs to rotate and/or twist; suggesting that the thoracic internal organs inertial load plays an important role in the ribcage response.

In summary, the absence of inertial load from the internal organs on the ribcage generated a weaker response. This weaker response was characterized by a larger compression rate at the sternum; by a mainly compressive response at both points on the 7th rib level; and by larger downward displacements for all tracked points on the ribcage.

3.5.2.5 Stiffer ribcage-no internal organs

For the stiffer ribcage-no internal organs state the stiffness was found to increase for all table top load cases. The increase was 23% for the hub and 3% for the distributed load cases. The sternal deflection decreased as well for all table top load cases; 14% for the hub and 3% for the distributed cases (Table 12). The differential deflection in the diagonal belt table top test was 25% smaller than the intact value. The difference between deflections on the 4th and 7th rib levels for the hub case also decreased compared to the intact state. These results suggest a more coupled ribcage trough general stiffness increase.
The sternal deflection increased in the sled test and was the largest deflection among all simulated ATD-like states. The deflection rate increased as well and it was very similar to that of the internal organs state, see Figure 57. This state was the only state where the trend in sternal deflection was the opposite between the table top and the sled tests. While the sternal deflection for the belt case on the table top was 14% less than for the intact state, it was 15% larger during the sled test. At the same time, the differential deflection only reached about half of the intact state value. As shown in Figure 58, both points on the 7th rib level suffered compression during the whole events, in contrast with all other states where some expansion was always present on the unbelted side. The ribcage displacement in the coronal plane followed a pattern similar to the state 80% mass on spine (
Figure 51).

An attempt to explain e the observed opposite trends in sternal compression in the table top and in the sled tests is sketched in Figure 70. The diagram shows a simplified model of the chest as proposed by Lobdell et al. (1973). Mass m_1 represents the impactor mass, in this case a seat belt. Mass m_2 collects the sternum, a portion of the ribs and thoracic viscera mass. Mass m_3 represents the spine mass. The springs and dashpots represent the elasticity and viscous damping of the skin, ribcage and thoracic viscera. The three diagrams on the first row correspond to the table top test and the three on the bottom row represent the sled test. For both tests, the sternal deflection was larger on the 80% mass on spine state

compared to the intact state since the thoracic viscera inertial load decreased. As previously described, the stiff ribcage-no internal organs state had stiffer ribs, cartilage and costovertebral ligaments, represented by thicker springs on the diagram. At the same time, the internal organs mass was attached to the spine for this state. For the table top tests and the ribcage-no internal organs state, the inertial loading from the internal organs was negligible since the spine was constrained. The registered decrease in sternal deflection was then a result of a stiffer ribcage structure. In contrast, during the sled test, the spine was able to move and then the thoracic viscera inertial load was so large that even a stiffer ribcage was not able to stop it without experiencing a larger sternal deflection. Summing up, a relatively large increase in stiffness (23% for the hub and 10% for the belt) as measured on the table top was not enough to bring the sternal deflection to a level similar to that in the intact state during the sled test.

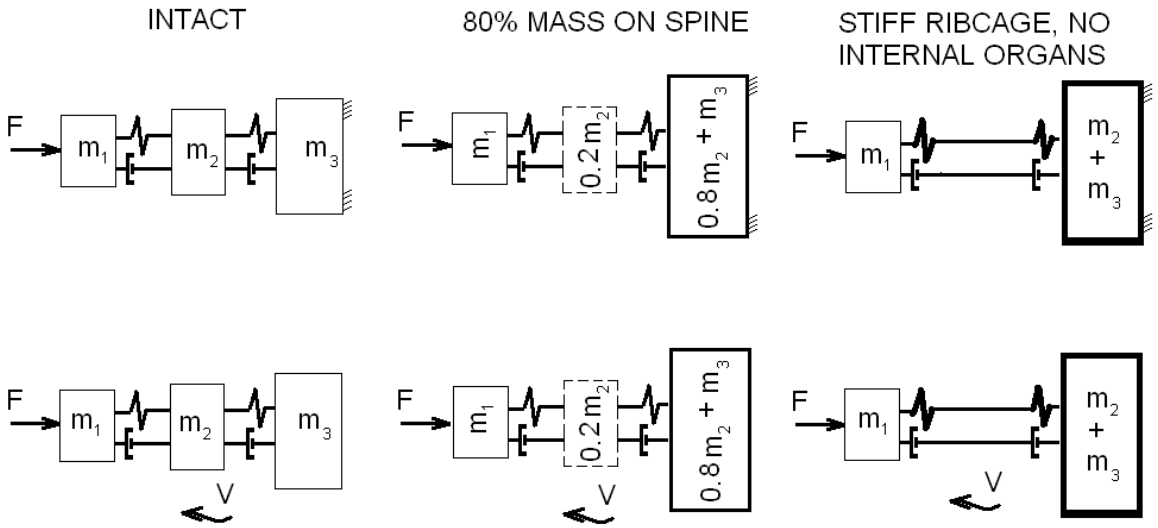

Figure 70. Diagram comparing the intact, internal organs: 80% mass on spine, and stiffer ribcage: 100% mass on spine states

3.5.2.6 Clavicle

The clavicle state was only studied in the sled test environment. The sternal deflection increased with 4% as compared to the intact state while the differential deflection decreased about 12%. The maximum DC value was unchanged. The compression of the upper right chest (belted side) decreased, as shown in
Figure 51, suggesting that the clavicle shielded the upper right chest region. At the same time, the deflection increased on the left side and this combination resulted in the largest difference between deflections for the left and right 4th rib levels among all states, as depicted in Figure 61.

The clavicle state also changed the model global kinematic response, mainly because of the change between the clavicle and shoulder belt interaction. The shoulder belt forces started to develop earlier for the clavicle state and they also reached a higher value compared to the intact state as shown in Figure 71. As a result of this earlier interaction, the clavicle state presented a larger yaw for the T1 and T8 vertebrae compared to the intact state during the first 80 ms, as shown in Figure 72. This larger yaw suggests that the whole trunk suffered a larger yaw rotation during the first 80 ms for the clavicle state, exposing the left ribs to higher belt loads. This could explain the larger compressions on the left thorax as shown in Figure 58.

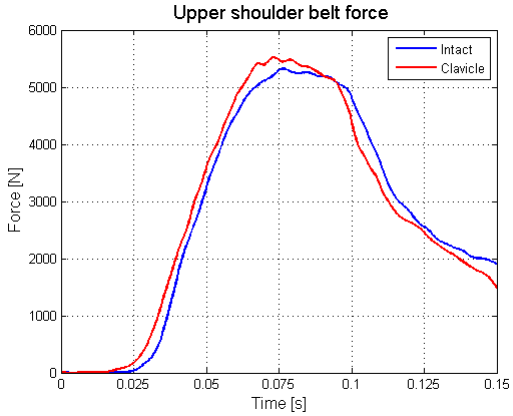

Figure 71. Shoulder belt forces for the intact and clavicle states

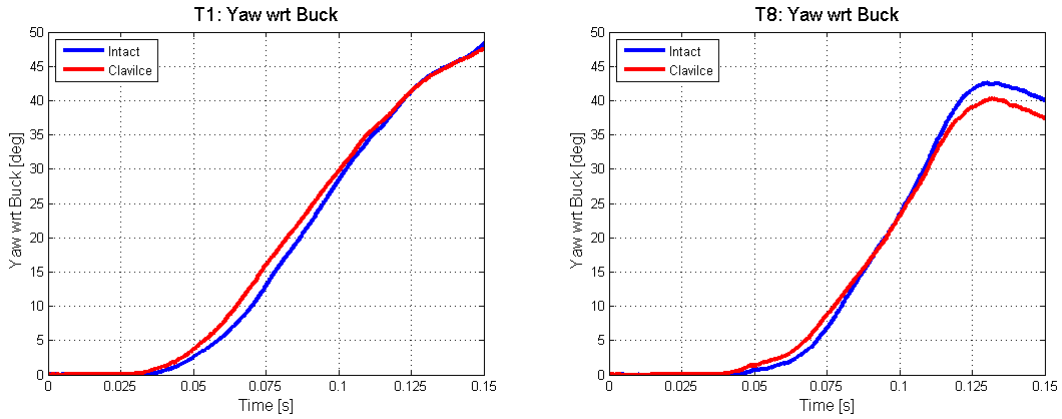

Figure 72. Yaw for the T1 and T8 during the sled tests wrt buck coordinate system

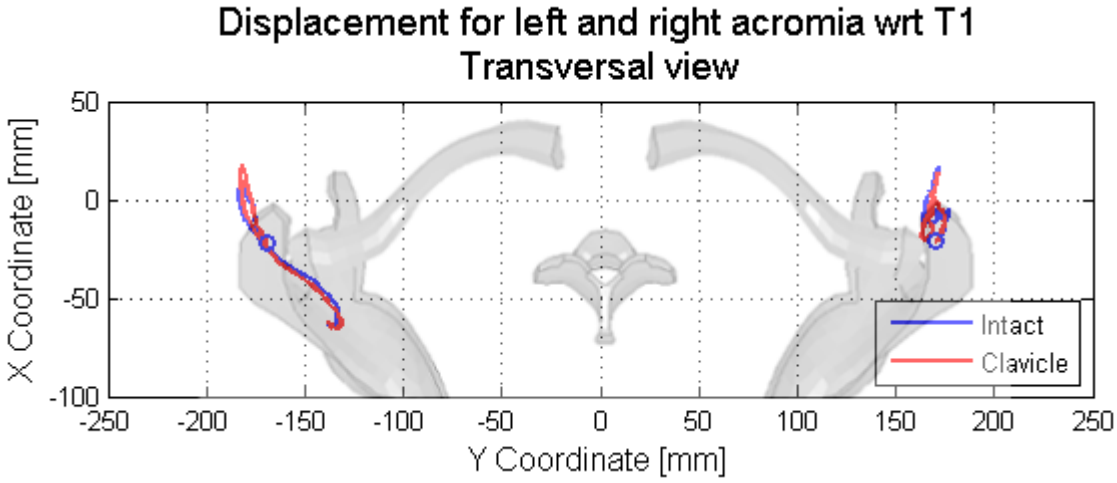

Figure 73. Left and right acromia trace on the transversal plane during sled test

3.5.2.7 ATD-like states summary

The head and T8 longitudinal displacements varied among the ATD-like states, as shown in Figure 48. The states with reduced thoracic viscera inertia presented larger forward excursions than all other states. The clavicle state showed less forward excursion. These states influenced the global kinematics, in contrast with the small variations that the weak states introduced.

Among the ATD-like states, the divided sternum state was the state that generated the smallest changes in thoracic responses. All other states had a large influence on the thoracic response.

A common result for the ATD-like states, except for the 80% mass on spine state, is that all of them presented smaller differential deflections than the intact state for the table top tests. These states had also a larger stiffness than the intact state for the table top tests. The 80% mass on spine state had a lower stiffness and larger differential deflection. These results suggest an inverse relationship between chest stiffness and differential deflection.

The opposite trends in sternal compression between the table top and sled tests for one of the states, the stiffer rib and 100% mass on spine, showed the importance of the thoracic viscera inertial load.

The clavicle state shielded the upper right chest. It also generated larger upper shoulder belt forces than the intact state, induced more T8 yaw rotation up to 80 ms and produced the shortest forward excursion. The chest defections were also different even though the maximum DC value remained similar to that for the intact state.

3.6 Limitations

There are some limitations on this work that are worth to mention. The first is that apart from the stiffer ribcage without internal organs state, no other state combinations were performed. This did not allow studying the interactions between different states.

To our knowledge, the THUMS version used in this work has not been validated against tests assessing ribcage coupling like those in Shaw et al. (2007). Despite this, the deflection on different thoracic points in THUMS showed a fairly good agreement with the experimental sled test results presented in Appendix B. One more concern about the THUMS model is the interaction between the ribcage and the abdominal organs. For the short cartilage state, an unrealistic interaction between the lower ribs and the abdominal viscera generated the maximum peak in sternal compression at 110 ms. This interaction did not represent a problem for the parametric study described in this work because the relevant parameters had their maximum before 100 ms, being the only exception the short cartilage state.

No element elimination was included on the THUMS ribcage, therefore no fractures were simulated. From the number of rib fractures and bulging out responses during the PMHS sled tests, it seems that greater number of fractured ribs led to larger bulging out values for the lower right chest which in turn generated larger differential deflections. As stated before, rib fractures were not simulated with the model and it is not planned to simulate them with THOR.

3.7 Conclusions

The conclusions of this work are divided into two sections. The first presents conclusions regarding the ATD design implications and the second about the DC criterion.

3.7.1 ATD Design

The whole kinematic response of THUMS was not substantially affected by the weak states. All three states that changed the kinematic response the most belong to the ATD-like category. These states were the 80 % mass on spine, the stiff ribcage – no internal organs, and the clavicle. The first two increased the forward excursion of the head and T8, while the clavicle state reduced that displacement. These results suggest that small changes on THOR ribcage stiffness will not affect its kinematic response, but changes on its clavicle and thoracic mass distribution will probably do.

Different tests on THOR indicate that it has a stiffer response than PMHS (Shaw et al. (2005)). The parametric study has shown that the weak ribs state decreased the effective stiffness the most. Hence, a large reduction in THOR chest stiffness could be achieved by a substantial decrease in the thickness or height of the ribs in the THOR.

In general, the different states suggested an inverse relationship between stiffness and coupling. All weak states responded with a lower effective stiffness than the intact state and all of them presented larger differential deflection that that for the intact state. One relevant state for the ATD design is the stiff ribcage – no internal organs state where the ribcage was stiffened up and the whole thoracic viscera mass was attached to the spine. In this case, the differential deflection was less than half of the value for the intact state; while the sternal deflection was 15% larger.

The thoracic viscera inertial load had a significant influence on THUMS kinematic and ribcage responses. The state stiff ribcage-no internal organs presented the largest chest deflection, deflection rate, and lowest differential deflection on the sled tests. On the other hand, this state responded with the largest effective stiffness during the table top tests. An even stiffer ribcage would have been needed to achieve a chest deflection similar to that for the intact state. Based on this parametric study results, it is expected that an increase in stiffness will be accompanied by an increment in coupling, larger caudal displacements on the ribcage.

The jacket in THOR is intended to represent the intercostal muscles. THUMS has a jacket to simulate the fat and muscular tissues around the ribcage, the intercostal muscles are included on the model. During the simulations with weak intercostal muscles, the unbelted side presented larger displacements on the Y and Z axes compared to the intact state while they were about the same value for the belted side. One possible explanation is that the THUMS jacket was compressed against the ribcage on the region engaged by the belt while it was barely in contact on the unbelted side, letting the ribs underneath to move more. There is a risk for the THOR jacket to act in a similar way. In that case, during the hub load case, the jacket would be engaging a small surface and therefore underestimating the intercostal muscles effect. While in the distributed load case the jacket would be engaging a large surface and increasing the intercostal muscles effect.

The state with the anteriorly displaced clavicle shielded the upper chest on the belted side. This state changed the kinematic response as well; THUMS had a 10 % shorter forward excursion and an earlier shoulder belt force development compared to the intact state.

Different states experienced a change on the displacement pattern in the coronal plane. This pattern change could modify the deflection results. For example, a larger caudal rib rotation may be interpreted as a larger rib compression. It is therefore suggested that the biofidelity requirements for ATD and HBM include 3D displacements for some points on the ribcage and not only their deflection.

3.7.2 DC criterion

The combined deflection criterion (DC) contains the sum of the sternal deflection (DC) and the differential deflection (dD), as defined in section 3.2.3. The following paragraphs will focus on these three variables.

Weak intercostal muscles and weak ribs were the states with largest dD, for both tabele top and sled tests. The smallest dD values for these tests were found on the sates shorter cartilage and stiff ribcage-no internal organs. As mentioned before, THUMS showed an inverse relationship between coupling and chest stiffness. This implies that for THUMS, an increase in chest stiffness is followed by a decrease in DS and dD.

For THUMS and during the sled tests, the states responded with different DS and dD peaks and with varying timings for those peak values. Since the DC value is reported as one value, corresponding to its maximum, and the DC is calculated as the sum of DS and dD, it is important to consider their timing. For example, the peaks for the clavicle state were separated 28 ms, while for the intact state this value was only 16 ms. It is therefore relevant to verify the influence that the changes performed on the ATD have on dD and DS timing.

4 Human body model studies into stiffness requirements for the rib cage: A parametric study on thoracic response part II

4.1 Introduction

Current two frontal impact dummies (HYBRID-III and THOR) do not represent organs, such as lungs and heart, and have rigid connections between the ribs and the spine. Does this simplification (called organ simplification in the following text) constitute a critical handicap for their biomechanical performance? In order to answer this question, it is important to quantify the influences of organs and rib-spine joints on the thoracic behavior of the human body. The HUMOS2LAB model was used to study into the influences. To do this, lungs, heart, stomach, liver, spleen, kidney and soft tissues between them were removed from the baseline model. The mass of these organs were added to the ribcage for half, and to the thoracic spine for the other half. Muscles in frontal of the lumbar spine were also deleted and their masses were added to lumbar spine. Following configurations were simulated with the baseline model and the modified model:

- Kroell frontal impactor test configuration at 4.3 m/s,
- Frontal sled test configuration with a 3-points belt restraint,
- Frontal sled test configuration with a combined 3-points belt and airbag restraint.

It is to be noted that simulations with organ simplification stopped at 65 ms for belt-only loading and at 69 ms for combined belt and airbag loading due to numerical instability. However, this early running stop does not affect the comparison of rib strain profile since rib fractures mainly occurred before and the calculation of strain profile considers only what happens before the occurrence of rib fracture.

4.2 Influence of organs and rib-spine joints on thoracic stiffness

Figure 74 shows influences of the organ simplification in frontal Impactor test at 4.3 m/s. Following observations can be made based on the comparison:

- Organ simplification affects little the thoracic stiffness in the onset phase, but significantly in the phase just after the onset.
- Thoracic deflection is 15% larger with organ simplification.

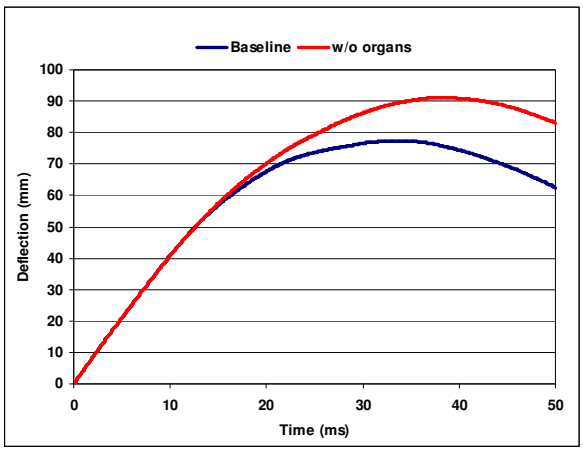

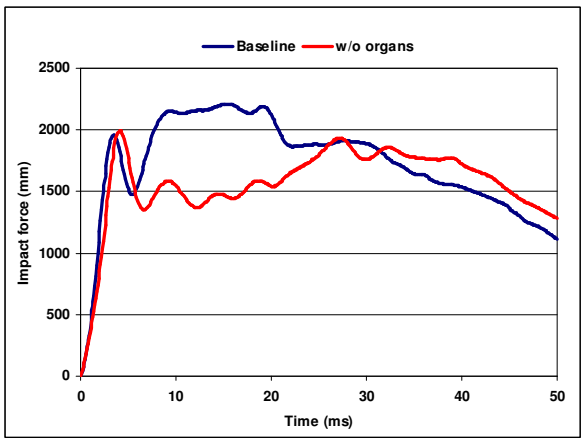

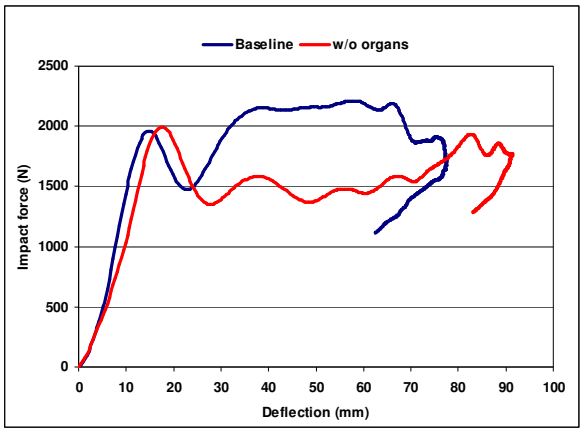

Figure 74. Comparison in frontal impactor test between the baseline model and the modified model where the internal thoracic organs were removed and the rib-spine joints were blocked.

4.3 Influence of organs and rib-spine joints on rib strain profile

Figure 75 Figure 76 and Figure 77 show the influences of organ simplification under three types of loadings:

- Frontal Impactor loading
- Belt loading in frontal sled test
- Combined belt and airbag loading in frontal sled test

The influences were examined in four different ways:

- Column 1 compares RMS (Root Mean Square of strain, refer to Section 2.2.3 for its definition), which is an indicator of global strain level sustained by the rib considered, and is proportional to deformation energy absorbed by the rib under a pure bending.
- Column 2 compares average normalized strain profile of each rib. The strain gauge measurement was normalized by RMS, and was averaged in the time interval between 10% and 99% of RMS max. What happens after rib fracture was not considered.
- Column 3 compares normalized strain profile at the time where the maximum of RMS was reached. What happens after rib fracture was not considered.
- Column 4 compares strain profile without normalization at the time where the maximum of RMS was reached. What happens after rib fracture was not considered.

Following remarks should be noted when examining this comparison:

- For identical loading conditions, RMS depends on anthropometry and mechanical properties of subjects tested. So this comparison should be examined with precaution: there is no normalization of results. This is true also for comparisons of column 3 and column 4.
- The average normalized strain profile should be privileged: it characterizes the best the strain profile for a given type of loading since results were normalized and averaged.
- Ribs 1 and 10 were instrumented with few gauges in PMHS tests, so precision should be considered with precaution.

- Positive strain corresponds to traction, and negative strain to compression.

Following observations can be made based on these comparisons:

- Globally, rib strain profile does not change very much with organ simplification.
- Ribs were far more strained with organ simplification, as RMS curves indicate.
- For loading configurations including a shoulder belt, organ simplification resulted in strain amplitude decrease on the no belt loading side of the lower ribs (7th, 8th, 9th and 10th ribs), but increase in their belt loading side, in particular near the spine. This means that the action of belt loading is locally accentuated with organ simplification. However, this modification of strain profile does not modify fracture locations, therefore does not constitute a fundamental change.

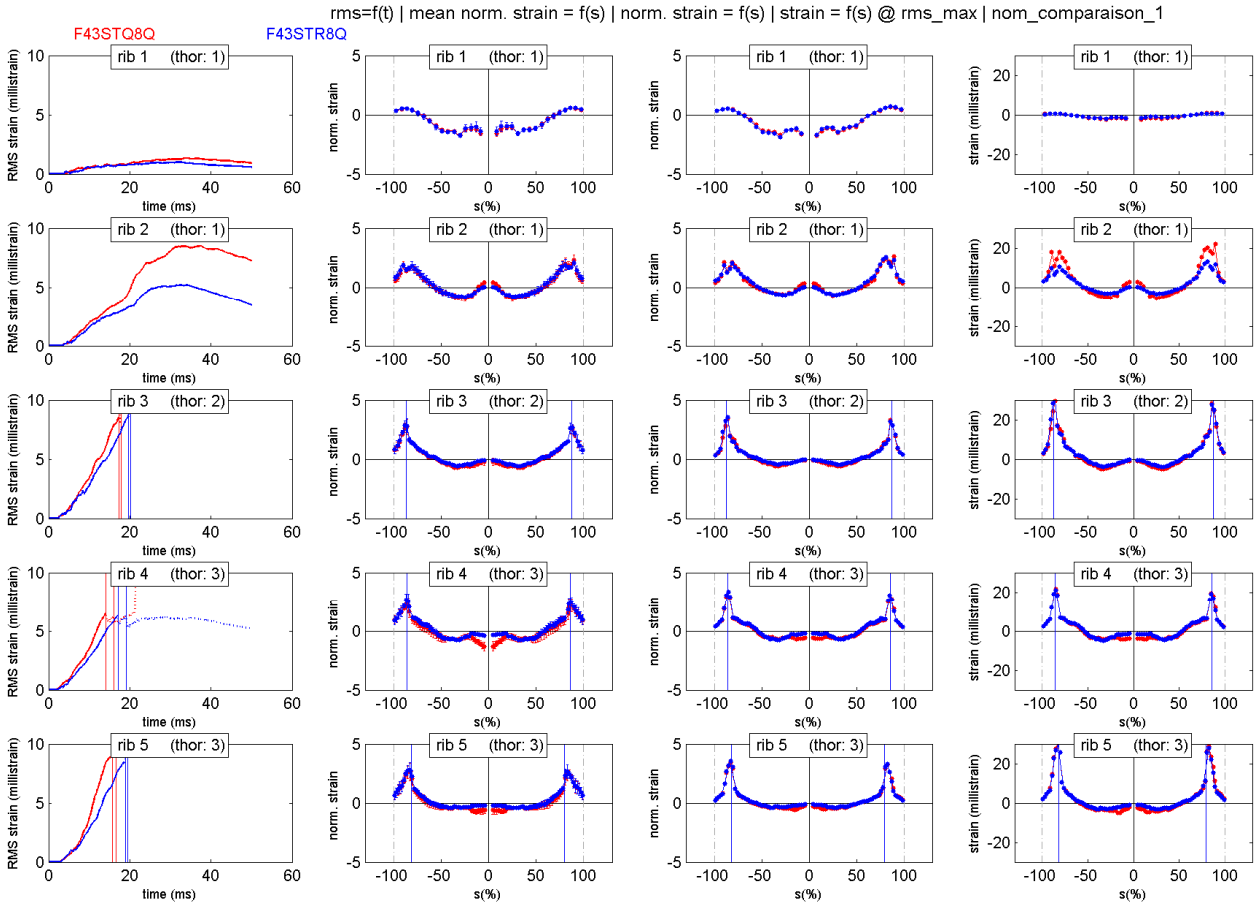

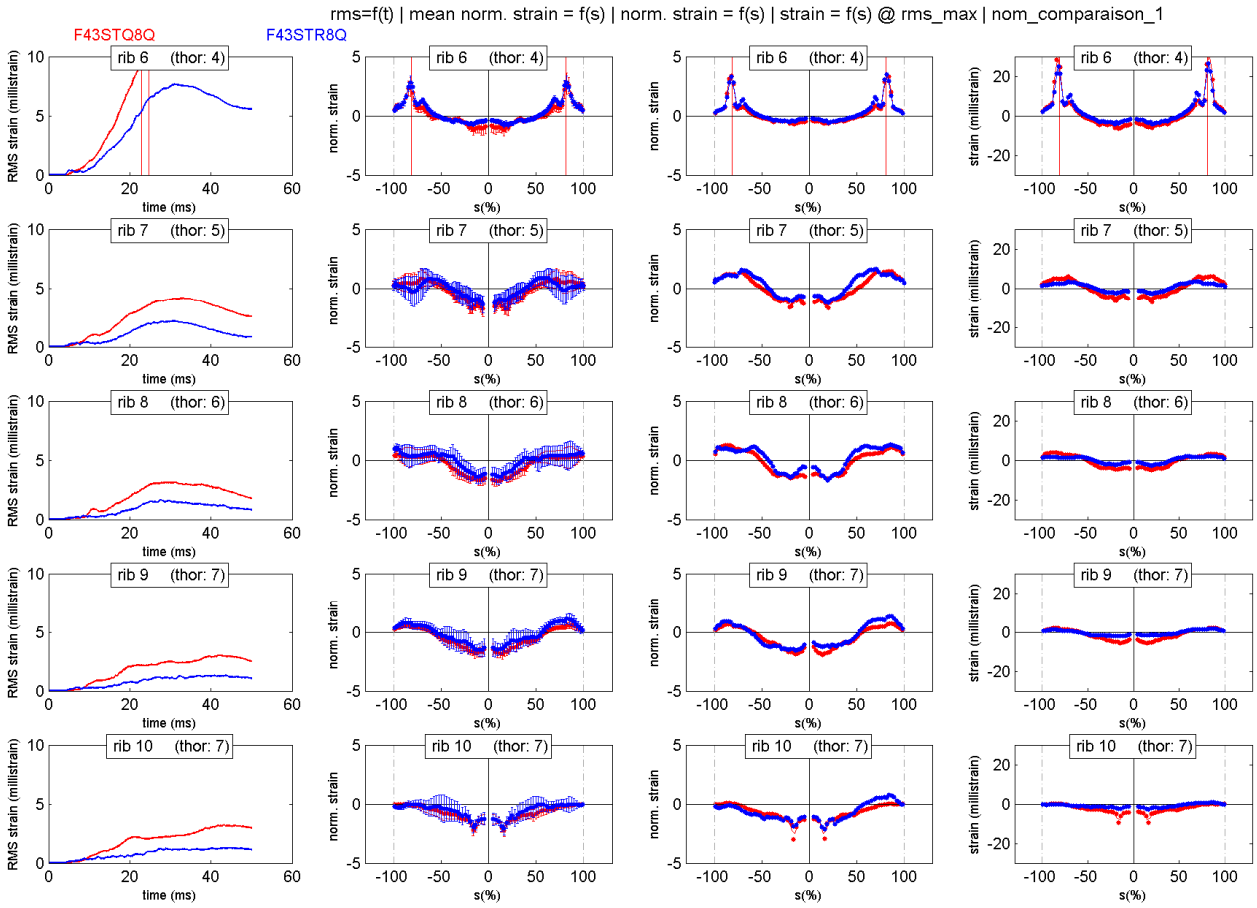

Figure 75. Rib strain profile comparison in frontal impactor test between the baseline model (in blue) and the modified model (in red) where the internal thoracic organs were removed and the rib-spine joints were blocked. For RMS curves, the portions beyond rib fracture were plotted in dot lines, and were not considered to calculate strain profile.

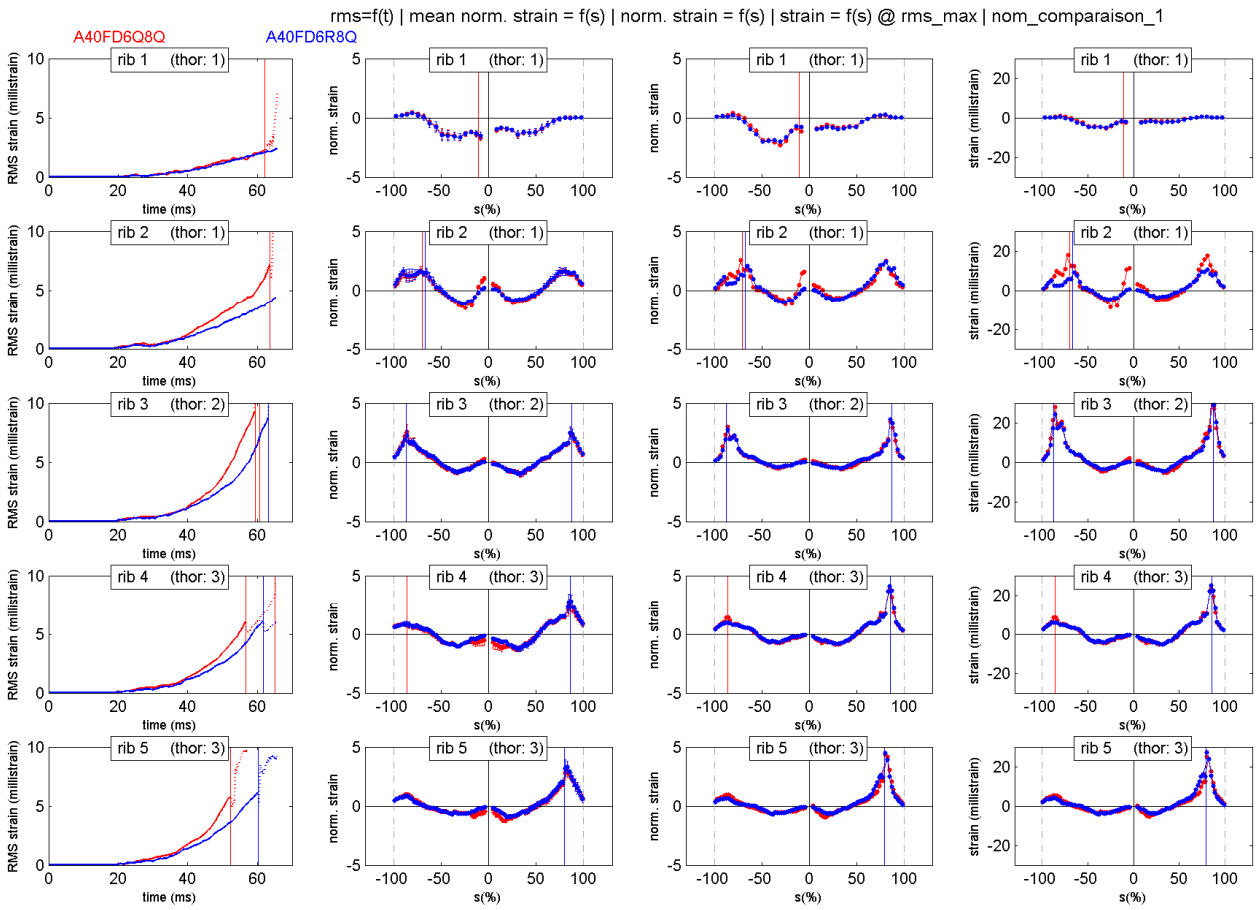
rms=f(t) | mean norm. strain = f(s) | norm. strain = f(s) | strain = f(s) @ rms_max | nom_comparaison_1
A40FD6Q8Q
A40FD6R8Q
rib 1 (thor: 1)
rib 2 (thor: 1)
rib 3 (thor: 2)
rib 4 (thor: 3)
rib 5 (thor: 3)
RMS strain (millistrain)
norm. strain
strain (millistrain)
time (ms)
s(%)

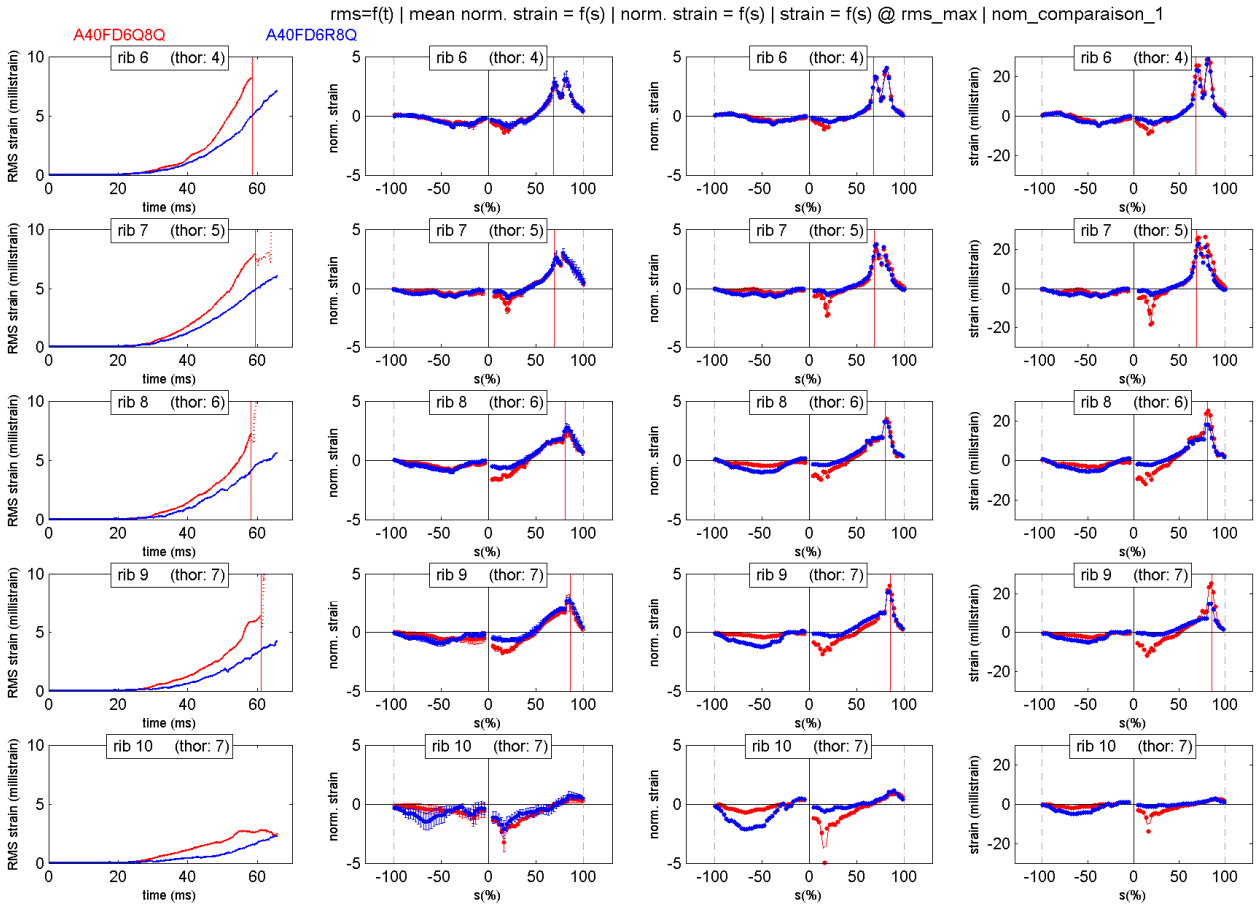

Figure 76. Rib strain profile comparison under belt only restraint in frontal sled test between the baseline model (in blue) and the modified model (in red) where the internal thoracic organs were removed and the rib-spine joints were blocked. For RMS curves, the portions beyond rib fracture were plotted in dot lines, and were not considered to calculate strain profile.

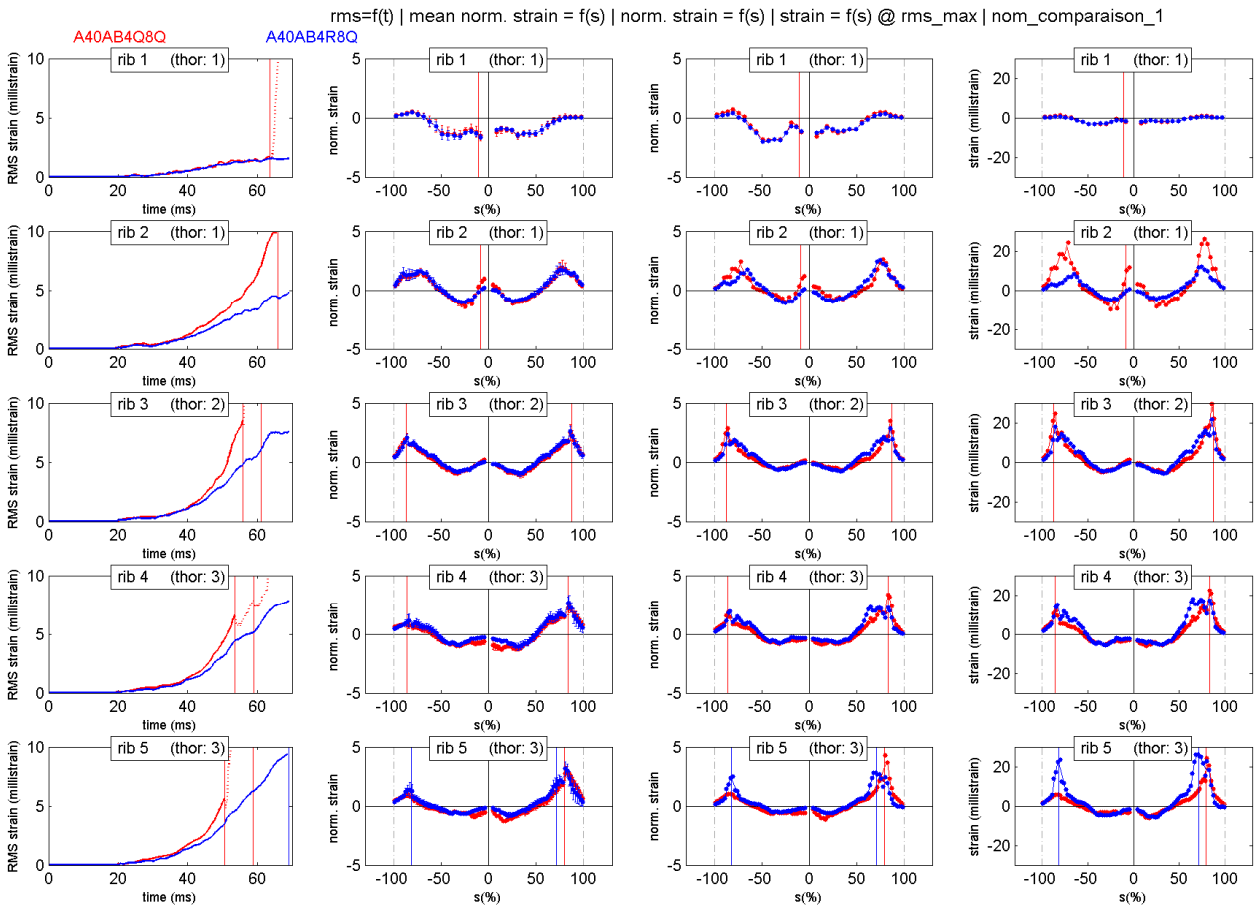
rms=f(t) | mean norm. strain = f(s) | norm. strain = f(s) | strain = f(s) @ rms_max | nom_comparaison_1
A40AB4Q8Q
A40AB4R8Q
rib 1 (thor: 1)
rib 2 (thor: 1)
rib 3 (thor: 2)
rib 4 (thor: 3)
rib 5 (thor: 3)
RMS strain (millistrain)
norm. strain
strain (millistrain)
time (ms)
s(%)

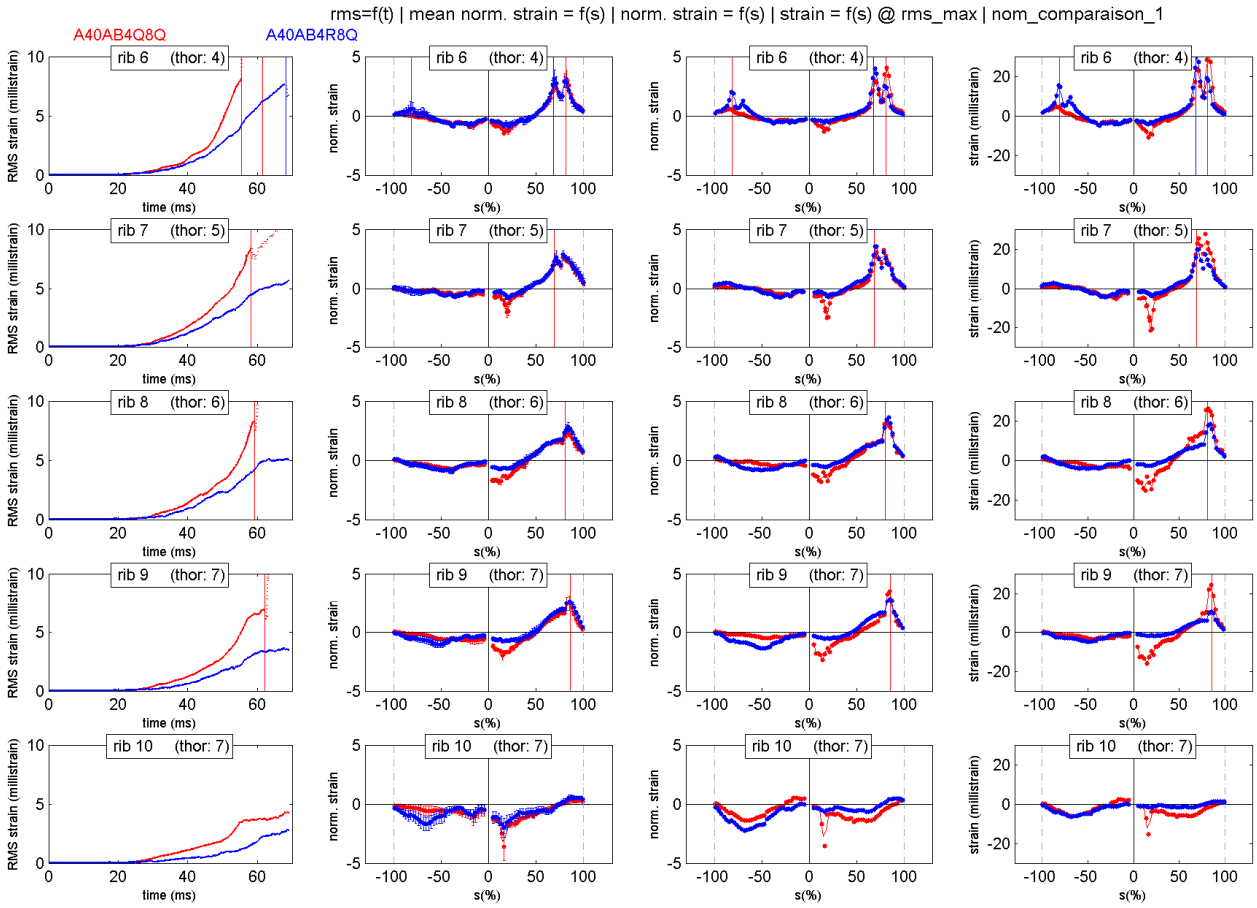

Figure 77. Rib strain profile comparison under combined belt and airbag loading in frontal sled test between the baseline model (in blue) and the modified model (in red) where the internal thoracic organs were removed and the rib-spine joints were blocked. For RMS curves, the portions beyond rib fracture were plotted in dot lines, and were not considered to calculate strain profile.

4.4 Conclusions

Based on above simulation results, it seems that organ simplification does not fundamentally change the thoracic behavior. The main features of rib strain profile remain the same, and the global stiffness decrease of the thorax may be compensated in a mechanical dummy by using stiffer rib materials. These conclusions suggest that it may not be necessary to represent organs and rib-spine joints in a mechanical dummy.

5 General conclusions

In the THORAX project, human body models were extensively used:

- to determine thoracic injury mechanism and define corresponding injury assessment criteria,
- to quantify the sensitivity of the suggested injury assessment criteria,
- to study thoracic stiffness and contributions of the various elements in the thorax to this stiffness.

Related to the studies on injury mechanism and injury assessment criteria it was concluded that:

- A human body model, the HUMOS2LAB, was validated with respect to four types of biomechanical data: 1) global force and deflection-based corridors, 2) rib strain profile, 3) spacial repartition of rib fractures and 4) ribcage damage evolution versus loading severity, under different loading types and regarding different impact directions.
- A series of simulations using the HUMOS2LAB model were performed, forming a "virtual" PMHS tests database. Five loading types were covered by this database: 3 points shoulder-lap belt restraint, 3 points shoulder-lap belt + airbag restraint, and airbag only restraint in sled test environment, airbag and cylinder impactor loading in static environment. For each simulation, rib fracture outcome was established and different metric of ribcage deflection were recorded.
- Based on these "virtual" PMHS tests, excessive strain, generated mainly by bending, was identified as mechanism of rib fractures.
- It was demonstrated that maximum peak strain of ribs does not predict number of fractured ribs correctly. It was suggested to directly use the NFR (Numbers of Fractured Ribs) as a global injury criterion. A scheme to use the NFR on a mechanical dummy, where ribs always remain in elastic state, is proposed. The NFR offers potential to be a universal injury criterion - restraint independent, impact direction independent and suitable for evaluating different levels of injuries.
- A more usual metric, named as Combined Deflection and noted as Dc, is also proposed. This metric is a global deflection-based predictor for serious injury (more than six fractured ribs). Injury curve and risk curve constructed with this criterion do not vary significantly from one loading type to another. It has potential to candidate as a restrain-independent injury predictor.
- Both the above mentioned criteria have been reported to the THORAX team and have been considered in the demonstrator THOR dummy. For the Combined Delfection criterion multiple point chest deflection measurement device (3D-ITRRAC) was developped. For the evaluation of the NFR criterion the chest cage of the demonstrator was instrumented with a suitable numbers of strain gages.

Related to the sensitivity study of the suggested injury assessment criteria, it was focused on the sternal deflection (C) and the differential deflection (dD) between the lower right and left thorax deflection. This part of the studies assesses the sensitivity of these parameters to design changes:

- In general, THUMS showed an inverse relationship between coupling and chest stiffness. This implies that for THUMS, an increase in chest stiffness is followed by a decrease in both the C and dD.
- Weak intercostal muscles and weak ribs were the states with largest dD, for both table top and sled tests. The smallest dD values were found when the cartilage was

made shorter and ribcage was made stiffer in combination with removal of the internal organs.
- For THUMS in the sled tests condition, the C and dD peak values varied in amplitude and timings. Since the DC value is reported as one single value, corresponding to its maximum, and the DC is calculated as the sum of C and dD, it is important to consider their timing. For example, the peaks for the clavicle state were separated 28 ms, while for the intact state this value was only 16 ms. It is therefore recommended to verify the influence that the changes introduced to an ATD have on dD and C in terms of timing.

Related to the thoracic stiffness studies using the THUMS model it was concluded that:

- The modified Total HUman Model for Safety (THUMS) version 3.0 showed a response very close to that of PMHS in pendulum impacts according to GESAC (2005), table top tests by Kent et al. (2003, 2004, 2005) and sled tests by Shaw et al. (2009). Also for denuded and eviscerated subjects the model performed well.
- The whole kinematic response of THUMS was not substantially affected by the weak states. All three states that changed the kinematic response the most belong to the ATD-like category. These states were the 80 % mass on spine, the stiff ribcage – no internal organs, and the clavicle. The first two increased the forward excursion of the head and T8, while the clavicle state reduced that displacement. These results suggest that small changes on THOR ribcage stiffness will not affect its kinematic response, but changes on its clavicle and thoracic mass distribution will probably do.
- Different tests on THOR indicate that it has a stiffer response than PMHS (Shaw et al. (2005)). The parametric study has shown that the weak ribs state decreased the effective stiffness the most. Hence, a large reduction in THOR chest stiffness could be achieved by a substantial decrease in the thickness or height of the ribs in the THOR.
- In general, the different states suggested an inverse relationship between stiffness and coupling. All weak states responded with a lower effective stiffness than the intact state and all of them presented larger differential deflection that that for the intact state. One relevant state for the ATD design is the stiff ribcage – no internal organs state where the ribcage was stiffened up and the whole thoracic viscera mass was attached to the spine. In this case, the differential deflection was less than half of the value for the intact state; while the sternal deflection was 15% larger.
- The thoracic viscera inertial load had a significant influence on THUMS kinematic and ribcage responses. The state stiff ribcage-no internal organs presented the largest chest deflection, deflection rate, and lowest differential deflection on the sled tests. On the other hand, this state responded with the largest effective stiffness during the table top tests. An even stiffer ribcage would have been needed to achieve a chest deflection similar to that for the intact state. Based on this parametric study results, it is expected that an increase in stiffness will be accompanied by an increment in coupling, larger caudal displacements on the ribcage.
- The jacket in THOR is intended to represent the intercostal muscles. THUMS has a jacket to simulate the fat and muscular tissues around the ribcage, the intercostal muscles are included on the model. During the simulations with weak intercostal muscles, the unbelted side presented larger displacements on the Y and Z axes compared to the intact state while they were about the same value for the belted side. One possible explanation is that the THUMS jacket was compressed against the ribcage on the region engaged by the belt while it was barely in contact on the unbelted side, letting the ribs underneath to move more. There is a risk for the THOR jacket to act in a similar way. In that case, during the hub load case, the jacket would be engaging a small surface and therefore underestimating the intercostal muscles

effect. While in the distributed load case the jacket would be engaging a large surface and increasing the intercostal muscles effect.

- The state with the anteriorly displaced clavicle shielded the upper chest on the belted side. This state changed the kinematic response as well; THUMS had a 10 % shorter forward excursion and an earlier shoulder belt force development compared to the intact state.
- Different states experienced a change on the displacement pattern in the coronal plane. This pattern change could modify the deflection results. For example, a larger caudal rib rotation may be interpreted as a larger rib compression. It is therefore suggested that the biofidelity requirements for ATD and HBM include 3D displacements for some points on the ribcage and not only their deflection.

Related to the thoracic stiffness studies using the HUMOS2LAB model it was concluded that:

- Organ simplification (i.e. without representing organs, such as lungs and heart, and using rigid connections between the ribs and the spine) does not fundamentally change the thoracic behavior. The main features of rib strain profile remain the same, and the global stiffness decrease of the thorax may be compensated in a mechanical dummy by using stiffer rib materials. These conclusions suggest that it may not be necessary to represent organs and rib-spine joints in a mechanical dummy.

6 Acknowledgements

This work was performed in the framework of the EU funded FP7 THORAX project. The authors would like to think the EU-Commission for the funding and the project partners for their collaboration.

7 References

7.1 References chapter 3

Bose, D., Pipkorn, B., Crandall, J., Lessley, D., Trowbridge, M. (2009) Multi-point thoracic deflection measurement as a predictor of rib injury in frontal collision. Proc. 30th International Workshop on Human Subjects for Biomechanical Research, Savannah, GA.

Bouquet, R., Ramet, M. (1994) Thoracic and pelvis human responses to impact. Proc. ESV1994 Munich.

Bouquet, R., Ramet, M., Bermond, F., Caire, Y., Talantikite, Y., Robin, S. and Voiglio, E. (1998) Pelvis human responses to lateral impact. Proc. ESV1998.

Burstein, A.H. et al. (1976) Aging of bone tissue : mechanical properties. Jouranl of Bone and Joint Surgery 58(A): 82.

Charpail, E., Trosseille, X., Petit, P., Laporte, S., Lavaste, F., Vallancien, G. (2005) Characterization of PMHS ribs: a new test methodology. Stapp Car Crash Journal 49: 183-198.

Kemper, A., McNally, C., Kennedy, E., Rath, A., Manoogian, S., Stitzel, J., and Duma, S. (2005) Material properties of human rib cortical bone from dynamic tension coupon testing. Stapp Car Crash Journal 49: 199-230.

Kemper, A.R., McNally, C., Pullins, C.A., Freeman, L.J., Duma, S.M., Rouhana, S.W. (2007) The biomechanics of human ribs: material and structural properties from dynamic tension and bending tests. Stapp Car Crash Journal 51: 235-273.

Kent, R., Lessley, D., Shaw, G., and Crandall, J. (2003) The utility of Hybrid III and THOR chest deflection for discriminating between standard and force-limiting belt systems. Stapp Car Crash Journal 47: 267-297.

Kroell, C., Schneider, D., Nahum, A. (1971) Impact Tolerance Of The Human Thorax I. Proc. 15th Stapp Car Crash Conference, pp. 84-134. Society of Automotive Engineers, Warrendale, PA.

Kroell, C., Schneider, D., Nahum, A. (1974) Impact Tolerance Of The Human Thorax II. . Proc. 18th Stapp Car Crash Conference, pp. 84-134. Society of Automotive Engineers, Warrendale, PA.

Lebarbé, M., Potier, P., Baudrit, P., Petit, P., Trosseille, X., Vallancien, G. (2005) Thoracic Injury Investigation Using PMHS in Frontal Airbag Out-of-Position Situations. Stapp Car Crash Journal 49: 323-342.

Lizee, E., Robin, S., Song, E., Bertholon, N., Le Coz, J.Y., Besnault, B. and Lavaste, F. (1998) Development of a 3D finite element model of the human body. Proc. 42nd Stapp Car Crash Conference, pp.115-138. Society of Automotive Engineers, Warrendale, PA.

Petitjean, A., Lebarbé, M., Potier, P., Trosseille, X., Lassau, J-P. (2002) Laboratory reconstructions of real world frontal crash configurations using the hybrid III and THOR dummies and PMHS. Stapp Car Crash Journal 46: 27-54.

Robin (2001). HUMOS: Human model for safety - A joint effort towards the development of refined human-like car occupant models. Proc. of the 17th Int. Tech. Conf. on the Enhanced Safety of Vehicles, Paper Number 297.

Shaw, G. et al. (2009) Rib Impact response of Restrained PMHS in frontal sled tests: Skeletal deformation patterns under seat belt loading. Stapp Car Crash Journal 53: 1-48.

Trosseille, X., Baudrit, P., Leport, T. and Valancien G. (2008) Rib cage strain pattern as a function of chest loading configuration. Stapp Car Crash Journal 52: 205-232.

Vezin, P., Verriest, J.P. (2005) Development of a set of numerical human model for safety. Proc. of the 19th Int. Tech. Conf. on the Enhanced Safety of Vehicles, Paper Number (05-0163).

Viano, D. (1989) Biomechanical responses and injuries in blunt lateral impact. Proc. 33th Stapp Car Crash Conference, pp.113-141. Society of Automotive Engineers, Warrendale, PA.

7.2 References chapter 4

Ali, T., Kent R., Murakami D. ,Kobayashi S. (2005). Tracking rib deformation under anterior loads using computed tomography imaging. SAE World Congress, Detroit, Michigan, USA, SAE International, Paper Number: 2005-01-0299.

Crandall, J. (2008), THOR NT advanced frontal crash test dummy, NHTSA Cooperative Agreement No. DTNH22-93-Y-07028,

GESAC (2005), Biomechanical response requirements of the THOR NHTSA advanced frontal dummy (Revision 2005.1), GESAC-05-03.

Hallquist, J. O. (2006). LS-DYNA Keyword user's manual. Version 970, Livermore Software Technology Corporation.

Kent, R., Lessley D. ,Sherwood C. (2004) Thoracic response to dynamic, non-impact loading from a hub, distributed belt, diagonal belt, and double diagonal belts, Stapp Car Crash J, 48: 495-519.

Kent, R., Murakami D. ,Kobayashi S. (2005). Frontal thoracic response to dynamic loading: the role of superficial tissues, viscera and the ribcage. International Research Council on the Biomechanics of Impact (IRCOBI), Prague, Czech Republic, pp. 355-365.

Kent, R., Sherwood C., Lessley D., Overby B. ,Matsuoka F. (2003). Age Related Changes in the Effective Stiffness of the Human Thorax Using Four Loading Conditions. International Research Council on the Biomechanics of Impact (IRCOBI), Lisbon, Portugal, pp. 249-264.

Lobdell, T. E., Kroell C. K., Schneider D. C., Hering W. E. ,Nahum A. M. (1973). Impact response of the human thorax, in: Human impact response: Measurement and simulation, Plenum Press, New York, pp. 201-245.

Murakami, D., Kobayashi S., Torigaki T. ,Kent R. (2006) Finite element analysis of hard and soft tissue contributions to thoracic response: sensitivity analysis of fluctuations in boundary conditions, Stapp Car Crash J, 50: 169-89.

Ruan, J., El-Jawahri R., Chai L., Barbat S. ,Prasad P. (2003) Prediction and analysis of human thoracic impact responses and injuries in cadaver impacts using a full human body finite element model, Stapp Car Crash J, 47: 299-321.

Shaw, C. G., Lessley D., Crandall J., Kent R. ,Kitis L. (2005). Dummy torso response to anterior quasi-static loading. Conference on Enhanced Safety of Vehicles, Washington, D.C., Paper 05-0371.

Shaw, C. G., Lessley D., Evans J., Crandall J., Shin J., Portier P. ,Paoloni G. (2007). Quasi-static and dynamic thoracic loading tests: cadaveric torsos. International Research

Council on the Biomechanics of Impact (IRCOBI), Maastricht, Netherlands, pp. 325-348.

Shaw, G., Crandall J. ,Butcher J. (2002) Comparative evaluation of the THOR advanced frontal crash test dummy, International Journal of Crashworthiness, 7(3): 239-254.

Shaw, G., Parent D., Purtsezov S., Lessley D., Crandall J., Kent R., Guillemot H., Ridella S. A., Takhounts E. ,Martin P. (2009) Impact response of restrained PMHS in frontal sled tests: skeletal deformation patterns under seat belt loading, Stapp Car Crash J, 53: 1-48.

Song E, Lecuyer E, Trosseille X (2011) Development of Injury Criteria for Frontal Impact Using a Human Body FE Model. Proc. of the 22nd Int. Tech. Conf. on the Enhanced Safety of Vehicles, Washington D.C., paper no 11-0330-O.

Toyota Motor Coorporation Toyota Central Labs Inc. (2008). User´s Guide of Computational Human Model THUMS - AM50 Occupant Model: Version 3.0-080225.

UNECE (2007), Uniform provissions concerning the approval of vehicles with regard to the protection of the occupants in the event of a frontal colission, Reg. 94

Untaroiu, C. D., Lim J. Y. ,Shin J. (2009) Evaluation of a thor dummy rigid-body model in frontal crash environment using objective rating techniques - biomed 2009, Biomed Sci Instrum, 45: 95-100.

Wu, G., Siegler S., Allard P., Kirtley C., Leardini A., Rosenbaum D., Whittle M., D'Lima D. D., Cristofolini L., Witte H., Schmid O. ,Stokes I. (2002) ISB recommendation on definitions of joint coordinate system of various joints for the reporting of human joint motion--part I: ankle, hip, and spine. International Society of Biomechanics, J Biomech, 35(4): 543-8.

Yaguchi, M., Ono K. ,Masuda M. (2008). Biofidelic responses of the THOR-NT and Hybrid III based on component tests. SAE World Congress, Detroit, Michigan, USA, Paper Number: 2008-01-0520.

8 APPENDIX A. Results of the HUMOS2LAB thorax model validation

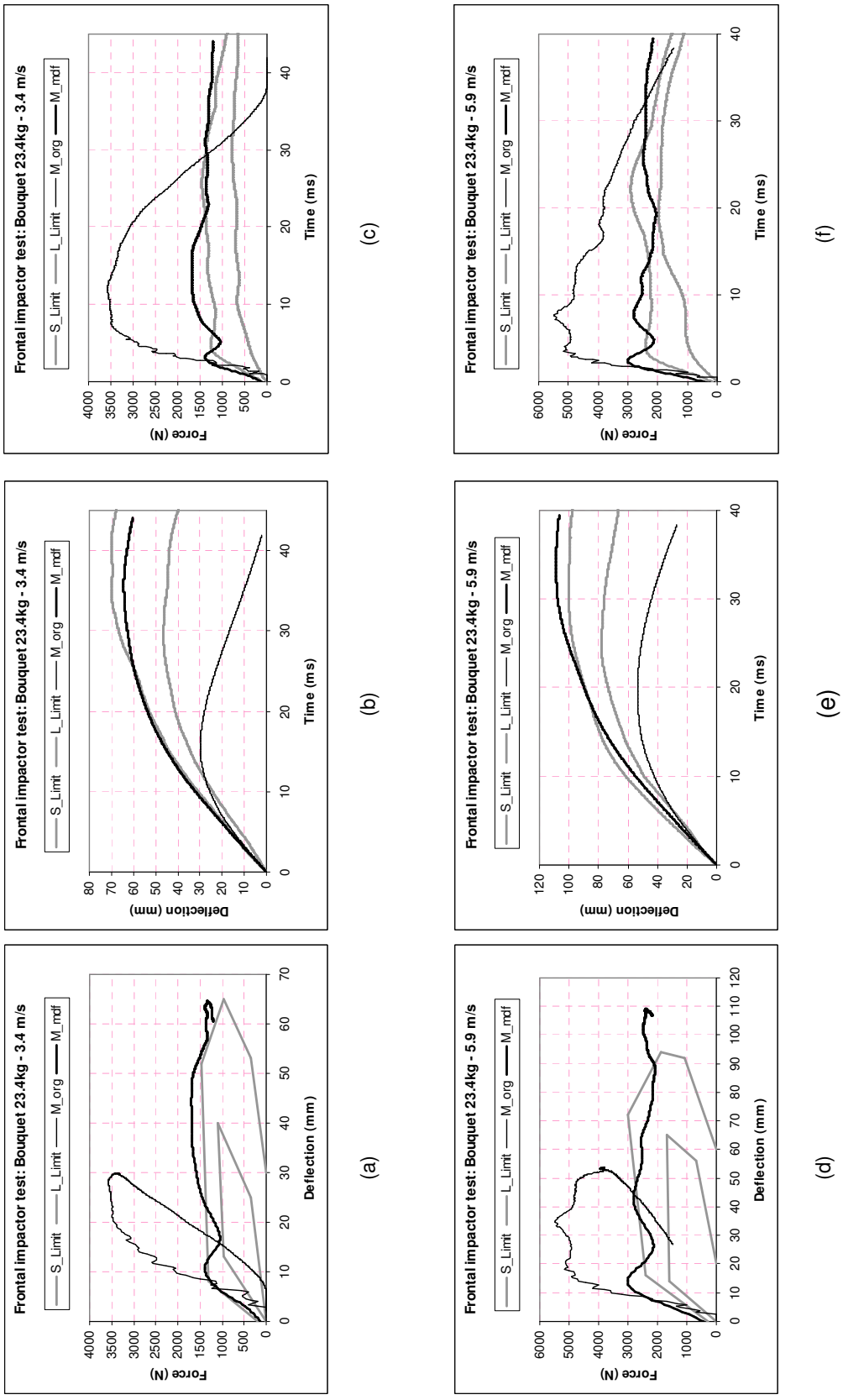

FIGURE A1. Validation of dynamic responses of the HUMOS2LAB model versus the Bouquet frontal impactor tests. S_limit and L_limit form experimental corridors, M_org and M_mdf are responses of the original model and the modified model.

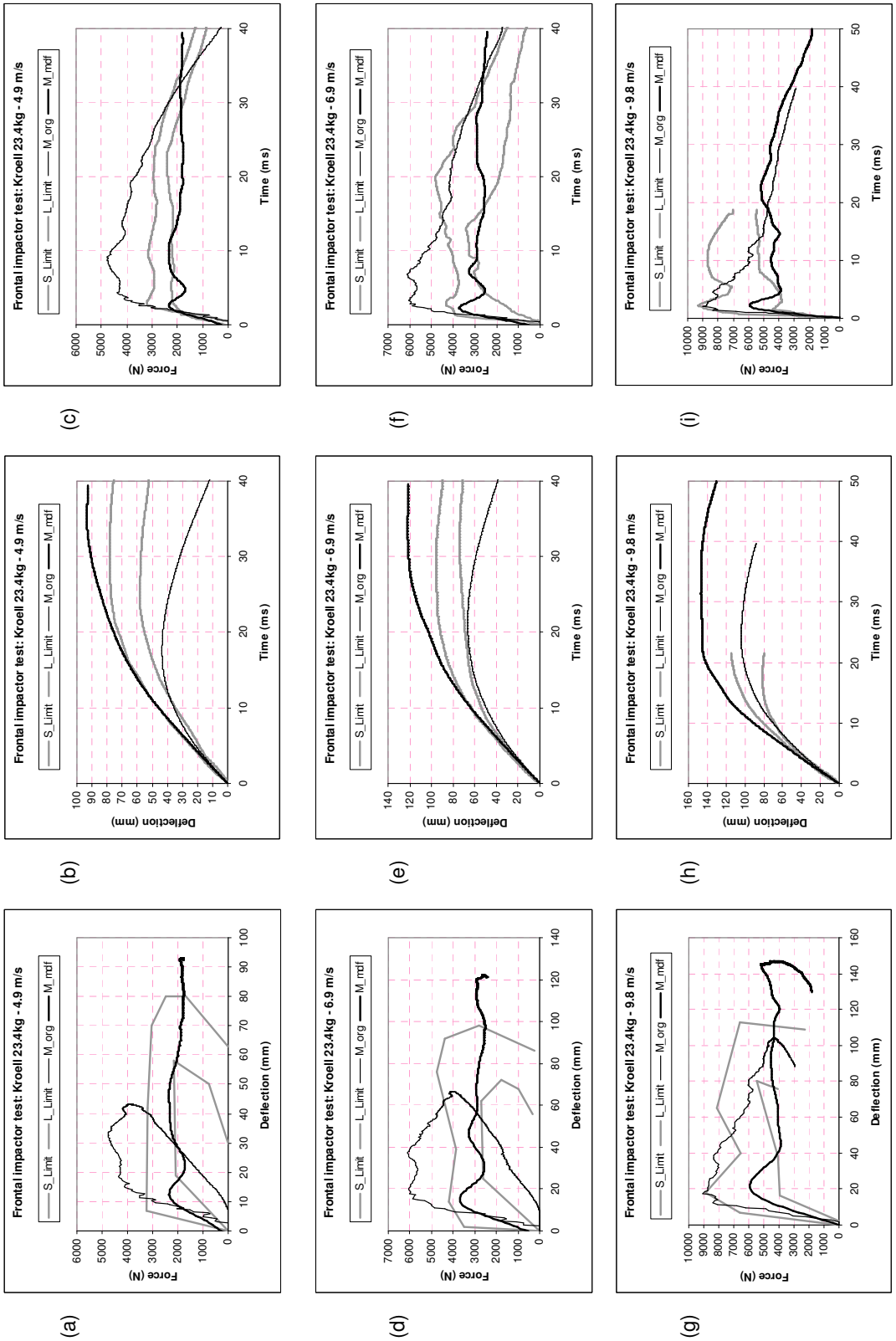

FIGURE A2. Validation of dynamic responses of the HUMOS2LAB model versus the Kroell frontal impactor tests. S_limit and L_limit form experimental corridors, M_org and M_mdf are responses of the original model and the modified model.

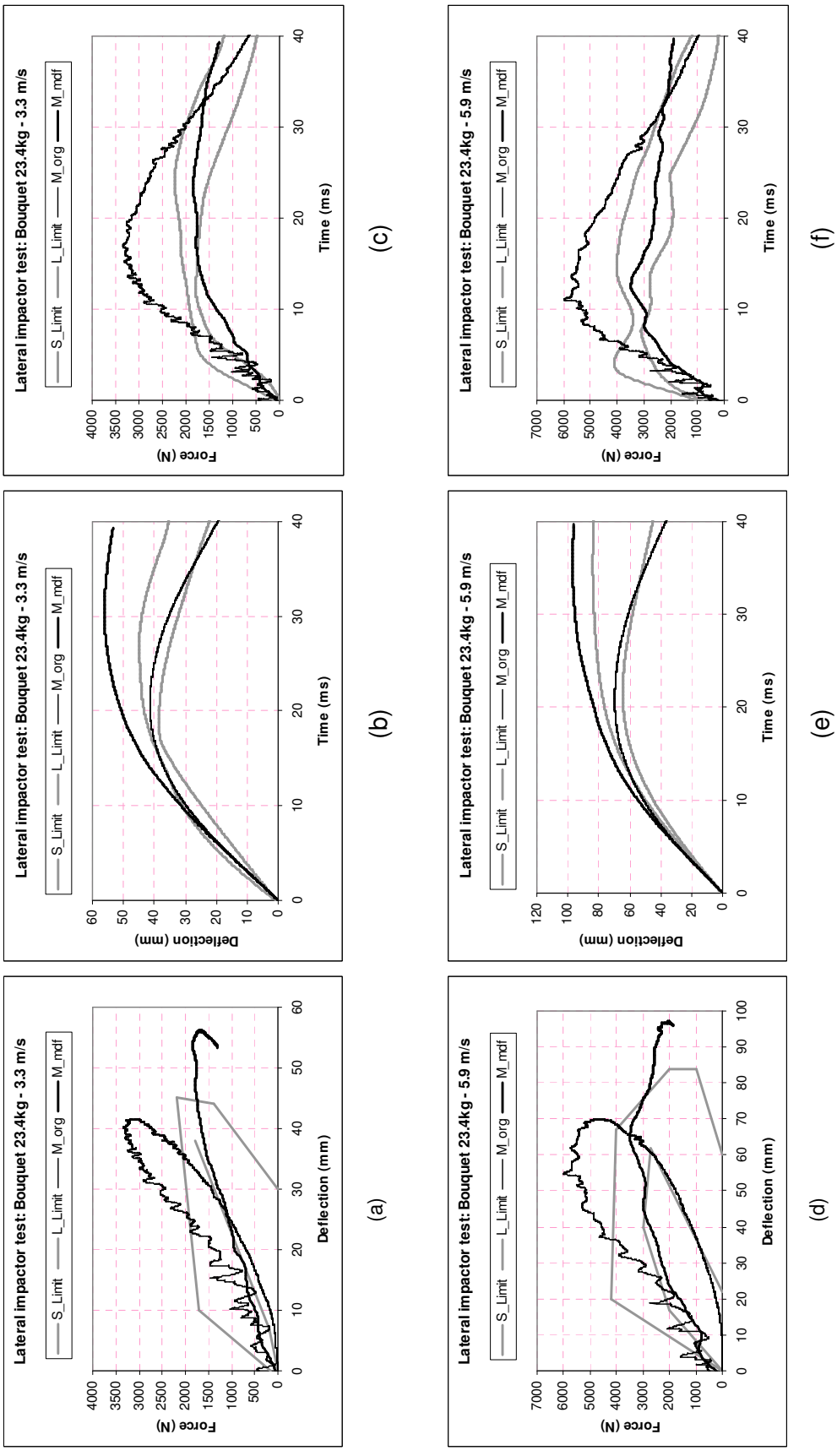

FIGURE A3. Validation of dynamic responses of the HUMOS2LAB model versus the Bouquet lateral impactor tests. S_limit and L_limit form experimental corridors, M_org and M_mdf are responses of the original model and the modified model.

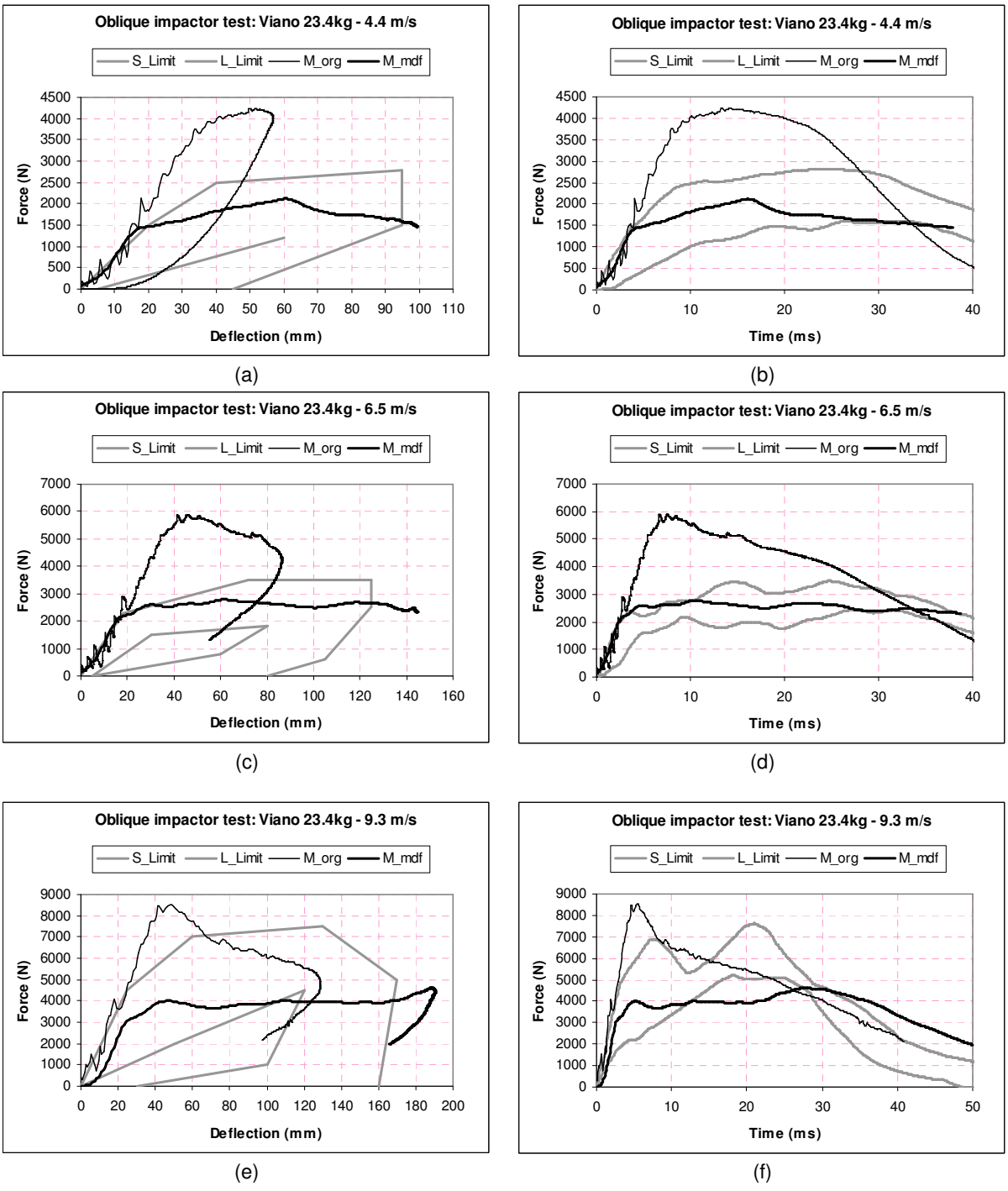

FIGURE A4. Validation of dynamic responses of the HUMOS2LAB model versus the Viano oblique impactor tests. S_limit and L_limit form experimental corridors, M_org and M_mdf are responses of the original model and the modified model.

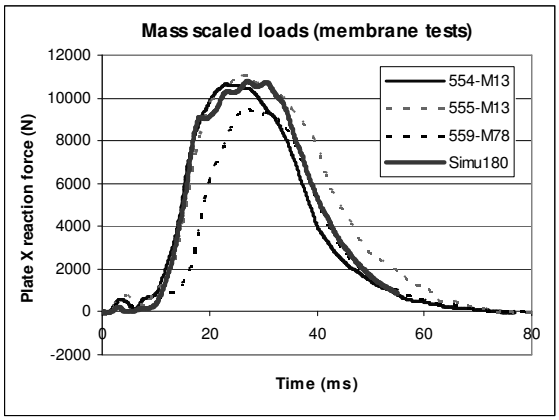

(a) Frontal airbag membrane loading

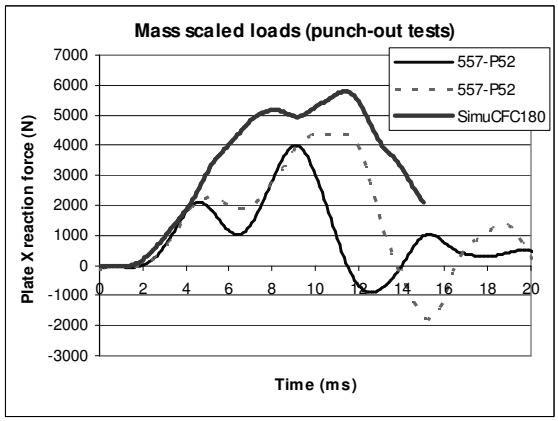

(b) Frontal airbag punch-out loading

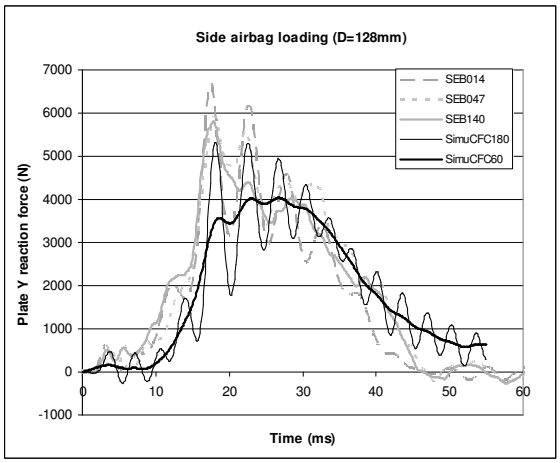

(c) Side airbag loading

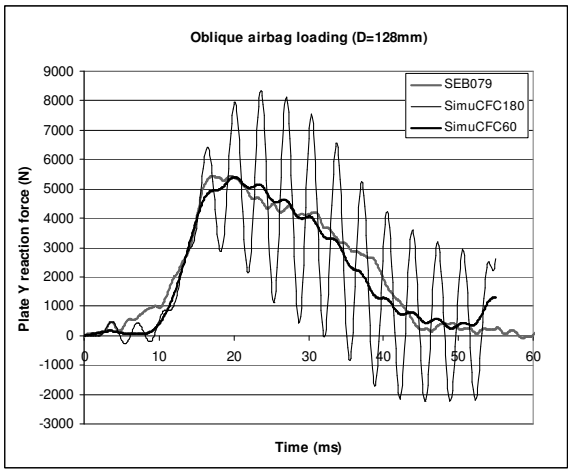

(d) Oblique airbag loading

FIGURE A5. Reaction force on the plate supporting the airbag. The airbag was close to the subject for frontal impact, and was distanced about 128 mm for side and oblique impact. All experimental results were filtered using CFC180, results of simulation for side and oblique loading were filtered using both CFC180 and CFC60.

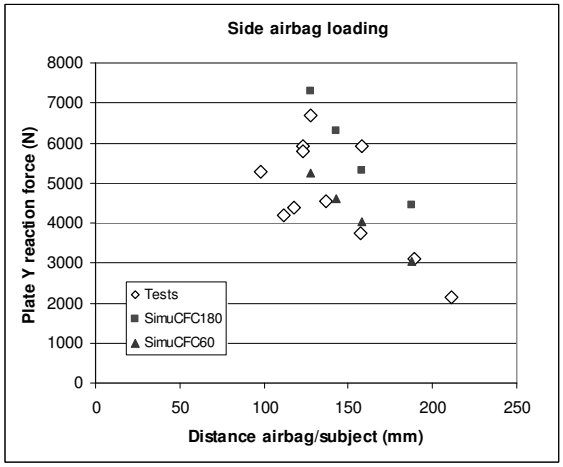

(a) Side airbag loading

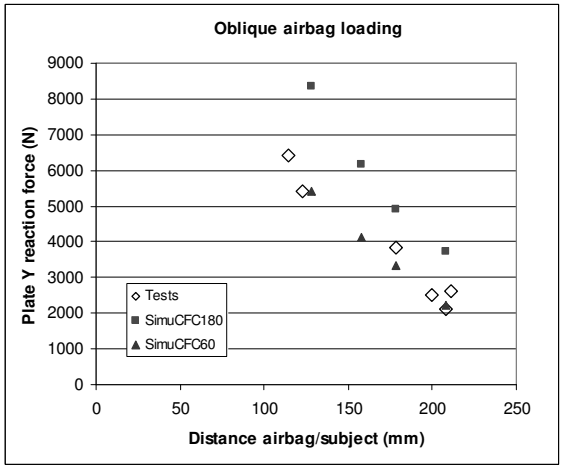

(b) Oblique airbag loading

FIGURE A6. Reaction force on the plate supporting the airbag versus distance airbag/subject. All experimental results were filtered using CFC180, results of simulation were filtered using both CFC180 and CFC60.

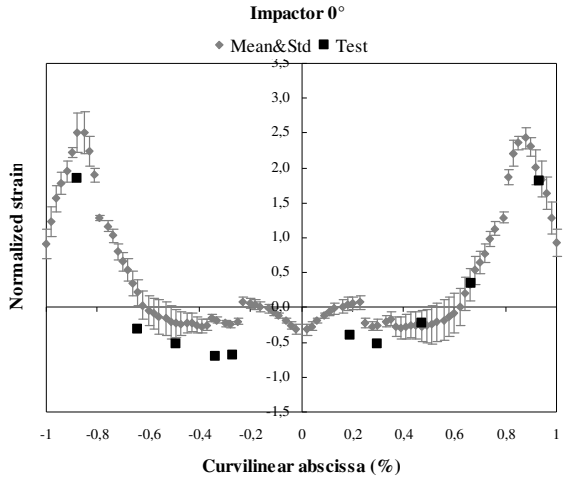

Impactor loading at 0°

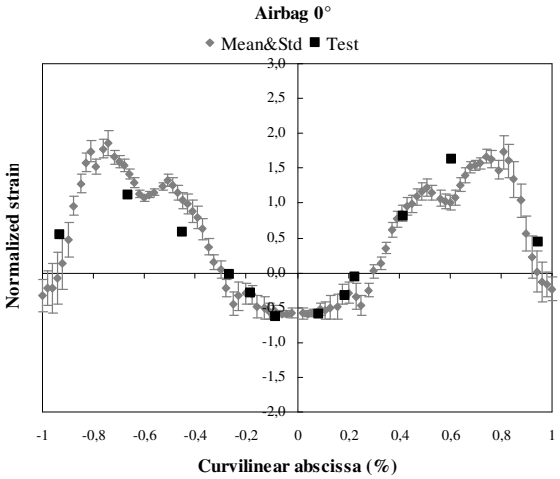

Airbag membrane loading at 0°

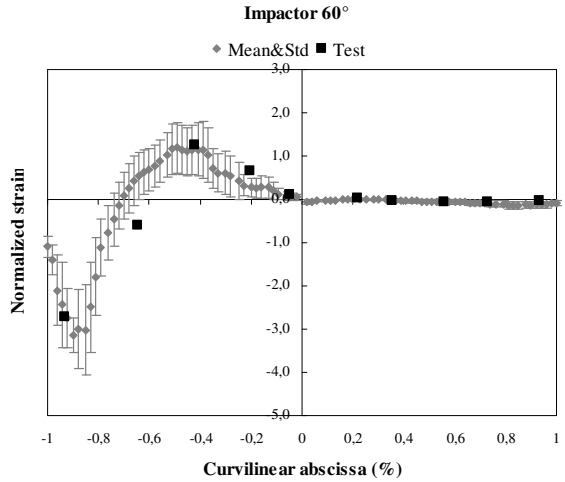

Impactor loading at 60°

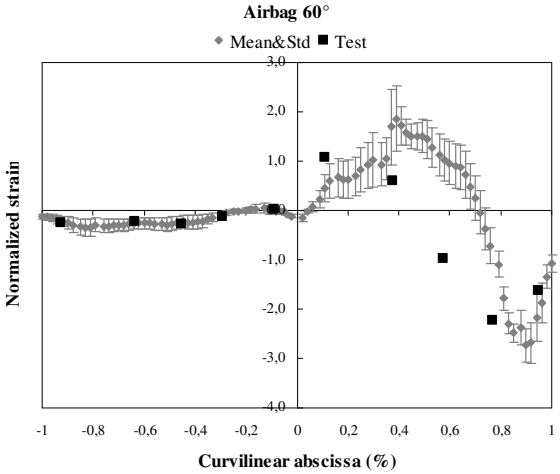

Airbag membrane loading at 60°

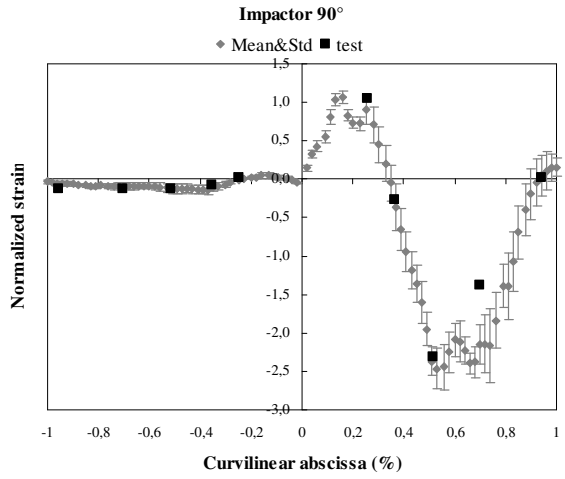

Impactor loading at 90°

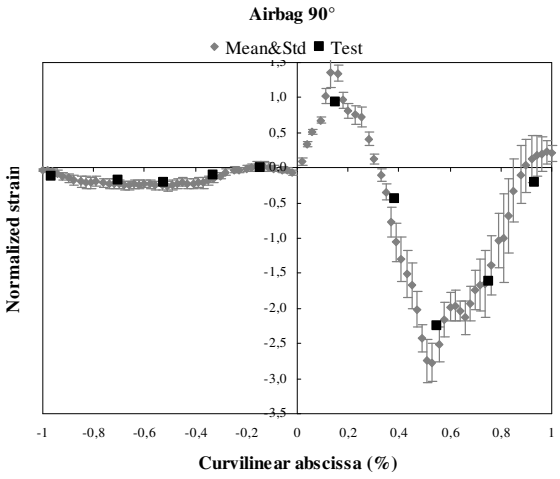

Airbag membrane loading at 90°

FIGURE A7. Comparison of the strain profile for the 5th rib between the HUMOS2LAB model and the experiment.

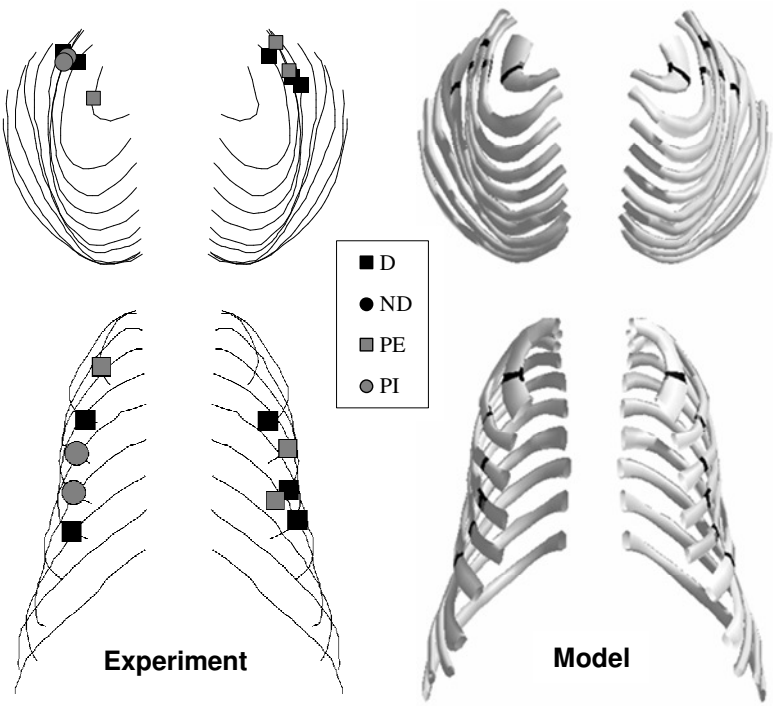

FIGURE A8. Comparison of the fracture regions between the model and the experiment for the impactor loading at 0° at 4.3 m/s.

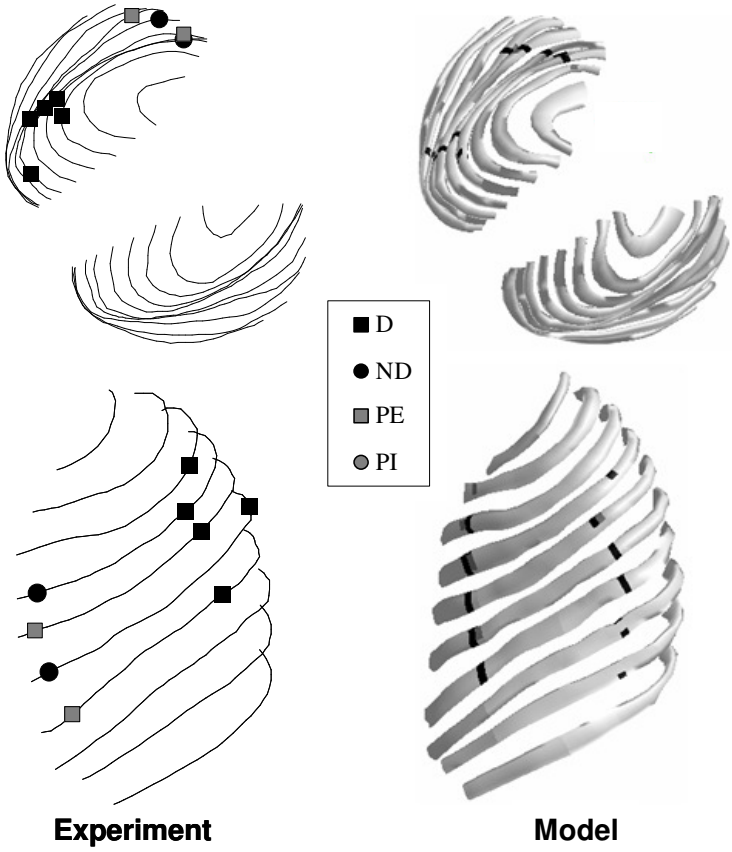

FIGURE A9 . Comparison of the fracture regions between the model and the experiment for the impactor loading at 60° at 4.3 m/s.

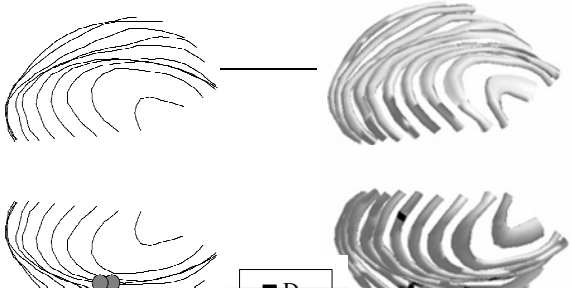

FIGUREB10 . Comparison of the fracture regions between the model and the experiment for the impactor loading at 90° at 4.3 m/s.

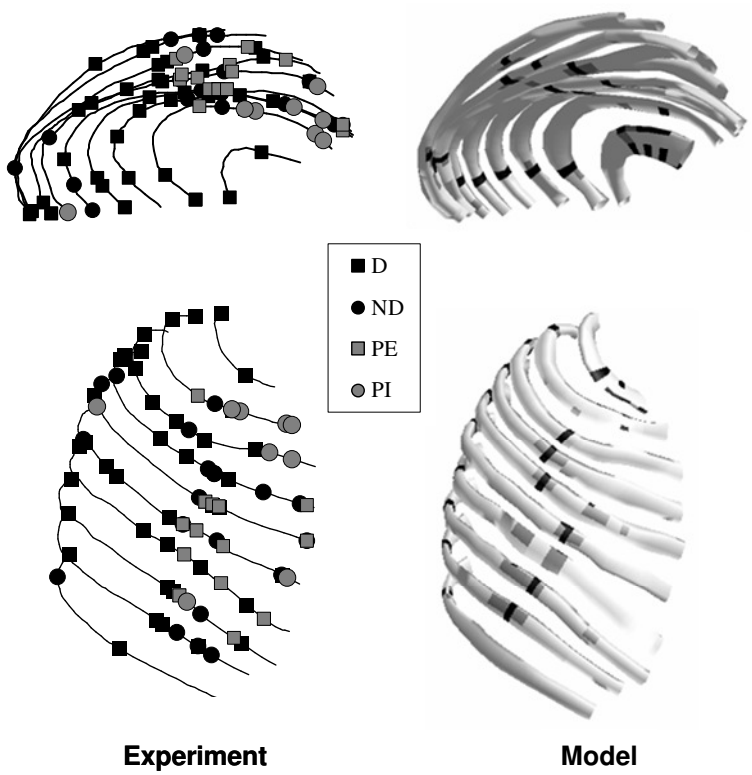

FIGURE A11 . Comparison of the fracture regions between the model and the experiments for the airbag loading at 90°.

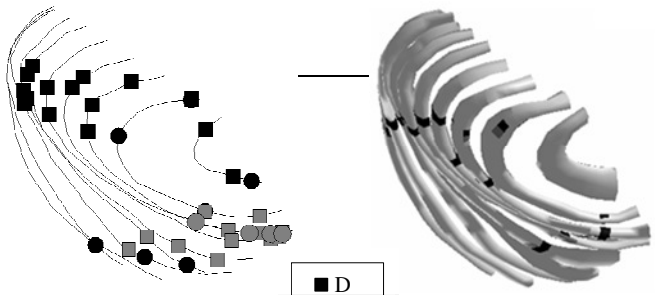

FIGURE A12 . Comparison of the fracture regions between the model and the experiments for the airbag loading at 60°.

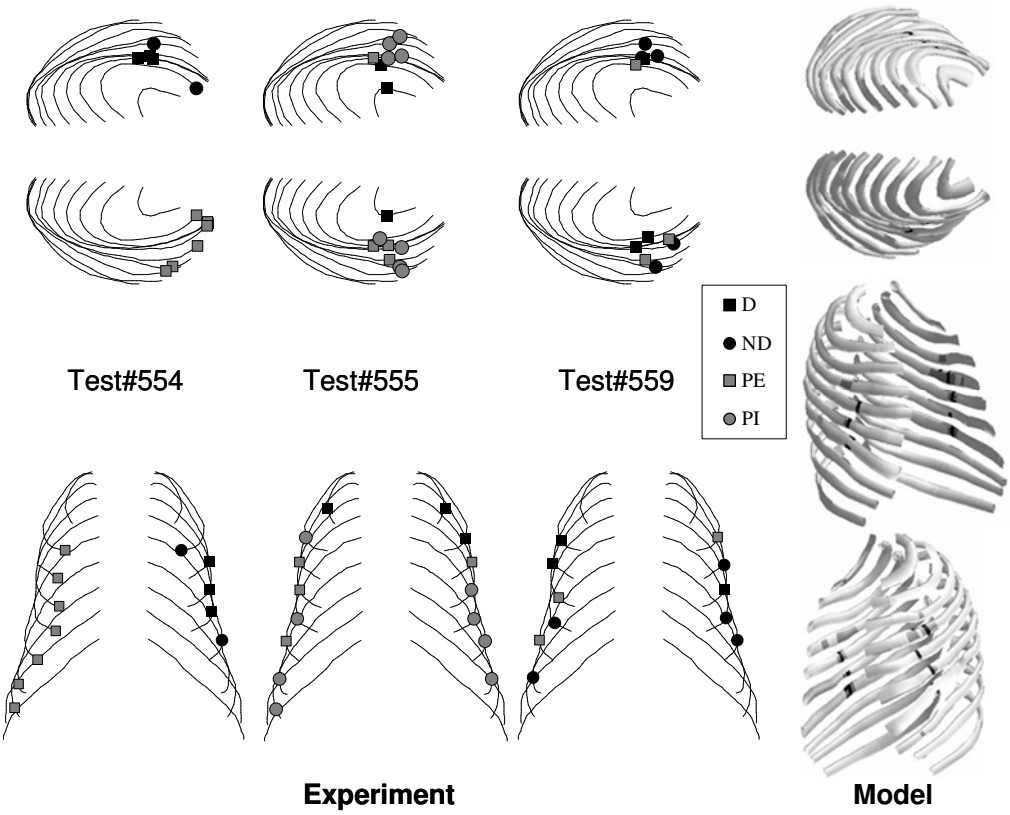

FIGURE A13. Comparison of the fracture regions between the model and the experiments for the membrane airbag loading at 0°.

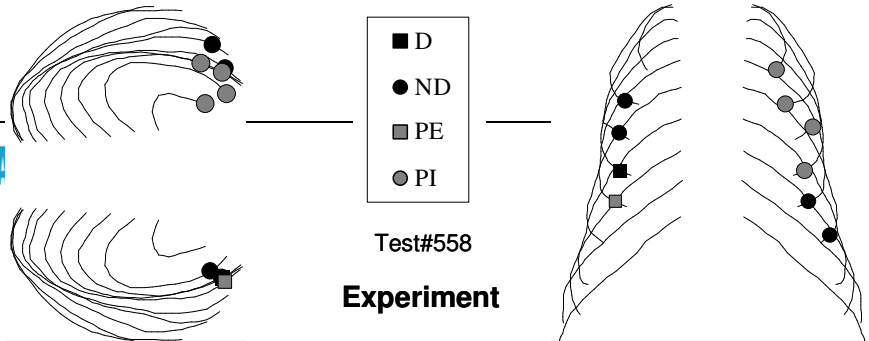

FIGURE A14 . Comparison of the fracture regions between the model and the experiments for the punch-out airbag loading at 0°.

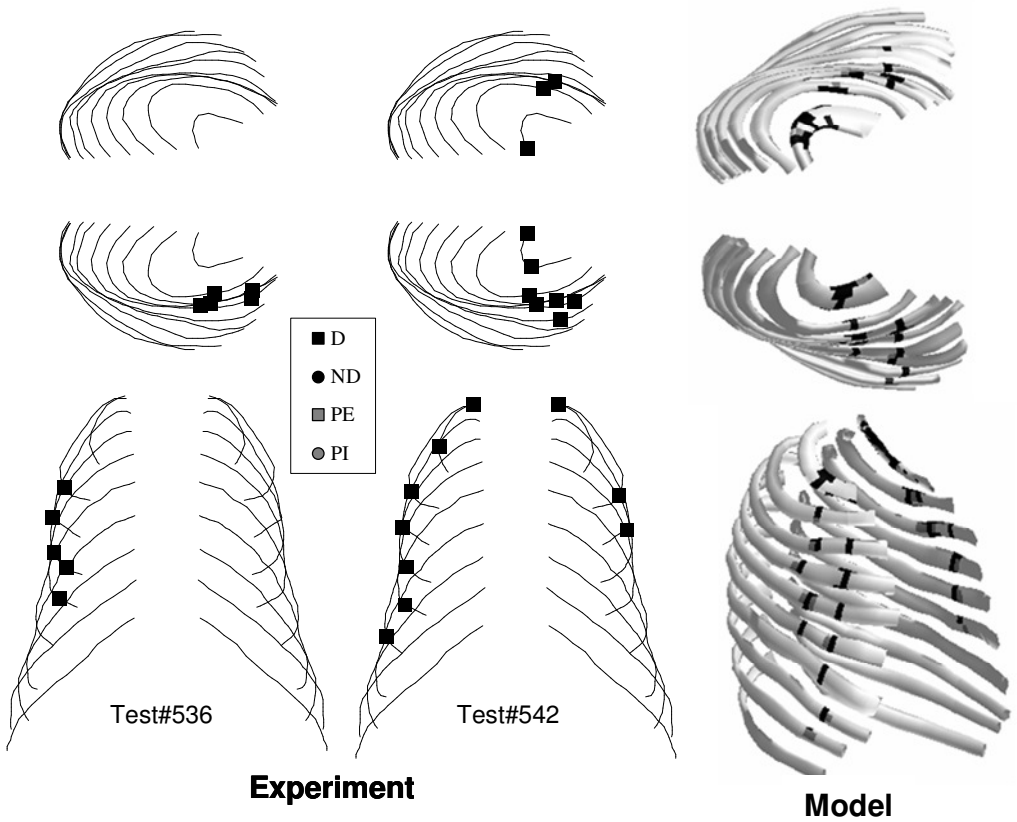

FIGURE A15. Comparison of the fracture regions between the model and the experiments for the frontal sled test with airbag and 4kN belt load limiter.

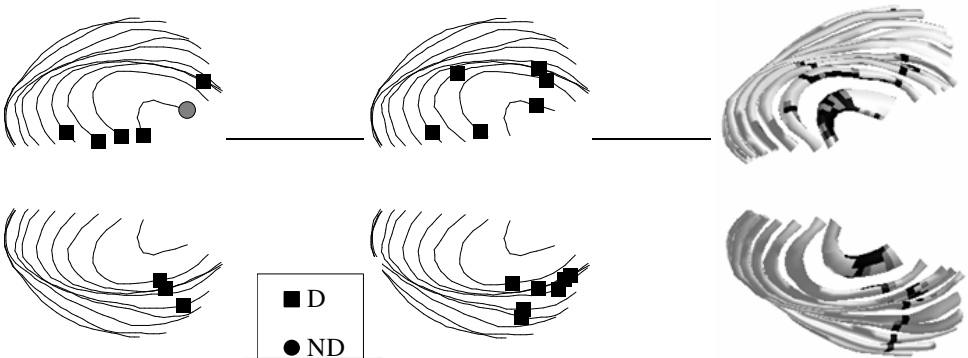

FIGURE A16. Comparison of the fracture regions between the model and the experiments for the frontal sled test with 6kN belt load limiter only.

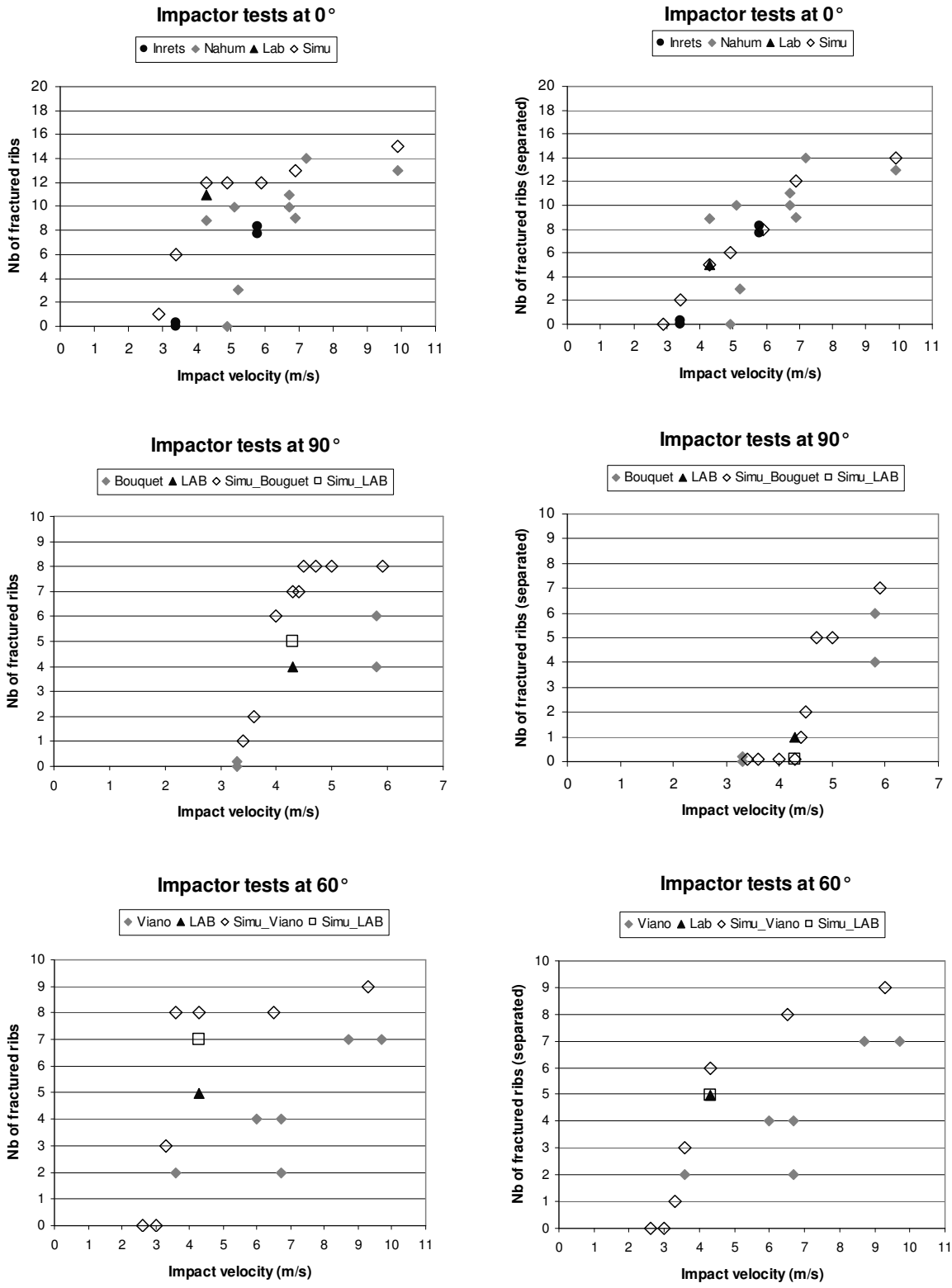

FIGURE A17. Variation of number of fractured ribs versus loading severity for impactor tests: comparison between the HUMOS2LAB model and the experimental data.

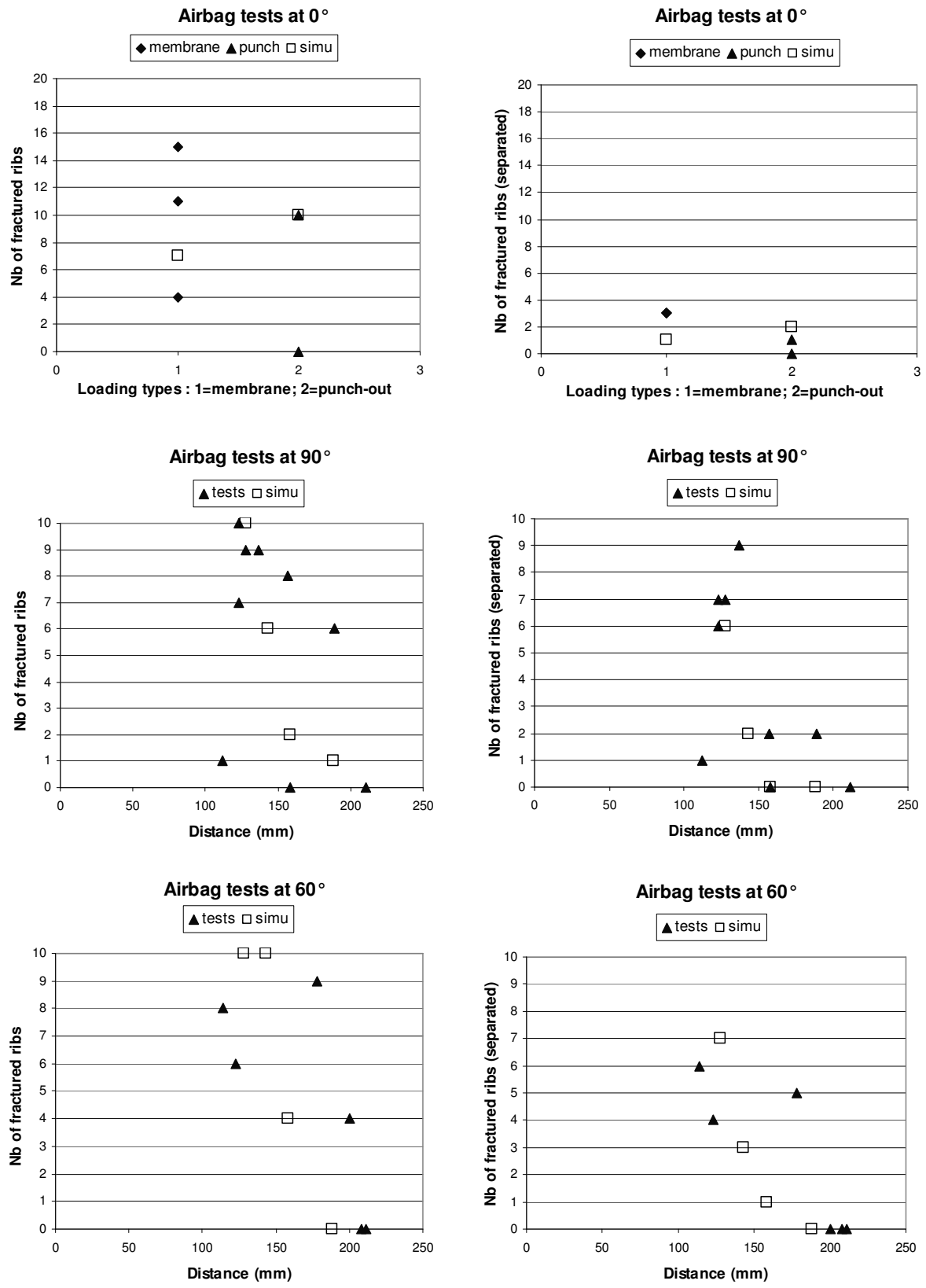

FIGURE A18. Variation of the number of fractured ribs versus loading severity for airbag tests; comparison between the HUMOS2 model and the experimental data.

9 APPENDIX B: Results of the THUMS-Chalmers thorax model validation

The Total HUman Model for Safety (THUMS) version 3.0 was used in this study. This HBM was originally developed by Toyota Motor Coorporation (2008) and modified by Chalmers University of Technology in cooperation with Autoliv. All simulations were performed using the Finite Element (FE) code LS-DYNA version 970 Hallquist (2006). Pre and post processing were done with LS-PREPOST (LSTC Inc.), MatLab (The Mathworks Inc.), Altair Hyperworks (Altair Engineering Inc.), and Oasys Primer (ARUP Inc.).

9.1 Appendix B:1 Human body model modifications

The THUMS with a refined thoracic mesh was modified to obtain a better agreement with the different PMHS tests. These modifications were mainly on the material properties used in the thoracic flesh and the lungs. The flesh was updated according to the material properties published in Ruan et al. (2003). The material for the lungs was modified by decreasing its stiffness to fit into the response from PMHS tests. The plastic strain dependant element elimination feature was removed from all materials in the ribcage. The HBM that resulted from these modifications will be referred as THUMS throughout this document.

9.2 Appendix B:2 Human body model biofidelity assessment

To assess the biofidelity of the HBM with the refined mesh and the introduced material property modifications, a set of simulations was carried out. The THUMS response was compared to pendulum impacts according to GESAC (2005) in the Appendix B1, table top tests by Kent et al. (2003, 2004, 2005) in Appendix 9.2.2, and sled tests by Shaw et al. (2009) in section 9.2.3. These three sets facilitate a comparison between the THUMS and the human response at range of deflection velocities Figure and load distributions.

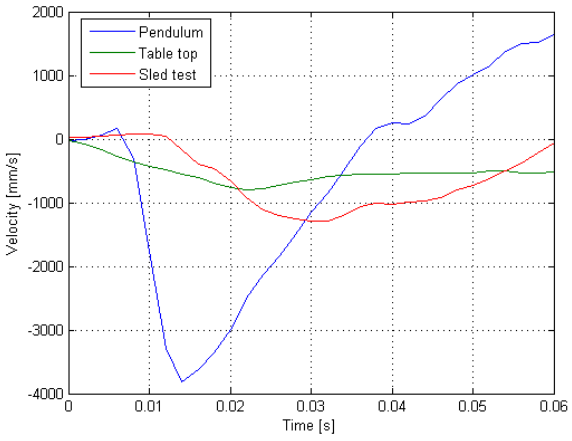

Figure B1. Mid sternum deflection velocity for the three different tests used to verify THUMS kinematic response

9.2.1 Pendulum impact

The force-deflection response of the HBM to pendulum impacts was compared to the low speed corridor defined as biomechanical requirement for THOR-NT according to GESAC (2005). This corridor considers a pendulum mass of 23.4 travelling at 4.3 m/s and impacting

at the 4th intercostal space. No compensation for muscle tension is included in the used response corridor.
The pendulum impact test was simulated using the THUMS. The model and the pendulum were positioned as in Figure B2. The pendulum was modeled as a rigid body with mass of 23.4 kg, a diameter of 152 mm and an initial velocity of 4.3 m/s. The data used to calculate the force deflection response for each test was:

a) The contact force between the pendulum and the THUMS, and
b) The distance between the center of the surface of the pendulum and the spine.

The sampling of both values started when the contact between the pendulum and the THUMS began. The results obtained from these tests are in Figure B3.

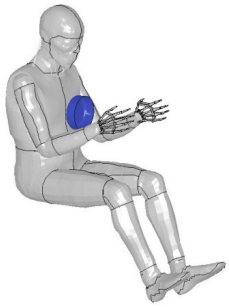

Figure B2. Pendulum impact configuration using the THUMS

The THUMS response is inside the corridor, with exception of the peak present at maximum chest compression. This peak is due to a contact between the lower tip of the sternum and the spine.

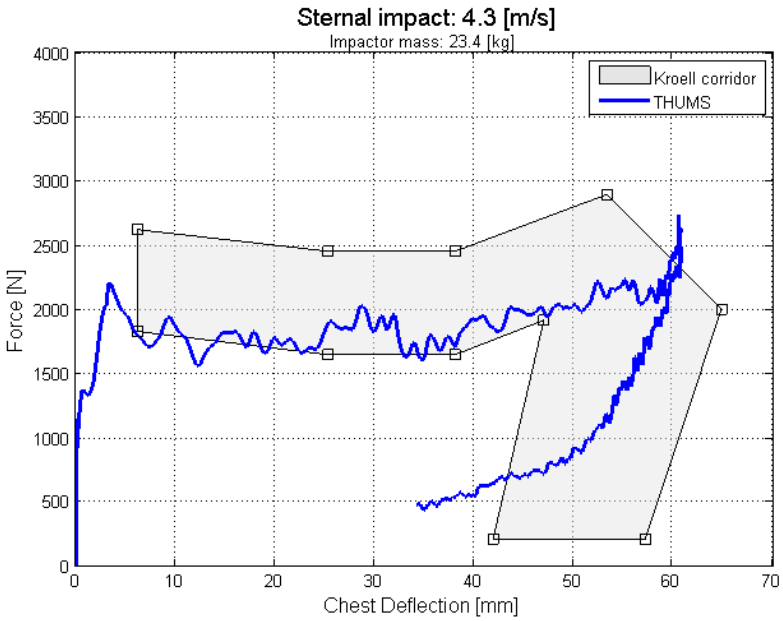

Figure B3. THUMS force deflection response to pendulum impact at 4.3 m/s and mass 23.4 kg

9.2.2 Table top tests

The THUMS was positioned on the table in a similar manner as described by Murakami et al. (2006). During the experiment, the PMHS head and hip rested on shims. Those shims and the table supporting the back of the THUMS were simulated as rigid plates with heights as depicted in Figure B4. Gravity acted on the THUMS under 150 ms in order to reach the stable laying position. The different loading devices were simulated according to the descriptions in Kent et al. (2004), refer to Figure B5. The rate at which the loading devices were pulled in the experiments was 1 m/s. The pulling rate in the simulations was defined so that the chest deflection rate measured at the mid sternum position matched the experimental deflection rate. The force used to calculate the force deflection response was the vertical component of the contact force between the plate supporting the back and THUMS back. The external chest deflection was measured at the center of the hub and at the node on the loader that was above the third intercostal space and on the sagittal plane for the belt and distributed conditions. The effective stiffness was then calculated as the slope of the linear regression of the force – chest deflection curve between 0 and 46 mm. It is expressed in force relative deformation, as expressed as deformation relative initial chest depth (N/%). The initial chest depth was assigned the value 230 mm.

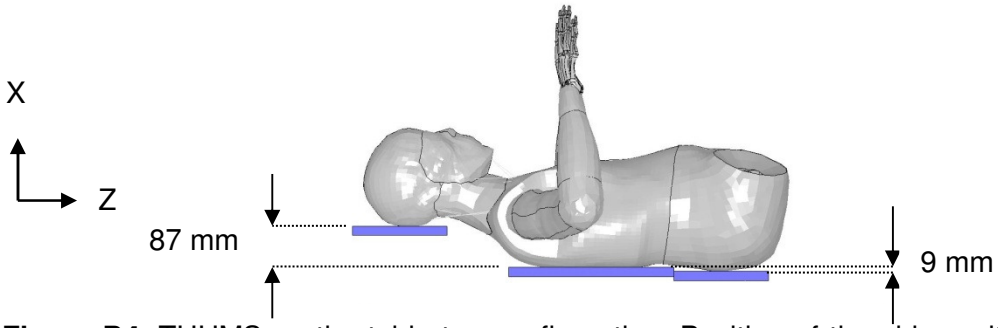

Figure B4. THUMS on the table top configuration. Position of the shims with respect to the back support during the intact state.

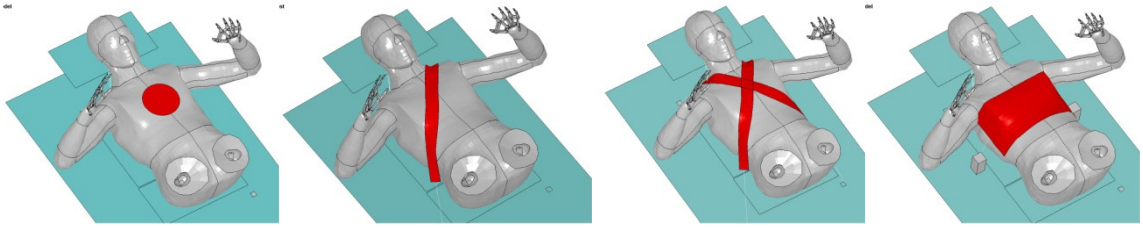

Figure B5. Table top configuration and four load types. From left to right: hub, belt, double diagonal belt and distributed.

The HBM responses in these tests were compared with the PMHS data corridors (Figure B6). The effective stiffness of the HBM under the four different loading conditions appears in

Table A16. The PMHS effective stiffness is based on results from ten subjects, as in Kent et al. (2003). The normalized stiffness displayed on the table was calculated as the stiffness in relation to the result for the load case DISTRIBUTED.

Table A16. Effective stiffness, non scaled data [N/%]

	PMHS, Kent et al. (2003)		THUMS	
	[N/%]	normalized	[N/%]	normalized
HUB	4750	0.30	3675	0.22
BELT	9862	0.64	11482	0.69
DOUBLE BELT	13706	0.89	14041	0.85
DISTRIBUTED	15397	1.00	16457	1.00

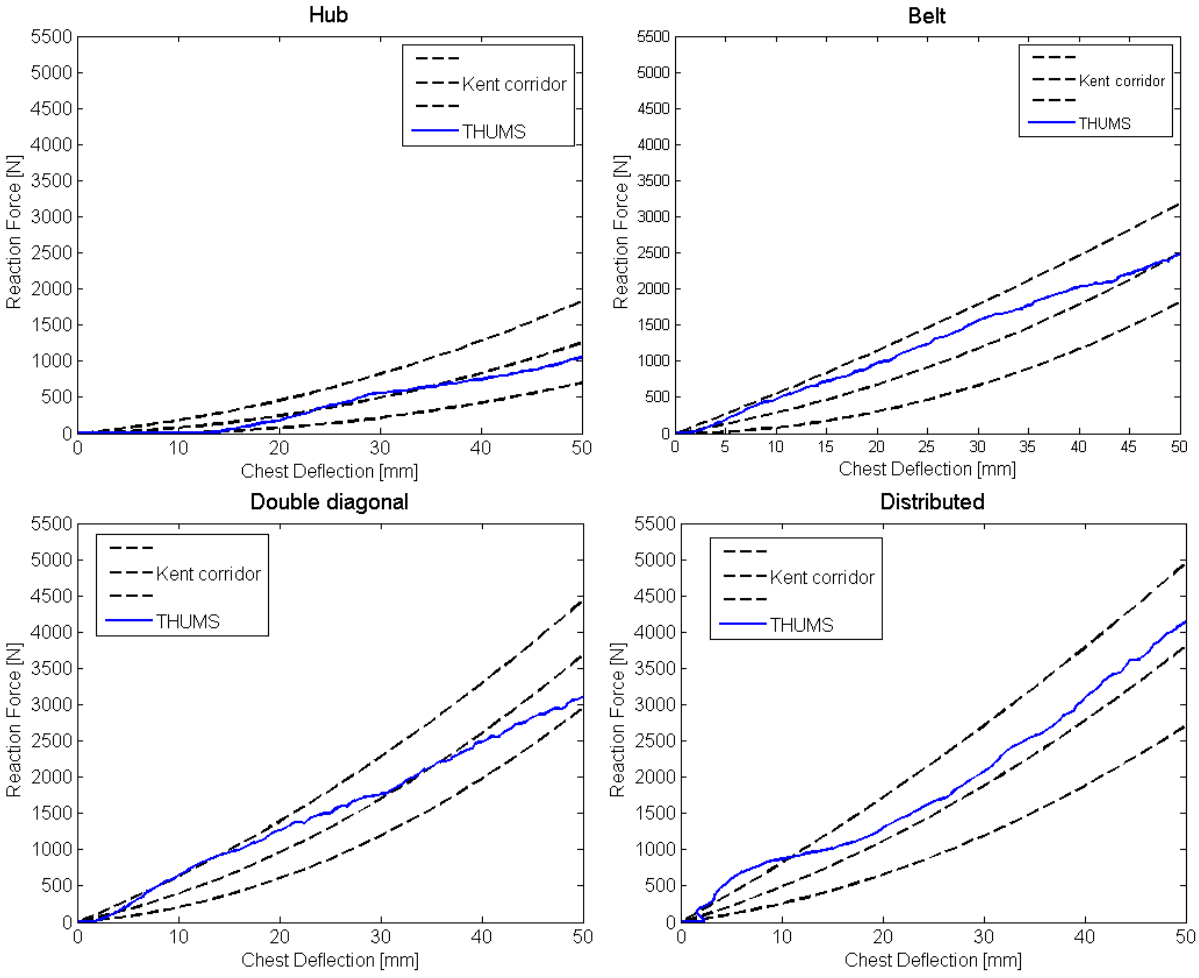

Figure B6. THUMS force – chest deflection response (blue line marked HBM) for four different loading cases compared to experimental corridors (dashed lines) by Kent et al. (2004). Upper left: hub loading, upper right: belt loading, lower left: double diagonal belt loading, lower right: distributed loading.

Figure B8 shows displacements on THUMS ribcage at 20% chest deflection under the four load conditions on table top tests. The results were measured on the THUMS ribcage at the points presented in Figure B7. The points on the 4th rib level were measured in a coordinate system with its origin in T8 whereas the points on the 7th rib level were measured in a coordinate system attached to L1. All points were located on the bones or cartilage as shown in Figure B7. Therefore the mid sternum compression was less than 46 mm. That corresponded to 20% of the external chest deflection. The point on the sternum was located

on the projection of the point where the thoracic deflection was measured on the PMHS tests. The other points were located on 4th and 7th ribs. The origin of the coordinate system was located on the initial position of the midsternal point. The XZ plane coincided with the sagittal plane, the X axis was orthogonal to the table and points upwards. The Z axis was orthogonal to the transverse plane and pointed towards the hip. These results cannot be compared with the experimental results since they were not measured on the tests with the PMHS. Nevertheless, they show deformation patterns similar to those obtained from computed tomography during quasi-static belt like and distributed like load on two PMHS, as reported by Ali et al. (2005). THUMS and the PMHS ribcage move laterally, away from the belt, and towards the abdomen while loaded with the diagonal belt. The ribcage displacement was mainly towards the abdomen while loaded with the distributed band. For both the PMHS and the THUMS, the intercostal spaces diminished while load was applied.

Figure B8 shows that all displacements were symmetric with respect to the sagittal plane, with exception for those of the belt load condition. The ribcage deformed mainly on the anterior posterior direction while loaded with the hub. The displacements in the X-direction under belt load were quite different, especially for the points located on the 7th rib. The displacements on X on the right side (belted) were around three times larger than those in the left side (unbelted).

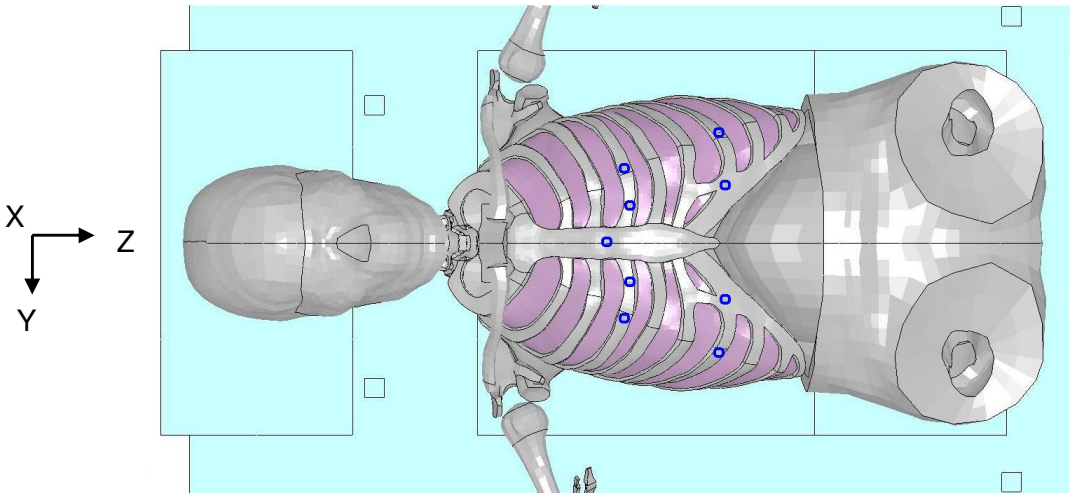

Figure B7. Location of the tracked points (blue circles) on the ribcage and coordinate system for the table top tests simulated with THUMS

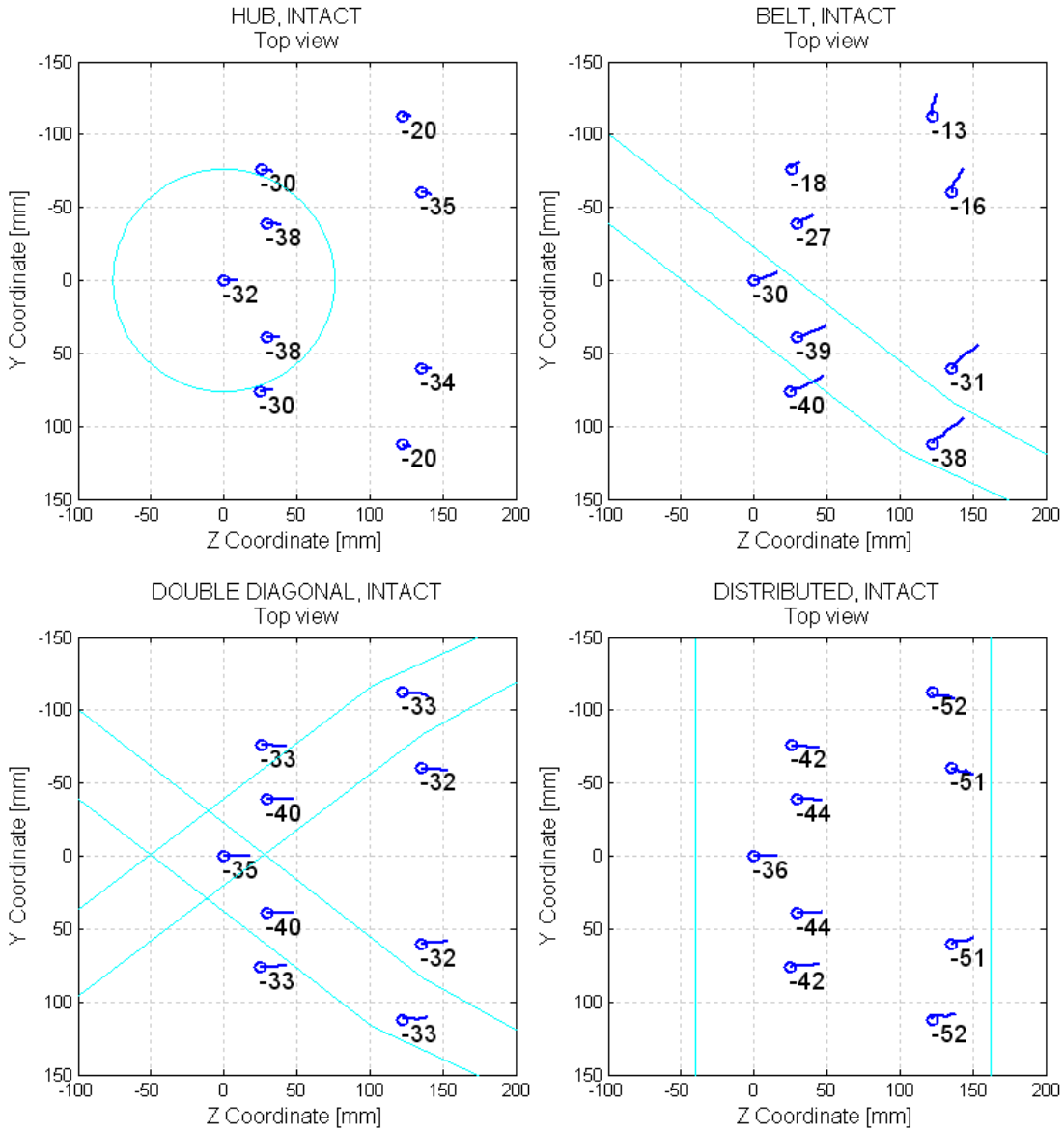

Figure B8. Displacements on THUMS ribcage at 20% external midsternal chest deflection under the four load conditions on table top tests. The blue circles indicate the initial position of all tracked points on the ribcage, the blue line illustrates the displacement of the tracked points on the YZ plane (coronal plane), and the number below each blue circle indicates the chest deflection (negative values indicate compression).

Kent et al. (2005) tested three additional PMHS using the same test procedure as described above. The characteristics of the tested PMHS are listed in Table B17. For these tests three different states for each of the PMHS torsos were tested:

1) Intact, where the torso was complete,
2) Denuded, when skin and soft tissues around the torso were removed, and
3) Eviscerated, when thoracic and abdominal organs, visceral fat, etc. were removed from the denuded subjects.

Table B17. PMHS characteristics, Kent et al. (2005)

PMHS	Age at time of death/Gender	Body mass [kg]	Stature [mm]
1	71/F	54	166
2	67/F	57	162
3	73/M	81	182
Average	70	64	170

As previously described, four different load cases were applied on each PMHS state; hub, diagonal belt, distributed load, and double diagonal belt. As expected, Kent et al. (2005) showed that the intact state had the stiffest response, followed by the denuded and then eviscerated state for all loading cases. The thoracic stiffness obtained for the loading cases involving only the rib cage, i.e. the hub and distributed load, were more sensitive to soft tissue removal than the loading cases engaging both the shoulder and the rib cage, i.e. the diagonal and double diagonal belt. For the hub and distributed loads, the denuded state stiffness was 60% of the intact state stiffness, and the eviscerated state stiffness was 30% of the intact state stiffness. For the diagonal and double diagonal belts, these figures were 85% and 55%.

The THUMS was used to simulate the four loading conditions and the three different states, i.e. intact, denuded and, eviscerated. The three different states set up and analyses differ in the following points:

1) Denuded: the shim supporting the hip was located as in Figure B9. The soft tissues surrounding the ribcage were deleted and the loading devices moved so that they were in contact with the ribcage.
2) Eviscerated: the shim supporting the hip was located as in Figure. Apart from removing the soft tissues around the ribcage, as in the denuded state, the internal thoracic and abdominal organs were removed.

The same procedure for laying the intact THUMS on the table, loading and analyzing the results as used previously was also applied to the denuded and eviscerated states.

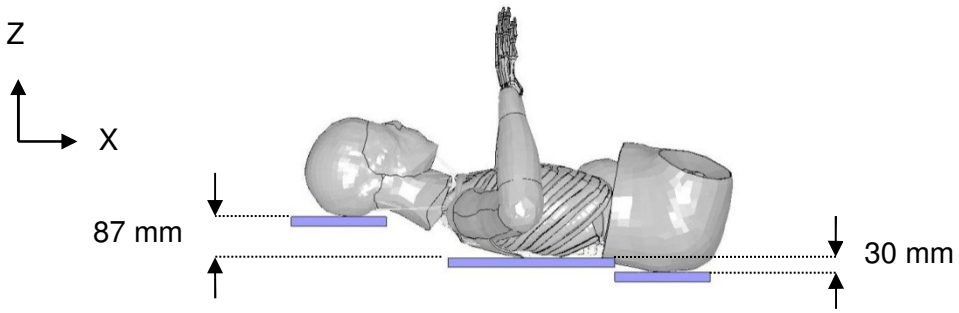

Figure B9. THUMS on the table top configuration. Position of the shims with respect to the back support during the denuded and eviscerated states.

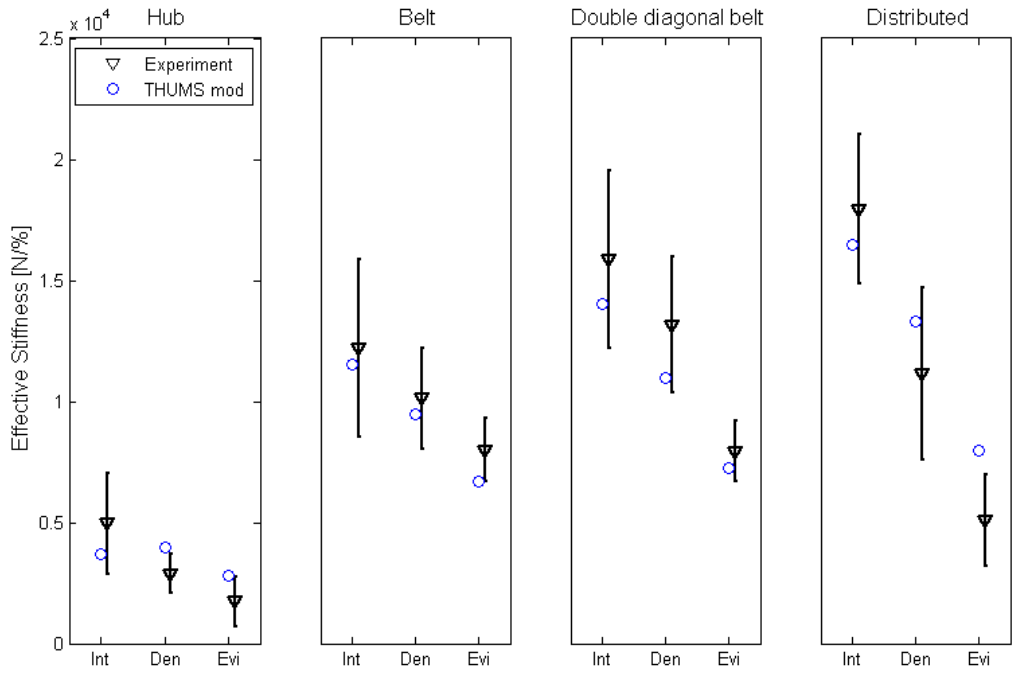

Figure B10. Effective stiffness for THUMS (blue) and unscaled experimental results for three PMHS (black, mean ±1 S.D.) under the four load cases and the three thoracic states, Kent et al. (2005)

The THUMS response under the three different states and the four loading conditions is summarized in FigureB9 and FigureB10. Under the two belted and the band loading conditions, the THUMS showed the stiffest response while in the intact state and the less stiff state while eviscerated. The THUMS response under the hub load was not as sensitive as the PMHS to the change from intact to denuded.

9.2.3 Sled test

The THUMS was positioned in the buck corresponding to this sled test, denoted GS, under action of gravity and according to the PMHS positions reported by Shaw et al. (2009), Figure. The footrest, seat and knee bolster were modeled as rigid bodies, as in Untaroiu et al. (2009), and adjusted to be in contact with THUMS at the beginning of the simulation. All parts in the model had an initial velocity of 40 km/h and the sled was subjected to a trapezoidal acceleration pulse, Figure2.

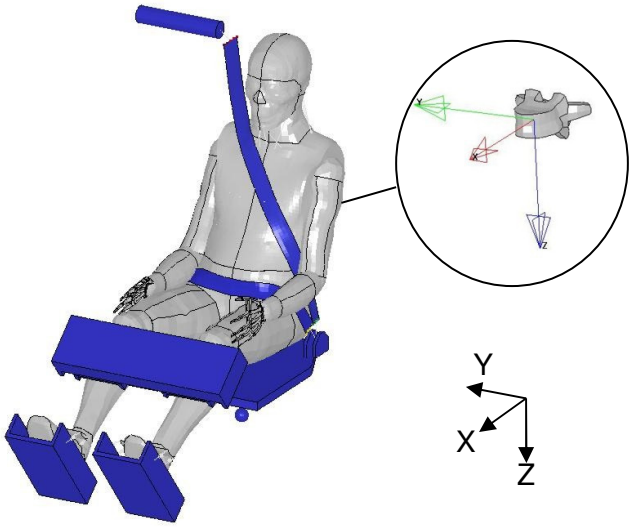

Figure B11. THUMS in sled test position. The buck coordinate system (black) and T8 coordinate system (encircled)

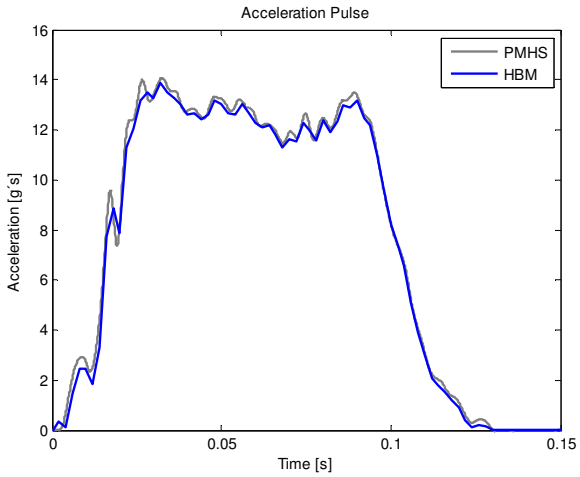

Figure B12. Acceleration pulse applied to the sled for HBM simulation (green) and representative experimental acceleration pulse (blue), Shaw et al. (2009)

The kinematic response of the THUMS was compared to the response of four PMHS under this sled test configuration. Figure3 shows the location of the points on the THUMS that were used on this comparison. The characteristics of the four tested subjects, selected to be included in this part of the study, are reported on Table B18. The kinematic data for the PMHS correspond to the un-scaled displacements calculated from the 3D motion tracking system and are given in two different coordinate systems. The first coordinate system is the buck coordinate system. It is parallel to the global coordinate system and it follows the buck throughout the test. The second coordinate system was the T8 coordinate system, defined similarly as in Wu et al. (2002), see Figure1. The T8 coordinate system moves and rotates along with the 8th thoracic vertebra.

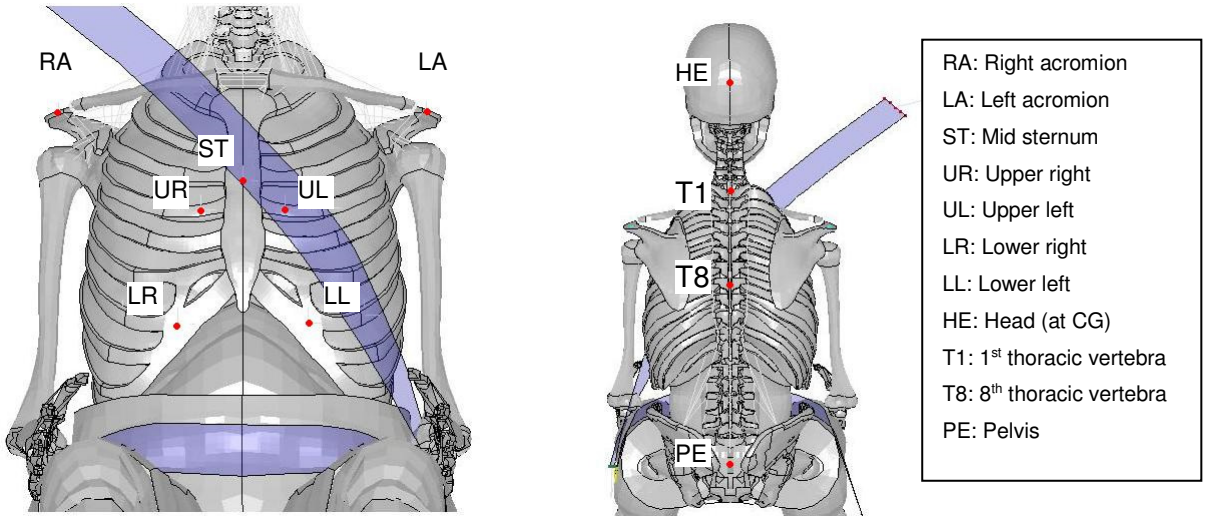

Figure B13. Location of the measured points on THUMS. Some parts have been hidden to facilitate visualization.

Table B18. PMHS characteristics, Shaw et al. (2009)

PMHS*	Age at time of death	Body mass [kg]	Stature [mm]
1	76	70	1780
2	81	81	1840
3	88	88	1790
4	78	78	1800
Average	81	79	1803

*One PMHS was excluded due to excessive number of rib fractures.

Overall, the THUMS showed a good agreement with the kinetic response from the PMHS tests, see Figure4. The longitudinal displacement of the head, T1, T8 and shoulders showed a good correspondence between the THUMS and the experimental data refer to Figure and Figure. The pelvic displacement rose earlier in the THUMS than in the experimental data, but reached maximum values comparable to those obtained from experiments. THUMS knee joint allowed some longitudinal displacement of the femur and it may explain this early raise. From Figure and Figure18 it can be seen that THUMS response matches with the experimental data at four of the five locations measured on the chest. The lower right chest point bulged out around 30 mm for the PMHS; while only 10 mm for THUMS. Furthermore, the lower right chest point on THUMS started to compress the tissue underneath at approximately 80 ms; while all PMHS were still bulging out at that time. Since THUMS was not simulating fractures, the integrity of the THUMS ribcage may have prevented the lower right chest point to move further away. One more factor that may have an influence on this response is the fact that THUMS has no liver modeled individually. Therefore there is no individual organ pushing the ribcage at the lower right point.

The movement of different points on the spine and head on the XZ and XY planes are plotted on Figure and Figure for THUMS and compared to PMHS results. In general, THUMS showed a better agreement with the PMHS results for the longitudinal displacements compared with the lateral and vertical ones. THUMS showed less initial vertical movement than the PMHS as well as less amplitude for the lateral displacements. These differences are more notorious after 100 ms

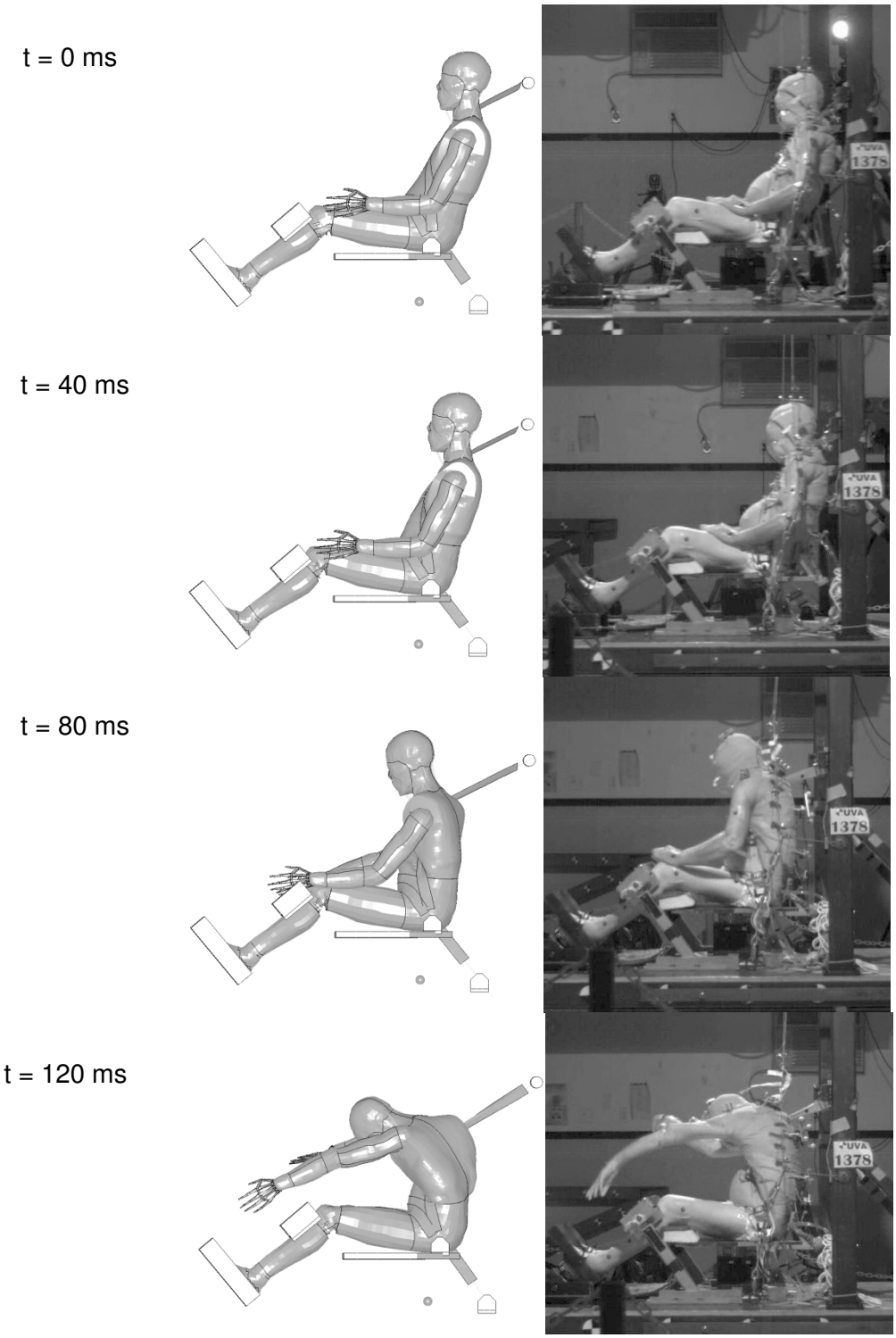

Figure B14. Illustrations of the HBM (left) and PMHS (right) positions during the sled test every 40 ms, experimental data from Shaw et al. (2009)

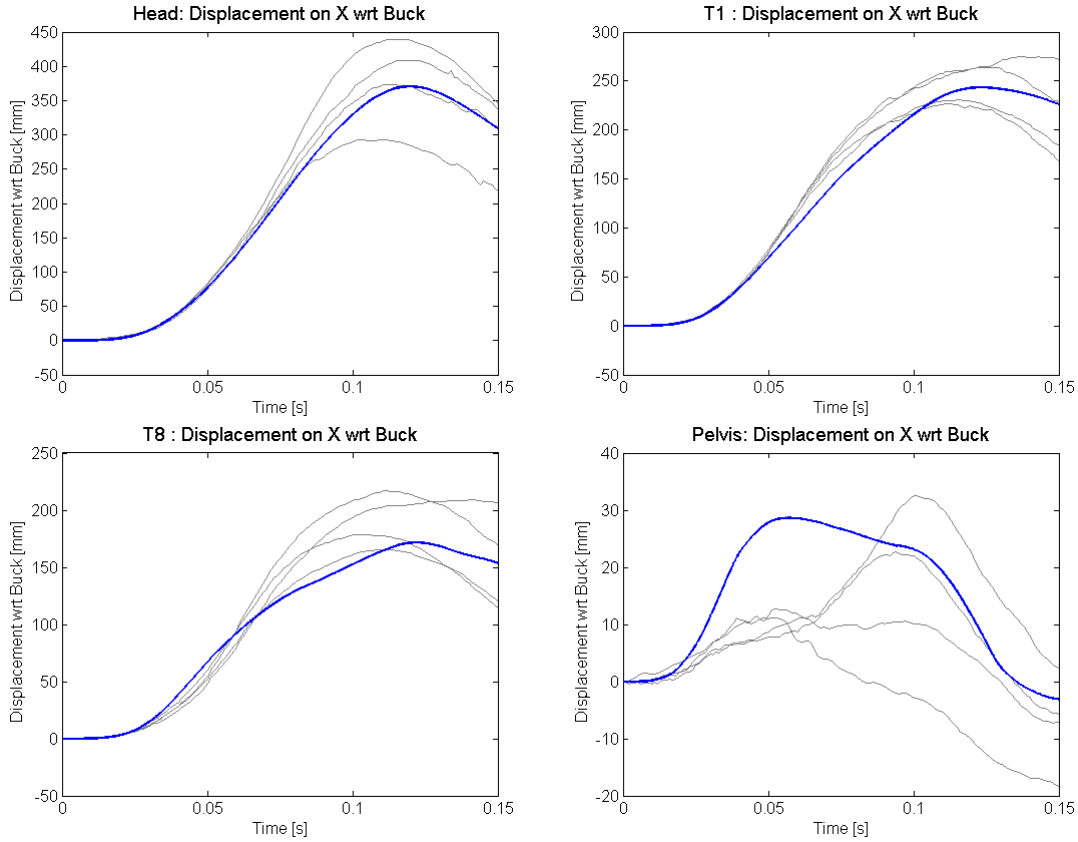

Figure B15. THUMS longitudinal displacements wrt buck coordinate system (blue). Compared to experimental data (grey) from Shaw et al. (2009). Upper left: Head, upper right: T1, lower left: T8 and lower left: Pelvis

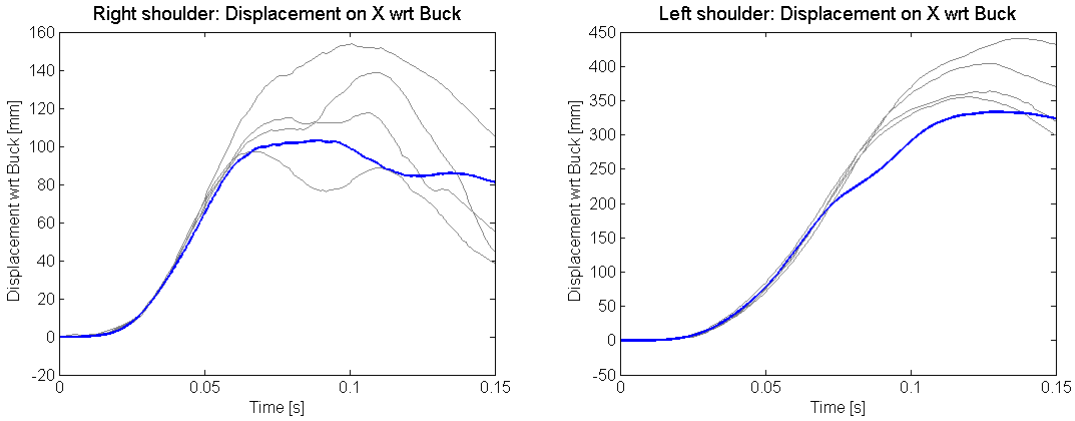

Figure B16. THUMS longitudinal displacements wrt buck coordinate system (blue). Compared to experimental data (grey) from Shaw et al. (2009). Left: right acromion, right: left acromion

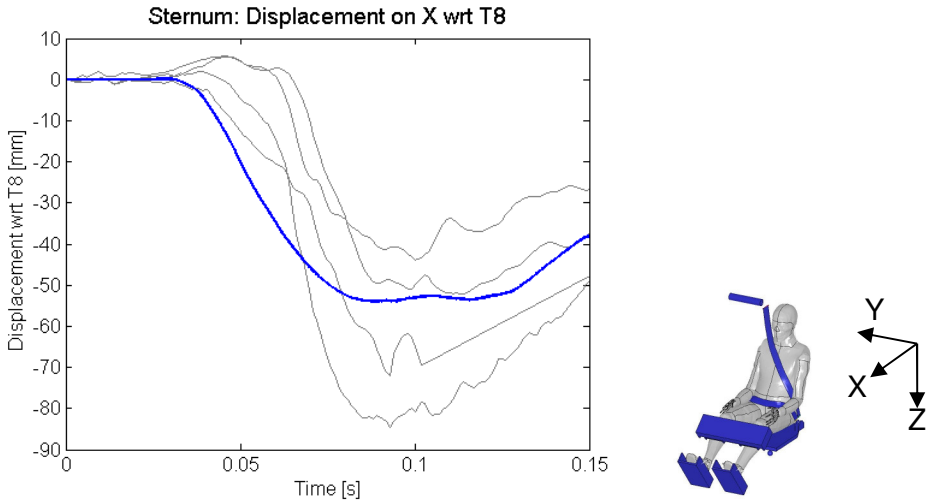

Figure B17. THUMS sternal displacement wrt T8 (blue). Compared to experimental data (grey) from Shaw et al. (2009). Negative values indicate chest compression.

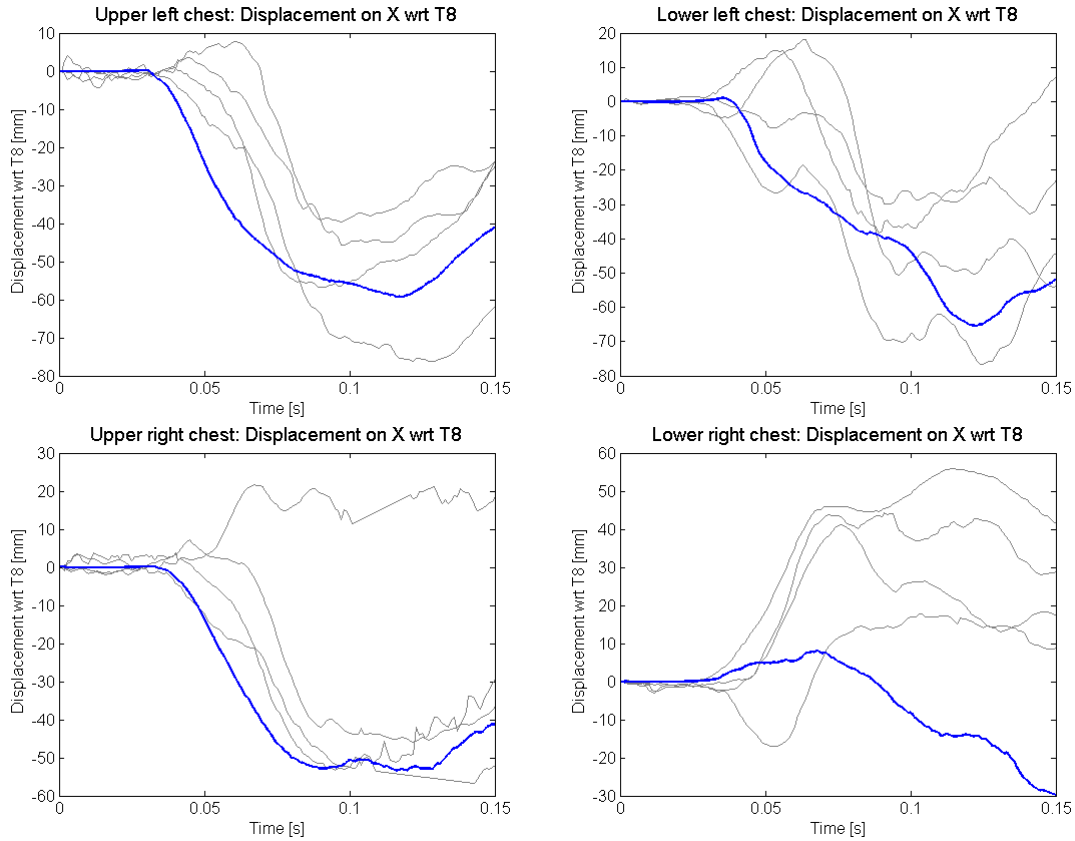

Figure B18. THUMS chest displacement wrt T8 (blue). Compared to experimental data (grey) from Shaw et al. (2009). Negative values indicate chest compression.

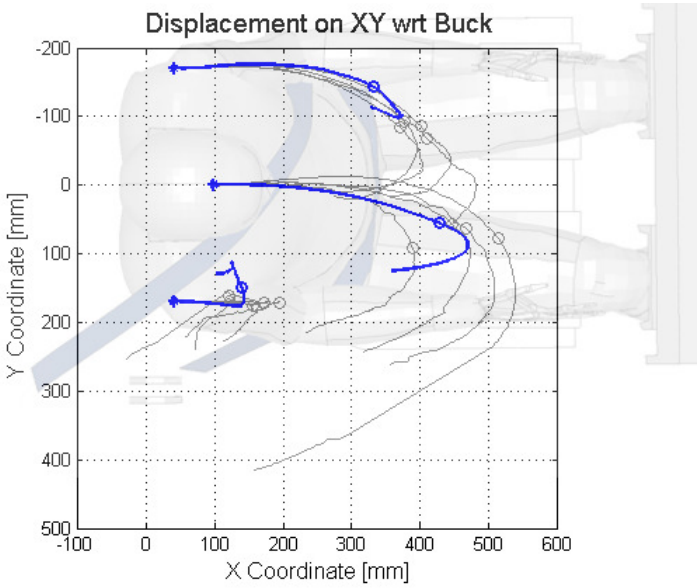

Figure B19. THUMS displacements on a horizontal plane for the shoulders and the head compared to PMHS results.

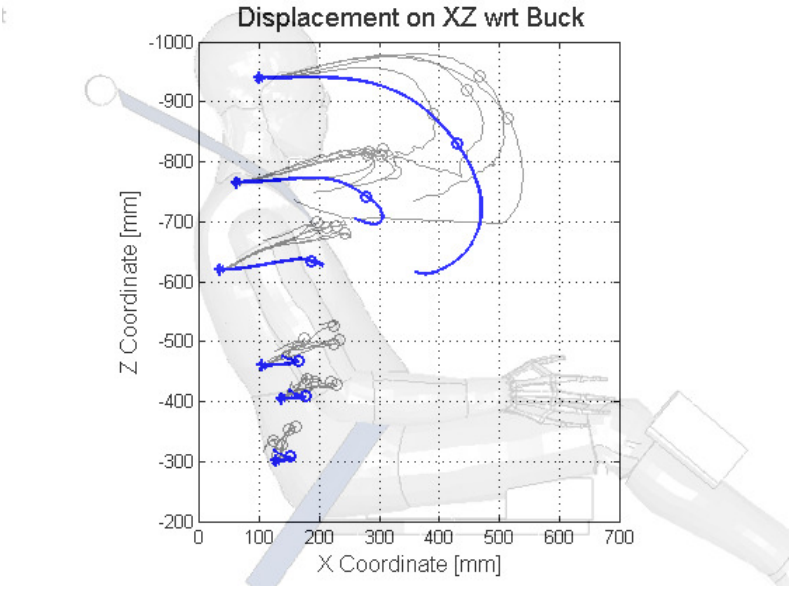

Figure B20. THUMS displacements on a sagittal plane for the head, T1, T8, L2, L4 and pelvis compared to PMHS results.

9.3 Appendix B:3 – Sled test: lateral and vertical chest displacements

Sled test: lateral and vertical chest displacements wrt T8 for the intact state compared to PMHS results

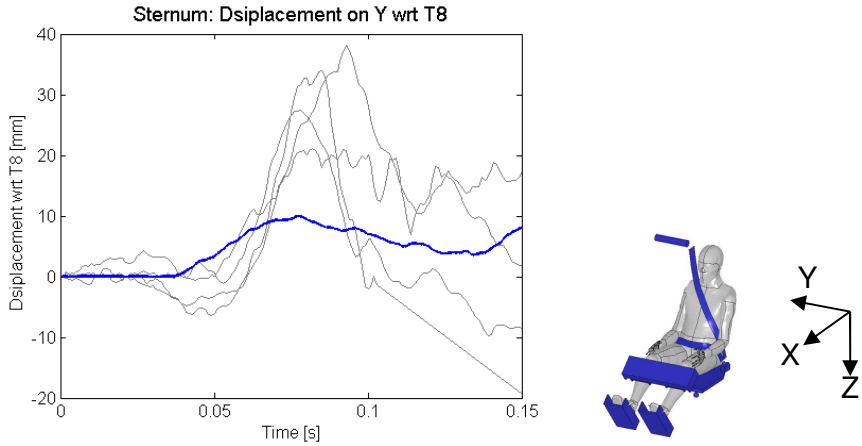

Figure B21. THUMS sternal displacement along Y axis wrt T8 (blue). Compared to experimental data (grey) from Shaw et al. (2009).

Figure B22. THUMS chest displacement along Y axis (blue) wrt T8. Compared to experimental data (grey) from Shaw et al. (2009).

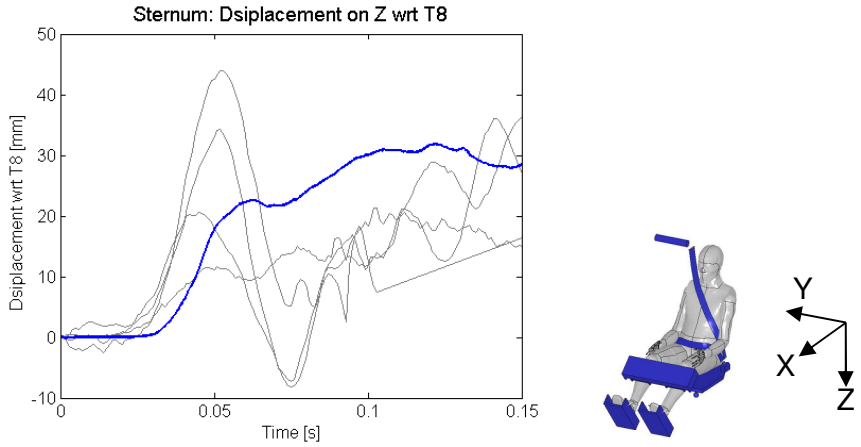

Figure B23. THUMS sternal displacement along Z axis wrt T8 (blue). Compared to experimental data (grey) from Shaw et al. (2009).

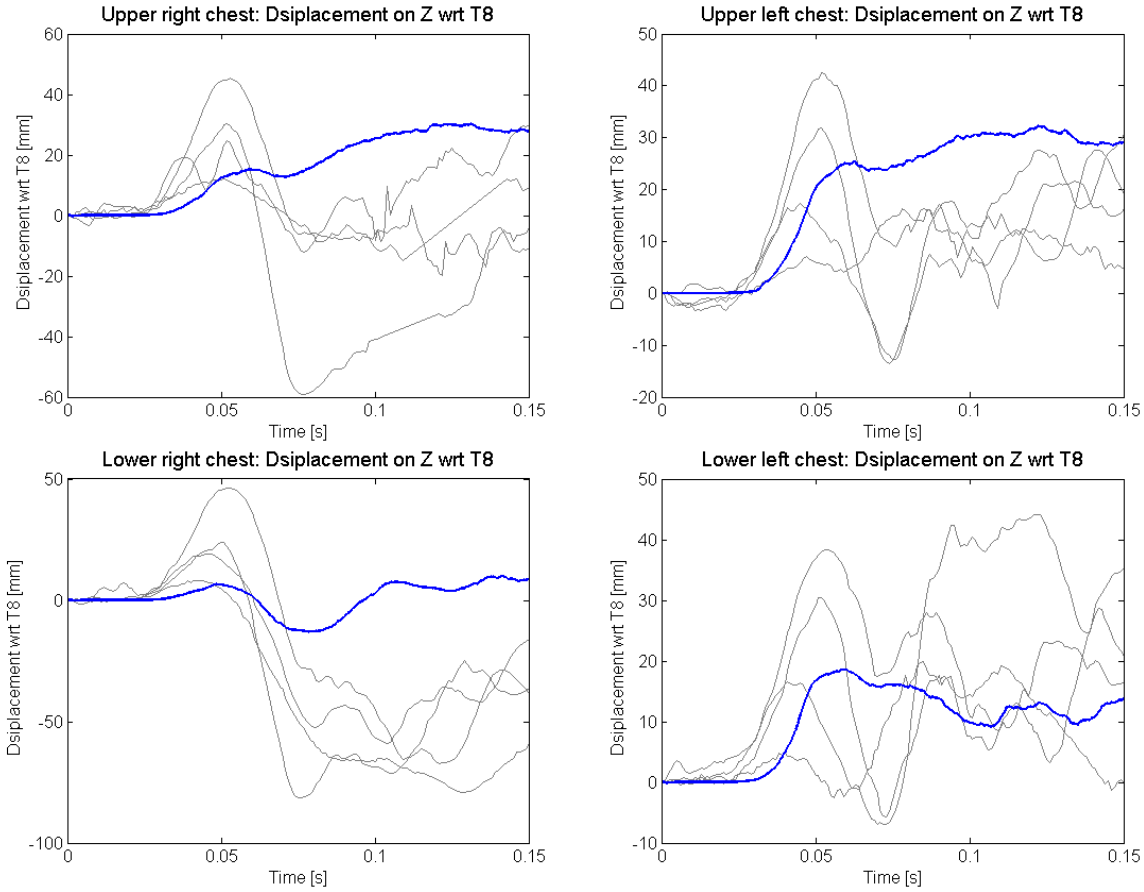

Figure B24. THUMS chest displacement along Z axis (blue) wrt T8. Compared to experimental data (grey) from Shaw et al. (2009).

9.4 Appendix B:4 – Sled test: T8 yaw and upper shoulder belt force

Sled test: T8 yaw and upper shoulder belt force for the intact state compared to PMHS results

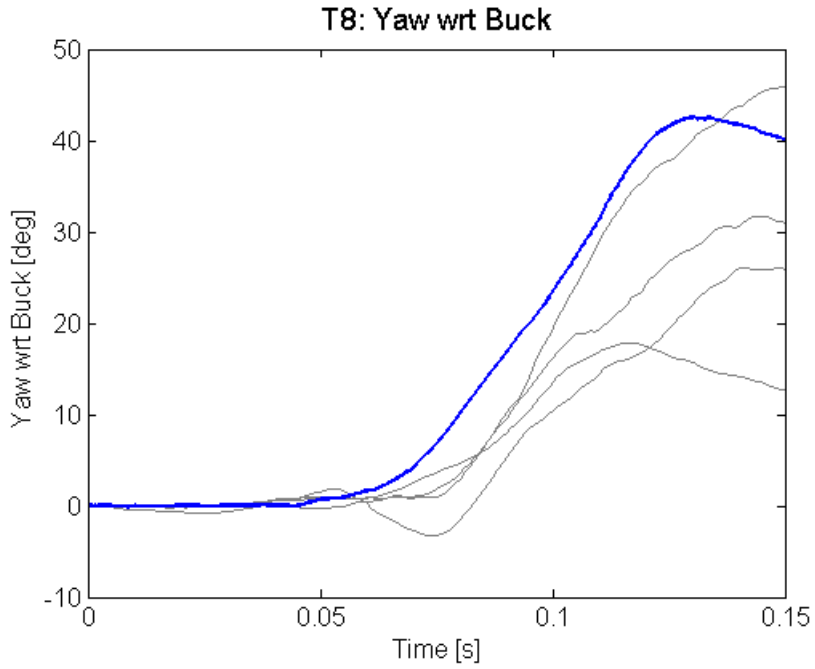

Figure B25. T8 yaw for THUMS (blue) in sled test compared to PMHS results (gray)

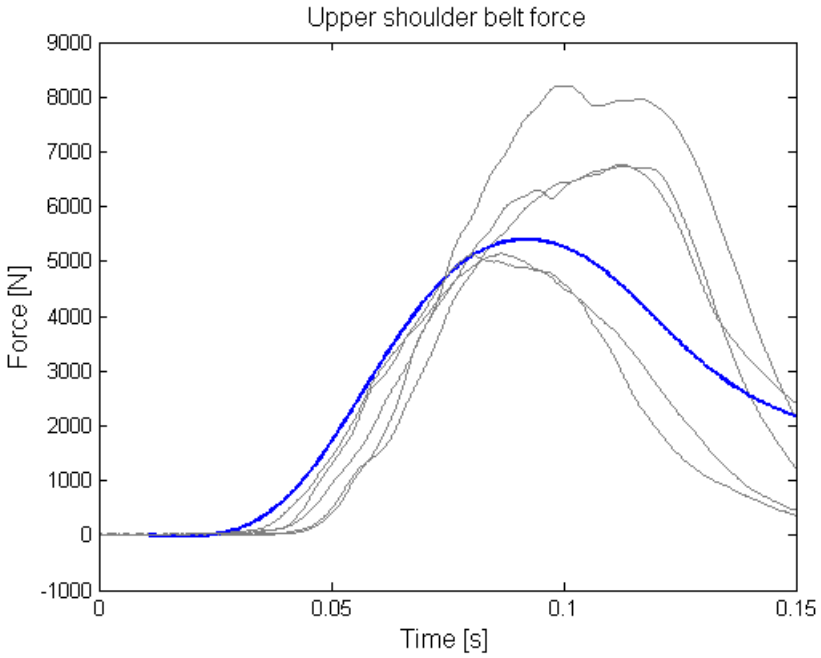

Figure B26. Upper shoulder force for THUMS (blue) in sled test compared to PMHS results (gray)